Reviews in Mineralogy & Geochemistry
Vol. 88 pp. 689–754, 2022

Synthesis of Diamonds and Their Identification

Ulrika F. S. D'Haenens-Johansson
Gemological Institute of America (GIA)
New York City, New York 10036, USA
ujohansson@gia.edu

James E. Butler
Cubic Carbon Ceramics
Huntingtown, Maryland 20639, USA
jimbutler29@comcast.net

Andrey N. Katrusha
Alkor-D Research
Kiev 03134, Ukraine
akatdps@gmail.com

INTRODUCTION

Since 1797, when Tennant demonstrated that diamond consists solely of elemental carbon by comparing the volume of carbon dioxide formed by burning identical weights of charcoal and diamond (Tennant 1797), scientists have been trying to synthesize diamond by converting various carbon-containing substances. Several attempts followed, but it would take over 150 years of continued research before the first successful report of diamond growth was published by scientists at General Electric (Bundy et al. 1955). Diamond synthesis by Union Carbide in 1952 and Allmänna Svenska Elektriska Aktiebolaget (ASEA) in 1953 predate the work at General Electric, but were not reported until later (Liander and Lundblad 1960; Eversole 1962; Angus 2014). The most familiar carbon allotropes are the crystalline phases of graphite and diamond. The hexagonal form of graphite consists of sheets of sp^2 hybridized carbon atoms in a hexagonal array, with each atom bonded to three equidistant nearest neighbor atoms. The layers are attracted to each other by weak van der Waals forces and may be arranged in a hexagonal, or rarely rhombohedral, stacking sequence. Meanwhile, the carbon orbitals in diamond are sp^3 hybridized, with each atom covalently bonded to four nearest neighbors in a tetrahedral arrangement. The prevalent diamond structure is cubic, though the hexagonal lonsdaleite form also exists. Figure 1 illustrates the pressure and temperature (*P, T*) phase and transition diagram for pure carbon. Theoretically and experimentally determined conditional phase boundary lines separate the diamond and graphite stability fields. The high cohesive and activation energies associated with the different carbon phases mean that other metastable forms can occur under conditions at which they are not thermodynamically stable. For instance, diamond exists at room temperatures and pressures, whereas graphite can survive pressures well into the diamond stability field (Bundy 1980; Bundy et al. 1996).

High quality single crystal diamonds can be synthesized using either the high pressure, high temperature (HPHT) or chemical vapor deposition (CVD) techniques. In the former, growers use an HPHT press to crystallize diamond from a carbon source such as graphite either by direct or indirect (catalytic) conversion methods (Fig. 2), applying temperatures and

1529-6466/22/0088-0013$10.00 (print)
1943-2666/22/0088-0013$10.00 (online)
http://dx.doi.org/10.2138/rmg.2022.88.13

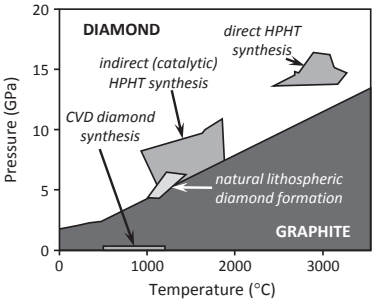

Figure 1. Carbon phase diagram as a function of pressure and temperature, illustrating the conditions for natural diamond formation in the lithosphere as well as those for laboratory-grown diamonds synthesized by chemical vapor deposition (CVD) and high pressure, high temperature (HPHT) methods. [Based on phase diagrams compiled by Bundy (1980) and Bundy et al. (1996), including natural diamond data presented by Stachel and Harris (2008).]

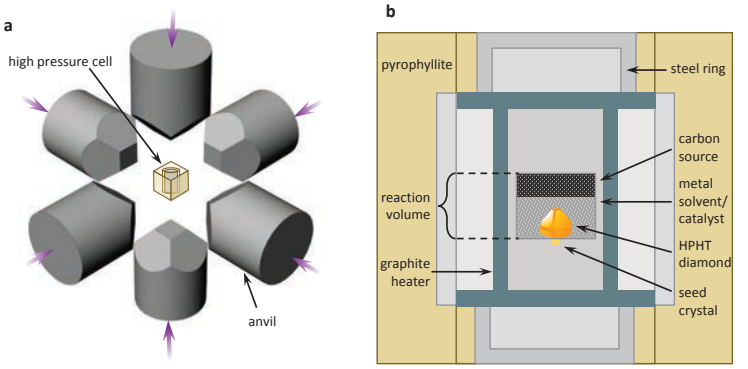

Figure 2. Illustrations of (**a**) the pressure transmitting anvil arrangement for a standard cubic press and (**b**) the high pressure cell (HPC). The internal reaction volume in the HPC contains the key ingredients for HPHT diamond synthesis: a carbon source (such as graphite), metal solvent/catalyst (typically Fe or its alloys), and one or more diamond seed crystals. For the temperature gradient method, the temperature is controlled such that the region with the carbon source is hotter than the seed crystal. The carbon dissolves into the metal solvent/catalyst melt, reaching supersaturation and recrystallizing as HPHT diamond material at the seed.

pressures at which diamond is the dominant phase. The latter technique is instead based on gas-phase chemical reactions involving hydrocarbon and hydrogen gases to deposit metastable diamond at low pressure in a CVD reaction chamber (Fig. 3). Though thermodynamically unstable, under the selected conditions diamond growth is kinetically favorable. This chapter reviews the principles, technology and current capabilities of these two different techniques, as well as the properties of the diamonds that they yield.

Although diamond's fame originates from its use as an attractive gemstone, research on the synthesis and characterization of their high laboratory-grown counterparts has historically been driven by a scientific community eager to manufacture materials specifically tailored to harness some of the remarkable combination of properties that this material or its lattice defects boast. Industrial and technological applications include diamond abrasives and cutting tools, quantum sensing, high power electronics, thermal management, optical windows, x-ray optics, and electrochemical devices for water treatment (Wort and Balmer 2008; Balmer et al. 2009; Field 2012; Shvyd'ko et al. 2017; Awschalom et al. 2018; Cobb et al. 2018; Koizumi et al. 2018; Donato et al. 2019; Yang et al. 2019; Achard et al. 2020). In the last couple of decades, laboratory-grown diamond quality improved and started to obtain gemological properties akin to natural diamonds, sparking interest in the gem and jewelry industry. Though long considered a niche product with limited distribution, in 2021 laboratory-grown diamonds were reported to account for 5 to 8% of the total global diamond (natural + laboratory-grown)

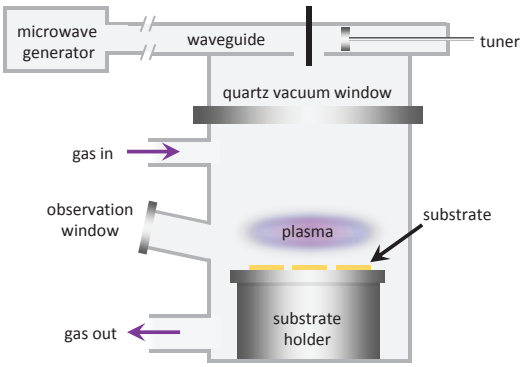

Figure 3. Schematic of a microwave CVD reactor. A hydrocarbon gas in an excess of hydrogen is introduced into the growth chamber. In this design, microwaves are used to activate a plasma, dissociating the gas components into species which can react with diamond substrates heated to 600–1200 °C, depositing new diamond material. [Modified after Martineau et al. (2004) *Gems and Gemology*, Vol. 40, Fig. 2, p. 4.]

jewelry market; this value was under 1.5% as recently as 2018 (Zimnisky 2021; Branstrator 2022). Market analysis estimated the annual production for laboratory-grown diamonds created for gem applications to be 6–7 million carats (1 carat = 1 ct = 200 mg) in 2020 (Linde et al. 2021). For reference, approximately 40% of the 140 million carats of natural rough diamonds mined annually are gem-quality (Zimnisky 2020). Competition between growers in this sector has led to dramatic rise in diamond sizes, producing faceted gems up to ~15 ct (e.g., Poon and Wang 2016; Wang et al. 2022). Further size increases may be tempered by consumer demand, though growers have been developing methods to synthesize 100 ct crystals. Despite global focus being placed on >1 ct faceted laboratory-grown diamond manufacturing, China has become a significant mass producer of melee-sized goods. Melee diamonds are loosely defined as those weighing 0.001–0.2 ct, but this may vary by country.

The introduction of laboratory-grown diamonds in the gem and jewelry industry has also led to concern that they may infiltrate the natural diamond stream and be sold without full disclosure of their man-made origin. In order to maintain transparency and protect gem and jewelry buyers, scientists and gemologists at grading laboratories have worked in tandem with the diamond physics and geology communities, as well as diamond growers from across the globe, to develop identification methods. This chapter presents a comprehensive account of the key gemological and spectroscopic characteristics that are used to confidently separate natural and laboratory-grown diamonds.

HIGH PRESSURE, HIGH TEMPERATURE GROWTH OF DIAMOND

Principles of growth

This section discusses the growth of high pressure, high temperature (HPHT) diamonds, synthesized at pressure and temperature conditions where diamond is the thermodynamically stable form of carbon. Commercial HPHT synthesis is generally conducted at higher temperatures and pressure with respect to the graphite–diamond boundary line (see Fig. 1), accounting for kinetic effects related to uncertainty in the boundary line position which may negatively affect the crystallization of diamond from the graphite phase, leading to growth plane incompleteness or inclusion entrapment.

Research teams at General Electric investigated two primary routes for HPHT diamond growth in the 1950s through 1970s: the direct and indirect (stimulated) conversion of graphite to diamond as presented in Figure 4 (Bundy et al. 1955; Bovenkerk et al. 1959; Bundy 1962, 1963; Wentorf 1971; Strong 1989). These approaches differ in technological complexity. Although the former growth method is faster, it requires specialized high-pressure control equipment

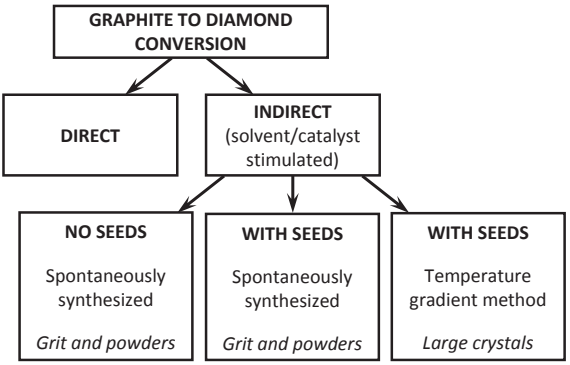

Figure 4. Schematic of the different graphite to diamond conversion processes.

that can generate and maintain pressures higher than 13 GPa at temperatures above 2000 °C, as well as technical staff capable of manipulating these parameters simultaneously. Thus direct graphite to diamond conversion tends to yield small diamond crystals ranging from a few nanometers to millimeters in size, which may be polycrystalline in nature (Bovenkerk et al. 1959; Bundy 1962, 1963; Irifune et al. 2003, 2004, 2014). Commercial diamond production is based on the indirect graphite to diamond conversion approach, where a carbon source material, usually graphite powder, is mixed with a solvent/catalyst and placed in a growth cell (the "reaction volume"). The solvent/catalyst is used to stimulate growth, transport carbon to the growing surface, and decrease the pressure and temperature requirements for diamond nucleation, with typical conditions of 5–6 GPa and 1300–1600 °C. The reaction volume may also contain diamond seed crystals to aid in nucleation. Diamond grit and powder production can occur with or without diamond seeds, whereas large diamond crystal production requires them. Generally, diamonds grown by the spontaneous nucleation method (no seeds) readily incorporate nitrogen impurities, resulting in yellow color (Chrenko et al. 1971), but specialized approaches can result in colorless diamonds with good morphology, as shown in Figure 5. Color-producing impurities in HPHT diamonds will be discussed in the section *Identification of HPHT diamonds: Absorption spectroscopy and color.* The temperature gradient catalytic growth method has been successfully used to synthesize multi-carat sized HPHT diamonds (Burns et al. 1999; Kanda 2000; Sumiya and Tamasaku 2012; Sumiya 2014; Sumiya et al. 2015; D'Haenens-Johansson et al. 2015a). Operating under pressures within the diamond stability field, the temperature of the reaction volume is increased so that the solvent/catalyst melts. A temperature gradient of ~20–50 °C is produced, resulting in a hotter environment for the carbon source than the seed region. The carbon source material dissolves in the melt, with

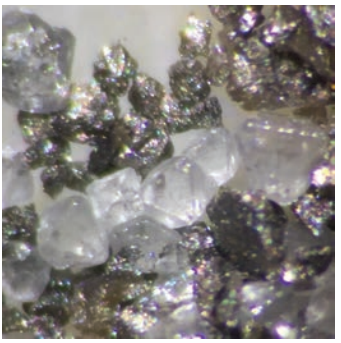

Figure 5. Colorless Type IIa HPHT diamond crystals with predominantly octahedral {111} morphology obtained by the spontaneous nucleation process (~50–150 μm in size). The gray shiny pieces are remains of the reaction medium after initial acid cleaning. [Diamonds synthesized by ANK with Alkor-D Ltd. Photograph by ANK.]

the carbon atoms being transported toward the cooler seeds. Under the selected conditions the carbon becomes supersaturated in the melt, crystallizing as HPHT diamond on the seeds. Figure 2 illustrates the key components of this method. HPHT growth occurs along different crystal directions with differing growth rates, typically resulting in crystals with well-developed cube {100} and octahedral {111} faces (cuboctahedral morphology) as shown in Figure 6 (Strong and Chrenko 1971; Kanda et al. 1980, 1989; Sunagawa 1984, 1995; Shigley et al. 1986, 1987, 1992, 1993a,b; Burns et al. 1999). Presently metal solvent/catalysts consisting of pure or alloy forms of Fe, Ni, Co, Mn, Cr, Ta, or Nb are used for industrial and gem diamond synthesis (see the upcoming section *Selection of metal solvent/catalyst*). Diamond crystallization using alternative non-metallic growth media such as carbonate-silicate, sulfide-carbon, sulfur-carbon, carbon-oxygen-hydrogen, and phosphorus-carbon systems have been reported, with experiments primarily geared toward gaining a better understanding of fundamental diamond formation processes in the mantle or creating unusually doped specimens. Such synthesis falls outside the scope of this chapter, as they are not used for large crystal diamond growth, however Palyanov et al. (2015a) present a detailed review.

Figure 6. HPHT diamond crystals (0.5–0.69 ct) grown by Jinan Zhongwu New Materials Company Ltd. of Shandong, China, showing characteristic cuboctahedral growth morphology. [Used by permission of the Gemological Institute of America, from Eaton-Magaña et al. (2017) *Gems and Gemology*, Vol. 53, Fig. 2, p. 266.]

Technology of growth

High pressure equipment capable of reaching pressures greater than 5 GPa—the minimum necessary for HPHT diamond nucleation—have been developed by several research groups across the world using different approaches for pressure generation and transmission. Excluding rare multi-stage high pressure machines with small (<1 mm^3) reaction volumes, the designs can be grouped into four main types: the belt, toroid, BARS, and cubic presses. Figure 7 illustrates the relationship between investment costs, reaction volumes, maintenance costs, and difficulty of usage for these presses. The belt and toroid presses are based on axial compression of the reaction cell, differing in side support design. With the former, a pair of pistons push into the chamber and are supported by binding rings forming a "belt" around the structure (Hall 1960a,b). In the latter, toroidal sub-cavities hold the pressure inside the main semi-spherical cavity (Kolchin et al. 1981; Khvostantsev et al. 2004). In contrast, the BARS and cubic systems apply pressure along multiple axes. BARS presses (referred to by the Russian abbreviation for their description) have a split-sphere multi-anvil block design, using hydraulic oil to generate pressure through an elastic membrane usually made from rubber or similar material (Shigley et al. 1993a; Palyanov et al. 2017). Cubic presses (e.g., Fig. 2) are based on six perpendicular anvils coupled to independent hydraulic cylinders compressing a cubic chamber (Zeitlin et al. 1961). The compression mechanism largely defines the weight and size of the presses. To generate the equivalent load on a similarly sized sample chamber, the mechanical piston hydraulics used for belt and toroid systems are approximately 2–3 times larger than those for BARS systems.

HPHT presses are manufactured globally, with certain regions specializing in a particular type. Factories in former USSR countries produce the most popular series of BARS presses, with the model names (300, 350, and 400) describing the diameter of the sphere in millimeters.

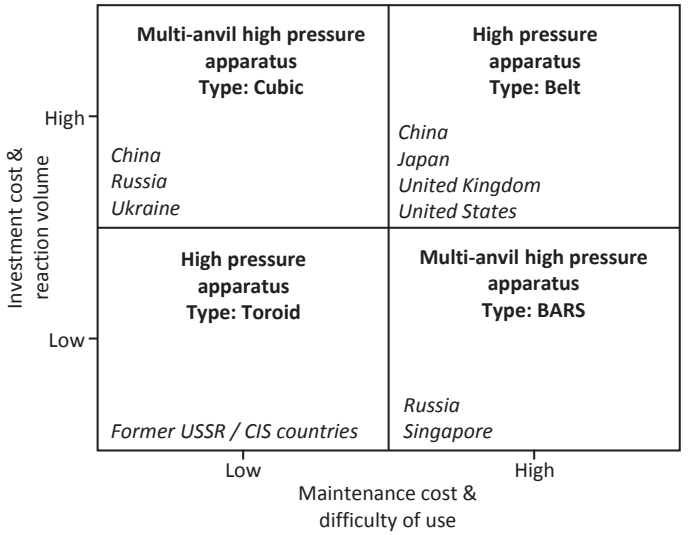

Figure 7. Comparison of the costs, reaction volumes, and difficulty of usage associated with high pressure, high temperature (HPHT) equipment presently existing in the market. Considering 2020 prices, the "low" regions indicate average investment costs of about $20,000–$30,000, while the "high" regions represent those greater than $100,000. For reaction volumes, the regions indicate either 1–5 cm^3 or 10–300 cm^3, respectively.

BARS presses use an oxide/halide ceramic cube (or parallelepiped) high pressure cell (HPC), where the edge defines the reaction volume, e.g., a 32 mm cube contains a 2 cm^3 reaction volume. These presses can produce loads of 6–12 MN (Feigelson 1983). Toroid systems also originate from this region, with central recess (lune) diameters of 20, 30 and 40 mm in combination with hydraulic press models DO043 or DO044. These presses are capable of generating 20 and 25 MN loads, respectively. The diameter of the lune defines the reaction volume, e.g., a 40 mm diameter provides an approximately 2 cm^3 reaction volume. Reaction volumes up to 10 cm^3 have been reported (Palyanov et al. 2015a). Belt systems from the United States are used for diamond grit production, with reaction volume sizes up to 1000 cm^3. The Chinese development of cubic systems has benefited from government support, leading to a continuous improvement in reaction volume sizes, ranging from the series 460 to the series 1000 (as of June 2020). The series number represent the diameter of the hydraulic cylinder in millimeters. The series 560, 650 and 750 cubic presses are the most widely used models for both grit and large diamond growth, attaining loads of 30–50 MN. As for BARS presses, the cubic HPC edge defines the reaction volume, e.g., 74 mm cubes have reaction volumes of about 40 cm^3.

All four press types consist of three main parts: the pressure generating machine, the pressure transmitting unit (referred to as the high pressure apparatus, HPA), and the sample containing HPC. In order to generate and hold the pressure on the sample, the force is transmitted from the press machine through the respective HPAs to the HPCs (Figs. 2 and 8). The HPA is made from cemented carbides composed of tungsten carbide and cobalt (WC-Co alloys, such as WC-6% Co, WC-8% Co and WC-10% Co). The geometry of the HPC is dictated by the shape of the compressive and tensile components of the HPA. Presently, the hardness and toughness of the HPA hard alloy set the upper limit for the achievable pressure in systems used for large volume diamond mass production. For further details regarding HPA and HPC design see Bundy (1988). Future improvements in large volume superhard HPAs would propel the diamond industry to increase production volumes, improve sample quality, and further explore promising unconventional growth media for diamond synthesis.

(a) (b)

Figure 8. (**a**) High-pressure cells (vessels) used for different high-pressure apparatus (HPA): toroid (**left**), belt (**middle**), and cubic (**right**). Belt and cubic systems benefit from higher reaction volumes. (**b**) High-pressure cells used in cubic high-pressure presses (series 650/750/850/950) from the 1990s till present. The largest version of the cell, with dimensions 88 × 88 × 88 mm (shown on the **right**) is currently the largest commercially available cell, and widely used. Larger cells exist, but are still in the experimental development phase. Cell dimensions from left to right: 58 × 58 × 58, 74 × 74 × 74 mm, and 88 × 88 × 88 mm. [Photographs by ANK.]

Heavy investment in diamond synthesis using cubic presses have led to design upgrades and regular breakthroughs in diamond volumes and qualities, warranting further detailed description of this press type. Cubic high pressure cells (Fig. 2b and 8b) are made of powder pressed pyrophyllite with a central cavity containing tens of concentric and axially assembled components designed for three main functions:

1. Pressure transmission to the sample reaction chamber;
2. Resistive heat generation to melt the metal solvent/catalyst;
3. Providing thermal and chemical insulation to prevent damage to other press components during high pressure and temperature experiments over long periods of time.

These functions are generally applicable to all HPHT systems. Components are made of advanced materials in order to fulfill these functions and withstand the combination of extreme pressures (5–7 GPa) and temperatures (1300–1800 °C) produced in the sample reaction chamber. Certain salts and refractory ceramics possess the required chemical inertness, high melting temperatures, and phase stability at high pressures. Boride and chloride salts, as well as ceramics in the form of oxides (Mg, Al, Zr, or Y) are commonly used by the diamond synthesis industry (Strong 1977; Zhu et al. 2019). The component materials may differ for systems that require higher temperatures, such as those used for HPHT annealing treatments to change diamond color.

The temperature in the cell is generated by means of graphite or composite material resistive heaters. A precise temperature field distribution is formed in the diamond synthesis region by careful selection of the geometry and physical properties of the electric system, considering how these may be affected when subjected to simultaneous temperature and pressure changes. Temperature gradients across the cell are undesirable for diamond grit production, with efforts made to minimize fluctuations close to the cell sides. In contrast, controlled axial and radial temperature gradients are the basis of the temperature gradient growth method used for large high quality diamond synthesis (e.g., D'Haenens-Johansson et al. 2015a). Careful component designs which consider detailed electric and heat conductance properties in the cell enable control of the heat generation and dissipation distributions, offering the flexibility to grow samples using either scheme. Finite element method (FEM) simulations are widely used to characterize the temperature field in the growth cell under different conditions (Li et al. 2013). The main drawback with this approach is that it cannot consider the component material properties at high temperatures and pressures. Results from complementary experiments analyzing real temperature distributions using thermocouples, as well as observations of phase transitions, provide the necessary feedback to improve the

simulated material properties. Temperature gradients as fine as 1 °C/mm can be predicted and realized within the cells, facilitating the set-up of the optimal carbon supersaturation conditions necessary for growth of high quality diamond crystals with flat faces and good morphology. In the case of suboptimal carbon supersaturation, growth is unstable, resulting in the formation of multi-crystal aggregates known as druzes (Fig. 9).

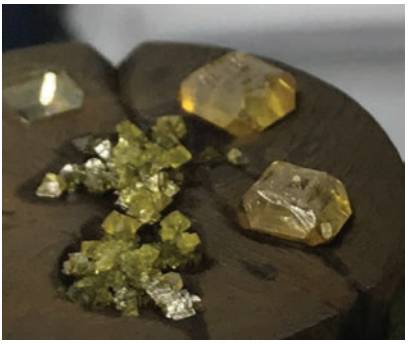

Figure 9. The simultaneous presence of optimal and oversaturated carbon flow during the HPHT diamond growth process resulted in the formation of high quality flat-surfaced single crystals (**upper right**) and multi-crystal aggregates (druzes, **lower left**) due to growth instability, respectively. The larger crystals weigh approximately 4 ct. The diamond materials are here imbedded in the remains of the growth medium after a short acid clean. [Diamonds grown by ANK with Alkor-D Ltd. Photograph by ANK.]

Selection of metal solvent/catalyst

Historically, HPHT diamond growers focused on selecting metal solvent/catalysts with the lowest possible diamond nucleation temperatures due to practical and economic reasons. Lower growth temperatures in turn also meant that lower pressures could be used, easing the demands on the press and increasing the lifespan of the HPA components. The costs of the metals used were also considered. Initially, the solvent/catalysts were Mn and Ni alloys (Bundy 1963). However, there was a great disadvantage to their use: the growing crystals readily trapped inclusions of carbides associated with these metals. Thus diamond crystal powders produced at the time were characterized by poor toughness. Inclusion uptake could be decreased, and the material properties improved, by operating at higher temperatures and pressures using Fe, Ni and Co alloys. Growth using a variety of solvent/catalysts composed of combinations of invar (Fe–Ni) and kovar (Fe–Ni–Co) alloys have been carefully analyzed (Strong and Chrenko 1971; Kocherzhinski and Kulik 1996; Sugano et al. 1996). Eutectic compositions are used as they lower the melting temperature.

Diamond growers devise proprietary melts with additional elements to decrease the pressure and temperature parameters or improve the crystal characteristics. Such additives may either be elements which are fairly chemically inert with respect to carbon (Cu, Sn, In, As, Zn, or Au), or they may be known to interact, forming carbides (Cr, Si, V, Mg, Nb, or Zr). These latter carbide formers are also strong nitride formers, and are usually added specifically to getter nitrogen that would otherwise readily incorporate into the growing diamond. As the molten solvent/catalyst should contain more than 10 at.% carbon, additives may be used to increase carbon solubility (Strong and Chrenko 1971; Kanda 2000). The resulting complex metallic mixtures have been tested for diamond production at a range of pressure and temperature conditions to optimize crystal quality. The conclusions are generally that growth benefits from higher temperature and pressure parameters. Intentional or inadvertent doping of the diamond crystals due to impurities in the melt ingredients, carbon source, or cell components further complicate growth and expand the variables that growers can customize. These dopants, further discussed in the section *Control of color center content and extended defects*, affect the HPHT diamond properties, most notably color. Large, high quality HPHT diamonds that are as-grown colorless, blue, green, and yellow can be produced.

The metal solvent/catalyst is one of the factors that affect the morphology of the growing crystal. For instance, Kanda et al. (1989) demonstrated that pure Ni melts resulted in cubic {100} and octahedral {111} faces, whereas Ni-alloys which included Co and Fe promoted the development of dodecahedral {110} and trapezohedral {113} faces. The solvent/catalyst composition also influences surface structures on the crystal faces, which may form dendritic, vein-like, lamellar or etch pit patterns (Kanda et al. 1980). The patterns correspond to the solvent/metal textures that are created during the quenching process that occur at the end of growth runs.

Diamond seed considerations

Large HPHT diamond growth using the temperature gradient method is initiated homoepitaxially on a diamond seed. Growth on the seed can follow two different approaches. Either all sides of the seed can be overgrown with HPHT diamond (like natural diamond growth), or growth can be restricted to one face, with greater control over the orientation. Figure 10 shows diamonds grown using the first method, with a yellow diamond seed enveloped by new colorless diamond material. For the second method the selected growth face of the seed is placed in contact with the metal solvent/catalyst, while the other faces are shielded by some barrier material (Wentorf 1971). The latter is the most commonly used approach for HPHT diamond growth.

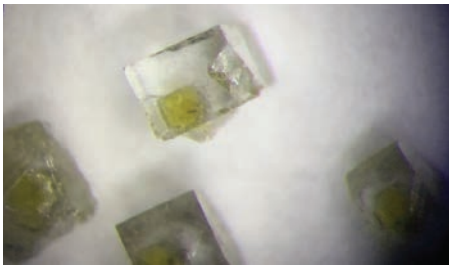

Figure 10. Experimental colorless Type IIa HPHT diamond crystals with cubic {100} faces obtained by the overgrowth method on yellow Type Ib laboratory-grown diamond seeds from usual diamond powder production. The size of the colorless crystals range between 1.0 and 1.5 mm. The cubic external morphologies seen here are extraordinarily rare for diamonds grown using high growth temperatures (>1850 °C), and were possible due to the use of non-traditional growth media based on magnesium. [Diamonds grown and photographed by ANK (Alkor-D Ltd.).]

The maximum size of each HPHT diamond is defined by the number of seeds simultaneously used as the growing diamonds compete for a limited amount of carbon source material and space within the reaction cell. It may be possible to increase the crystal output if the reaction cell is large enough to be segregated into a multi-layered growth structure. An example of multiple seeds for a two-layered growth cycle is shown in Figure 11. During growth the layers were vertically adjacent to each other, and advanced techniques were used to generate the necessary temperature gradient across the system to initiate diamond nucleation and growth under the appropriate pressure and temperature conditions.

The orientation of the diamond nucleation face on the seed defines the crystallographic orientation of the first atomic-scale HPHT overgrowth layer. The growth directions of subsequent atomic layers are influenced by the pressure and temperature parameters as well as the chemical composition of the growth environment, usually resulting in the characteristic cuboctahedral morphology (Strong and Chrenko 1971; Kanda et al. 1980, 1989; Burns et al. 1999). Typically, the upper growth face of the HPHT diamond has the same orientation as the nucleation face on the seed, unless the sample has experienced significant variations in growth conditions. Consequently, growers are able to exercise some control over the growing crystal morphology. Figures 6, 9, 11, and 12 present examples of HPHT diamonds grown on (100)-oriented (cubic) seeds, while Figure 13 shows samples grown on (111)-oriented (octahedral) seeds. Although intentional growth on alternative seed facet orientations such as (113), (115), or (110) are also possible, in practice it is mainly restricted to fundamental growth research as seed preparation is challenging and availability is limited.

Seed size selection has to balance material costs (larger seeds are more expensive) and the grower's ability to initiate and control growth without multiple nucleation sites. Seeds range from tens of micrometers to a few millimeters in size. There is a plentiful supply from the industrial diamond grit and powder manufacturing sector.

Figure 11. Typical example of HPHT diamonds resulting from multiple seed and multiple layer growth methods. The view is from the seed side (the bottom of the reaction volume illustrated in Fig. 2b), where the growth medium has been partially dissolved by acid cleaning. Average crystal size is ~4 mm each. [Diamonds grown and photographed by ANK.]

Figure 12. Nitrogen doping influences the color of HPHT diamonds, with yellow color being observed with increasing isolated substitutional nitrogen concentrations ([N_S^0]). These concentrations were controlled by including nitrogen getters in the growth capsule. Each diamond crystal is ~7 ct in size. [HPHT diamonds synthesized and photographed by ANK.]

Figure 13. Deep blue to black Type IIb HPHT diamonds grown on {111}-oriented diamond seeds. Sizes range from approximately 6 to 15 ct. The upper face has a {111} orientation, reflecting that of the seed. The sizes and orientations of the other faces depend on the pressure and temperature conditions in the growth cell. [HPHT diamonds synthesized and photographed by ANK.]

Effect of growth temperature and pressures

Growth temperature affects the crystal morphology, with the primary faces changing from {100} to {100} + {111} and then {111} as temperatures are increased when using standard ferrous solvent/catalysts (Satoh et al. 1990; Sumiya et al. 2002). Temperature ranges for good crystal quality are narrow, with reported windows spanning only about 10–40 °C, depending on the applied pressure and the type of diamond being synthesized. At lower temperatures skeletal crystals start to form, where growth primarily proceeds along corners and edges rather than at the crystal faces. At higher temperatures inclusion uptake increases. However, there are exceptions to this behavior. Rare pure rhombidodecohedral {110} (12-faced crystal form of {110} with cubic crystal symmetry) diamonds can be grown under certain pressure and temperature conditions for a given metal solvent/catalysts, as shown in Figure 14. The relationship between the pressure, temperature, solvent/catalyst, and resulting grown diamond morphology is complex. For example, the HPHT diamonds shown in Figure 10 were grown at high temperatures (>1850 °C), yet are dominated by {100} faces. These diamonds were grown using an atypical Mg-based solvent/catalyst.

The solubility of impurities such as nitrogen into the solvent/catalyst rises with temperature, potentially leading to lower impurity concentrations in the growing diamond (Burns et al. 1999). Furthermore, increasing temperatures leads to a decrease in the efficiency of impurity getters (Kanda and Lawson 1995). Hence drifting or fluctuating local temperatures at the growth fronts can modify the distribution of impurities within growth sectors, defined as volumes within a diamond that were grown with common growth planes (Kanda and Yamaoka 1993; Burns et al. 1999). Further discussion of growth sectors is presented in the section *Identification of HPHT diamonds: Growth sectors*. Higher temperatures in nitrogen-containing growth can also lead to the formation of aggregated nitrogen defects (nearest neighbor nitrogen-pairs known as A-centers) (Davies 1976; Kanda et al. 1990; Vins et al. 1991; Babich et al. 2000, 2004).

Pressure influences significantly the nucleation rate in the indirect graphite to diamond conversion growth method (Bundy et al. 1955), whereas for the temperature gradient method its influence is relatively small and restricted to the effect of "widening" the effective technological growth zone. It has been observed that pressure has some influence on the solubility of carbon in melted solvent/catalysts, so that fluctuations also affect the crystal growth.

While diamond nucleation and/or seeded growth have been achieved using many pressure and temperature combinations, temperatures exceeding 1600 °C and pressures above 7 GPa have been identified as suitable for stable mass production of diamonds. However presently such parameters are not economically viable to generate in larger volume high pressure systems since production costs would be much higher than the sale price of the product, without much improvement in the diamond properties.

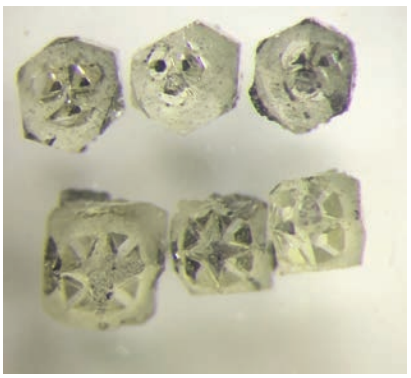

Figure 14. Example of extremely rare HPHT diamond single crystals with pure rhombic dodecahedral {110} external morphologies. The upper and lower rows show crystals with 3-point and 4-point joining tips, respectively. The light yellow hue of the crystals is a result of nitrogen doping occurring due to loss of nitrogen-getter efficiency at high growth temperatures (>1850 °C). [HPHT diamonds grown by ANK with Alkor-D Ltd. Photograph by ANK.]

Doping and control of color center content

Diamond is a wide-bandgap semiconductor with a bandgap energy of ~5.48 eV, making it transparent from the ultraviolet, through the visible, and into the infrared range (~225 nm–2.6 μm) (Clark 1959; Collins 1982). Consequently, perfect, impurity-free diamond consisting solely of carbon atoms is a colorless material. The growth environment, as well as post-growth conditions or treatments may however introduce color-producing impurities and defect complexes. Diamond has one of the highest atomic densities (atoms/cm^3) of any terrestrial material. This is due to the small size of carbon atoms and the four strong and short carbon to carbon sp^3 bonds per each carbon atom in the lattice. As a result, it is difficult to fit larger atoms into the lattice. Nitrogen, boron, and possibly phosphorus atoms are known to occupy lattice sites, while larger atoms such as silicon and nickel usually are accompanied by vacancies for them to fit in the lattice. Defects related to carbon interstitials are observed and there is evidence for atomic hydrogen and protons associated with elemental impurities. Defects can change the electrical, optical, thermal, and structural properties of diamonds. Thus the ability to manipulate the defect content in laboratory-grown diamonds through doping or growth control measures are important. Many defect centers absorb light, fluoresce, luminesce, and/or phosphoresce, enabling their identification, as discussed in detail in the section *Separation of natural and laboratory-grown diamonds*. Collins (1982, 1992, 1993a), Ashfold et al. (2020), and Green et al. (2022, this volume) present reviews on diamond defects.

Nitrogen and boron are the most widespread impurities in both natural and laboratory-grown diamonds (Collins 1993a,b; Ashfold et al. 2020). Unintentional contamination with them during HPHT synthesis is common due to their availability in the growth environment. Air, which has 78.09% nitrogen by volume, is easily trapped in pores and cavities within the reaction cell or its components. Trace amounts of both nitrogen and boron can be found in the carbon source, metal solvent/catalyst, and cell materials. Whereas the purity of the solvents and graphite can be controlled with high accuracy (up to 0.001 wt%), the purification process of the total assembled growth capsule is highly complicated and not reproducible due to constraints in press operation. For these reasons, precise control of nitrogen and boron content in the grown diamonds primarily relies on a chemical approach—the use of impurity getters (Mg, Al, Zr, Ti, V, Cr) or compensators (B, S, N, P). Getters act as chemical absorbers of the undesirable elemental impurity, for instance by forming nitrides, minimizing the element's availability for dissolution into the diamond lattice (Strong and Chrenko 1971; Wentorf 1971; Sumiya and Satoh 1996; Burns et al. 1999; Wakatsuki et al. 1999). Rather than preventing impurity incorporation into the growing crystal, compensators form lattice defects that interact with those formed by impurities, donating or accepting electrons and reducing the concentration of a specific defect charge state which produces unwanted properties (e.g., color) (Burns et al. 1990).

Figure 12 shows the effect of careful addition of getters to control the concentration of nitrogen in HPHT diamonds. As the getter content is decreased, there is an increase in the concentration of isolated nitrogen defects and a transition from Type IIa, to IIa + Ib (where the crystal contains both Type IIa and Ib material), to Ib (see *Identification tools* section below for an explanation of diamond types). There is a stark change in the appearance of the diamonds as the isolated nitrogen defect is associated with yellow color (Chrenko et al. 1971), as discussed in *Identification of HPHT diamonds: Absorption spectroscopy and color*. This control opens up the possibility of defect engineering, where specific concentrations of desirable color centers are produced, either in "as-grown" (untreated) material, or through treatment. Nitrogen-vacancy (NV) centers, which can produce an attractive pink color in gem quality diamonds (e.g., Fig. 15), are also of great interest to the scientific community as they develop methods to harness properties of the negatively charged state of the center (NV^-) for uses in quantum technology and other fields. NV centers can be created by irradiating and annealing HPHT diamonds with

suitable isolated nitrogen concentrations (Moses et al. 1993; Shigley et al. 2004a). The addition of nitrogen getters narrows the range of temperatures at which diamonds with good crystallinity can be grown, and leading to higher uptake of melt inclusions and associated carbides (Sumiya and Satoh 1996; Burns et al. 1999, 2009; Sumiya et al. 2002). It is thought that nitrogen getters decrease the solubility of carbon in the metal solvent/catalyst, or prevent the diffusion of carbon. Group Ib metals (Cu, Ag, Au, etc.) can be used to decompose the carbides (Wakatsuki 1966). Nitrogen getters can also affect the crystal morphology (D'Haenens-Johansson et al. 2015a).

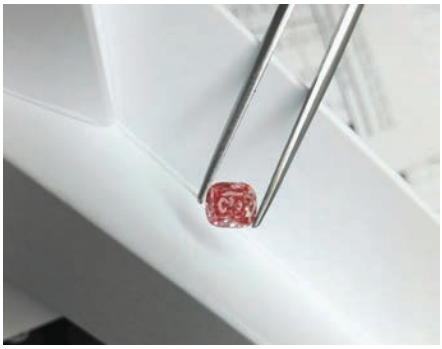

Figure 15. 2.55 ct HPHT-grown gem diamond with a saturated pink color due to high concentrations of nitrogen-vacancy centers. These color centers were obtained by a multi-step process: the original Type IIa + Ib HPHT diamond, containing a low concentration of substitutional nitrogen, was first electron irradiated and finally annealed at a moderate temperature. [HPHT diamond produced and photographed by ANK.]

Uncompensated boron gives rise to blue color in HPHT diamond (Collins and Williams 1971) (see also *Identification of HPHT diamonds: Absorption spectroscopy and color*). Impurity uptake in HPHT diamonds is sensitive to the orientation of the growing face, growth rates and temperature (Strong and Chrenko 1971; Burns et al. 1990, 1999; Satoh et al. 1990). Boron concentrations are typically higher in {111} growth sectors, followed by {110} sectors, whereas nitrogen concentrations follow {111} > {100} > {113} > {110} (Burns et al. 1990). Even blue color can only be achieved by reducing nitrogen concentrations in the diamond to less than 10^{18} cm^{-3}. Otherwise, the resulting material will contain both yellow Type Ib and blue Type IIb growth sectors, which may produce an overall green hue (Shigley et al. 1992, 2004a,b; Fritsch and Shigley 1993; Rooney et al. 1993; Hainschwang and Katrusha 2003). Both Type IIb or IIa + IIb HPHT diamonds are thus grown by adding a nitrogen getter and a boron dopant (e.g., amorphous boron). An example of sector-dependent boron uptake is shown in Figure 16. Further discussion on this phenomenon is presented in *Identification of HPHT diamonds: Growth sectors*.

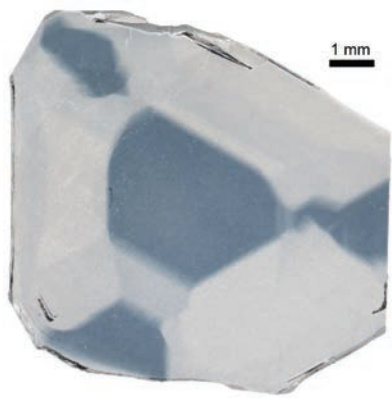

Figure 16. Example of the growth sector dependent incorporation of impurities in large laboratory-grown diamonds. The blue zones indicate the higher concentrations of uncompensated boron present in {111} sectors. [Modified after Howell et al. (2019) *Diamond Related Materials*, Vol. 96, Fig. 1, p. 209.]

Although nitrogen and boron are the most studied impurities in HPHT diamonds, several other elements such as nickel, cobalt, silicon, and germanium can be introduced during synthesis, forming vacancy-containing defect complexes (Collins and Spear 1982; Collins et al. 1990; Lawson and Kanda 1993a,b; Lawson et al. 1996; Sittas et al. 1996; Palyanov et al. 2015b, 2017). These impurities often originate from the solvent/catalyst and its additives.

Large HPHT diamond growth

The growth of extra-large diamond single crystals with high crystalline quality has been simultaneously a dream and one of the biggest challenges for diamond researchers during the last 60 years. Progress was tempered by the technological expertise required, the high associated costs, as well as underdeveloped applications for the final product. Before around 2010 large diamonds were grown using modified belt presses that include large volume HPAs with precise cooling water, hydraulic pressure suspension and in-cell temperature control. De Beers Diamond Research Laboratory grew a 34.80 ct yellow-brown Type Ib HPHT diamond in 1992 (pictured in Kanda (2005), while Sumitomo Electric Industries synthesized 10 ct colorless Type IIa diamonds (Sumiya and Tamasaku 2012; Sumiya 2014; Sumiya et al. 2015). The team at New Diamond Technology (NDT) Ltd. (headed by the present author ANK) adapted cubic series 750 and 850 presses to grow large diamond crystals, and in 2015 announcing the growth of a 32.26 ct colorless diamond that was later cut into a 10.02 ct E color gem (Deljanin et al. 2015). Continuous improvements in their growth capabilities led to increasing rough HPHT diamond sizes from 1 to 60 ct for a reasonable cost and in short time periods up to about 2 weeks. Previously the generally accepted averaged mass growth rate for good single crystals was 1–2 mg/hour, whereas the NDT team could achieve rates as high as 45 mg/hour in those record stones (Deljanin et al. 2015; D'Haenens-Johansson et al. 2015a). To date NDT has produced the largest faceted gem laboratory-grown diamonds reported, including 20.23 ct Fancy Vivid yellowish orange, 15.32 ct H color, and 10.08 ct Fancy deep blue diamonds (Poon and Wang 2016; Ardon and Eaton-Magaña 2018; Wang et al. 2022). As of the year 2020 at the facilities of Alkor-D Ltd. the author ANK has broken the 100 ct limit of single crystal rough HPHT diamonds, as shown in Figure 17. They have also produced a Guinness World Record-breaking 150.42 ct blue HPHT diamond (28.55 × 28.25 × 22.53 mm), not pictured (IGI 2022). Notably these Type IIa and IIb diamonds were grown using extremely fast average growth rates (>64 mg/hour). The limited reaction volume resulted in some deterioration of the exterior of the samples.

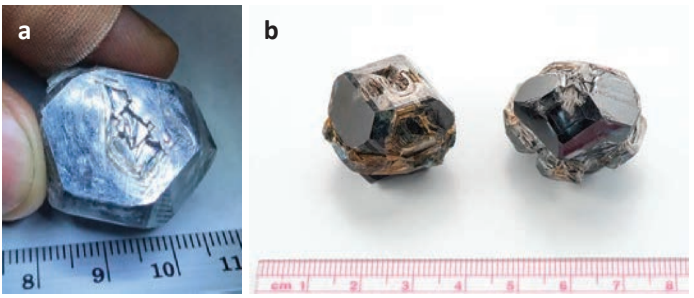

Figure 17. Examples of super large HPHT diamonds grown by ANK with Alkor-D Ltd. (**a**) This Type IIa "colorless" crystal weighed 94.30 ct (22.16 × 23.70 × 18.88 mm), while the (**b**) Type IIb nearly-black crystals shown here left and right weigh 109.81 ct (25.72 × 24.74 × 19.84 mm) and 115.65 ct (28.42 × 24.71 × 23.36 mm), respectively. [Photographs taken by (a) ANK and (b) Jia Xin (Jae) Liao for GIA.]

There are three factors that are extremely important when growing extra-large diamond single crystals: temperature control and reproducibility within the given in-cell isotherm pattern, high chemical stability of the hardware materials used to withstand prolonged exposure times (up

to 400 hours), and the availability of a large growth volume for the solvent bath and the necessary quantity of carbon source. It is expected that increasing the maximum achievable cubic press load up to 80–90 MN and increasing the high pressure cubic cells to span 90–100 mm will make it possible to grow diamonds weighing as much as 500 ct (100 g). In addition to attracting interest from the gem industry, future applications include manufacturing single crystal diamond plates with pre-determined characteristics (e.g., high crystalline purity, charge carrier mobility, thermal conductivity or electrical conductivity), with uses as varied as substrates for CVD growth or diamond x-ray optics components (Stoupin et al. 2016; Shvyd'ko et al. 2017).

CHEMICAL VAPOR DEPOSITION OF DIAMOND

Principles of growth

This section discusses the growth of diamond by chemical vapor deposition (CVD) under conditions where diamond is not the thermodynamically stable form of carbon, as highlighted in Figure 1. The earliest reports of verifiable diamond growth under metastable conditions (low pressure) date to the 1950s to 1970s, initially in the United States, Russia, and then Japan (Angus 1994; Fedoseev 1994; Setaka 1994). A detailed summary of the history of chemical vapor deposition of diamond is provided by Angus (2014). The inclusion of hydrogen as a key reactant/solvent initiated the use of hot filaments and plasmas for creating atomic hydrogen and activating the reactants which demonstrated growth of mm-sized crystals. The mid 1980s then saw an explosion of interest in CVD diamond research forming the basis of our current understanding and diverse applications of diamond materials by groups primarily in Japan, US, and Europe (Angus 2014).

Crystalline diamond can be grown by chemical vapor deposition with a multitude of different gaseous reactant activation techniques: hot surfaces (hot filaments), plasmas (DC, RF, microwave, e.g., Fig. 3), and combustion flames. As will be presented later, there are many common chemical processes to these apparently dissimilar techniques. In the hot filament and plasma-based techniques, the reactant gases contain primarily hydrogen and a dilute amount of some hydrocarbon (generally less than 10%). The reactants are activated at pressures between ca. 1 mbar to several bar (typically between 20 and 500 mbar) to create many molecular, radical, and ionic species. Figure 18 presents a schematic of the diamond CVD process. In this schematic, the reactants are introduced into a pressure containment vessel (reactor) and the pressure is maintained with a throttle valve to the exhausting system (pump). The hot filaments (typically tungsten at 2000–2500 °C) or the plasma (gas temperature in the range of 2000–5000 °C) dissociate the reactants and initiate complex gaseous chemical reactions while the gas is transported by forced flow, convection, and/or diffusion toward the growing diamond crystals whose surface temperature is maintained at between 600 and 1200 °C. "Boundary" layers are formed just above the growth surfaces with strong temperature gradients, reactant gradients, and gas stagnation. Growth then proceeds on the surfaces of the diamond crystals. Generally, diamond seed crystals of sizes between several nm to several cm are provided to start the process, commonly referred to as "substrates." However, nucleation techniques for forming the diamond seeds from stable carbon/carbide clusters on the surface are also used (Liu and Dandy 1995).

CVD diamond materials can be polycrystalline agglomerates with a continuum of grain sizes from nm to cm, or single crystal blocks or plates. Various properties of these materials can also be tuned by controlling the grain size, defects, and impurities (Butler and Windischmann 1998; Butler and Sumant 2008).

The CVD growth of crystalline diamond is one of the most complex of any chemical vapor deposition or physical vapor deposition process (PVD) (Butler and Woodin 1993; Goodwin and Butler 1997; Butler et al. 2009a,b). Its study involves many scientific disciplines: chemical kinetics, plasma chemistry, fluid dynamics, thermal transport, surface chemistry, and possibly, diffusion processes in solids.

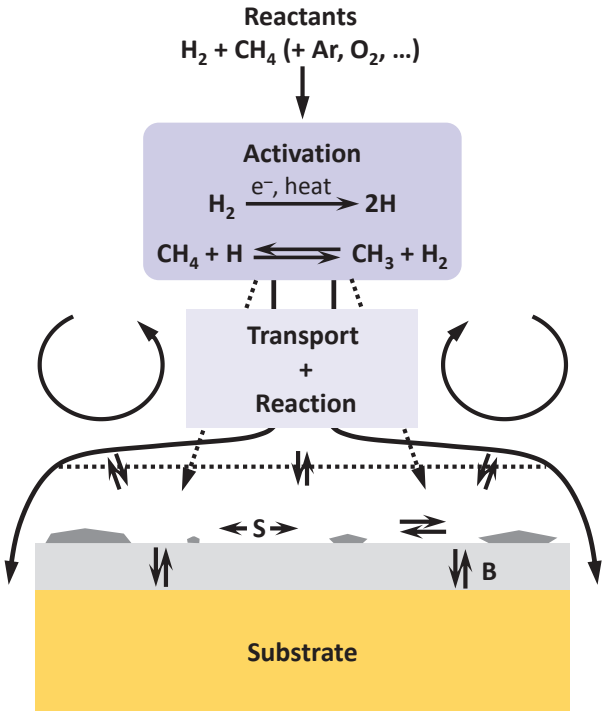

Figure 18. A schematic of the diamond CVD process. Various reactive and transport processes are shown in the gas-phase and surface (**S**). Diffusion through a boundary layer (**dashed line**), and into the crystal bulk (**B**) are also depicted. [Modified after Celii and Butler (1991), *Annual Review of Physical Chemistry*, Vol. 42, Fig. 2, p. 647.]

Surface vs. bulk temperatures

The temperature of a gas, surface, or solid is an extremely important parameter for controlling the kinetics of reactions and transport of species. While there are reports of very slow, poor-quality diamond growth by CVD at temperatures as low as ~300 °C, the optimal surface temperature is generally between 800 and 1200 °C for excellent crystallinity and reasonable growth rates. Surfaces at over 800 °C are sufficiently hot to break even the strongest of single chemical bonds that an adsorbate might make with the surface. Reactants can only bond to the surface with very strong bonds, and even those that can bond are likely to desorb back to the gas after a short time. Hence, the incorporation of species into the growing bulk will likely involve the formation of multiple chemical bonds to the surface, while desorption of reactants to the gas will dominate over the mobility or diffusion of reactants across the surface.

Bulk processes like structural rearrangements or diffusion of atoms are very unlikely at the bulk temperatures of diamond CVD (less than 1200 °C), because of the extremely high "Debye" temperature of bulk diamond, ~1800 °C. The Debye temperature is a parameter measuring the transition of the heat capacity of a solid from quantum phonon statistics to classical thermodynamics, and as such is a measure of the thermal motion of atoms in the bulk. Heating diamond to approximately its Debye temperature initiates the transition to the more thermodynamically stable form of carbon—graphite—catalyzed at defects and surfaces (Evans 1979). A consequence of this is that there is very little thermal motion in the diamond lattice during growth, with diffusion possible only for lattice vacancies and interstitials, and with little repair of structural defects.

Nucleation vs. growth

The nucleation of diamond on non-diamond substrates can happen, but is a poorly understood process. Important factors include a source of carbon to form clusters of carbon on or within the surface, bonding of the carbon cluster to the substrate to prevent desorption at the surface temperatures, and etching/rearrangement reactions within the cluster to convert to local sp^3 diamond structure. See Pehrsson et al. (1993) and Liu and Dandy (1995) for more detailed discussions. For the most part, current researchers and growers of CVD diamond who grow on non-diamond substrates will prepare the substrate for growth by treating or seeding the surface with crystalline diamond particles (Clausing et al. 1989; Inspektor et al. 1989; Philip et al. 2003; Buijnsters et al. 2005). Depending on the application, these particles can range in size from nm to mm. Then subsequent growth is homoepitaxial growth of diamond on diamond.

Diagnostics of growth environment

The important insight enabling the growth of diamond at low pressure was the recognition of the role of hydrogen in stabilizing the surfaces of diamond and in etching non-diamond carbon. This is discussed at length in the review of the early history by Angus (2014). One major advantage of CVD diamond growth over HPHT techniques, or diamond growth in the mantle of the earth, is that scientists can employ a range of in situ analytical techniques to study the process. The first in situ examination of the gas phase composition during diamond CVD with infrared absorption spectroscopy detected the conversion of the reactants (methane 0.5% in hydrogen) to C_2H_2 and CH_3 in a hot filament activated deposition chamber (Celii et al. 1988). Direct detection of ground state atomic H in the gas phase of hot filament and plasma based reactors followed (Celii and Butler 1989; Celii et al. 1990a,b). Optical emission from excited states of atomic hydrogen was also observed in plasma activated diamond CVD (Stalder and Sharpless 1990; Chu et al. 1991; Muranaka et al. 1991). Mass spectroscopy sampled in situ from a hot filament reactor detected CH_4, C_2H_2, and C_2H_4 inferred the presence of methyl (CH_3) radical and H atoms in the complex gaseous chemical processes (Harris et al. 1988; Harris and Weiner 1990; Hsu 1991). Sampling of the exhaust gases from a microwave plasma detected CH_4, C_2H_2, and C_2H_4; and CO and H_2O when O_2 was added to the reactant gases (Johnson et al. 1990; Hsu et al. 1994).

Which chemical species are important for the CVD growth of diamond? The conclusion reached by many experiments is atomic H and the CH_3 radical. Kinetic and isotopic experiments support that the bulk of the carbon incorporated into the diamond crystal is from CH_3. For an extensive review, see Goodwin and Butler (1997). The typical growth environment involves a gas pressure above 30 mbar and a relatively long gas residence time in the reactor, allowing for the complex gaseous kinetics to approach a stable equilibrium. An approximate model of the observed gas phase composition was presented and is shown in Figure 19 (Butler et al. 1989). In this model, the detailed composition of the gas phase can be approximated by the thermodynamic composition of the input reactants placed in a container at an equilibrium temperature of the plasma or hot filament source. An important consequence of the model is the implication that diamond growth is not sensitive to the specific nature of the hydrocarbon reactant, but just to the ratio of carbon to hydrogen in the reactants. While this "zero order" approximation is useful in a general sense, the gaseous chemistry is far more complex than this due to the spatial and temperature gradients in the growth environment.

The interconversion of the dilute hydrocarbon species in atomic and molecular hydrogen is shown schematically in Figure 20. In the hotter portions of the gas (in the plasma), the chemistry is driven toward the lower right of the figure, by the conversion of CH_n to C_2H_n, while in the colder portions of the reactor, near the reactor walls and the growing surface, the chemistry is driven to the upper left by atomic hydrogen reactions (C_2H_n to CH_n) (Ma et al. 2009).

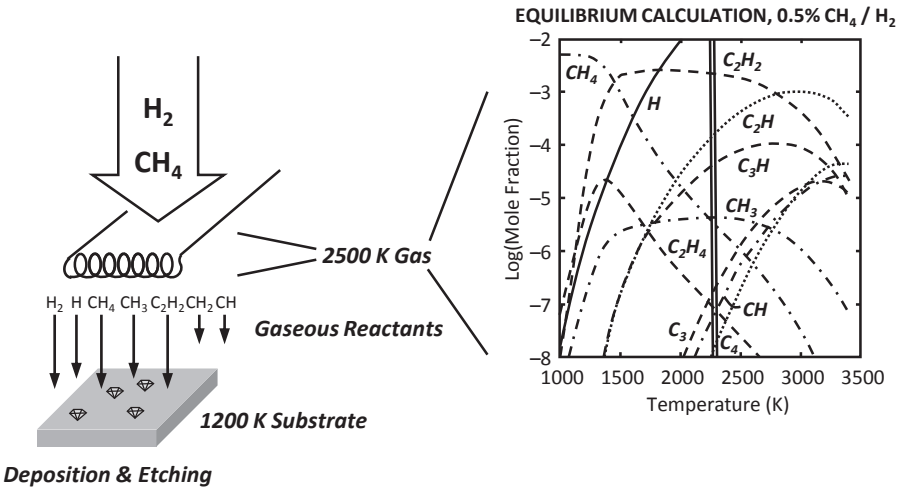

Figure 19. A simple model of the gaseous processes occurring in filament-assisted diamond CVD. On the right are the results of a thermodynamic equilibrium calculation of the mole fraction of various species present versus the equilibrium temperature. The schematic on the left summarizes the gaseous transport of species. [Modified after Butler et al. (1989), *High Temperature Science*, Vol. 27, Fig. 8, p. 193.]

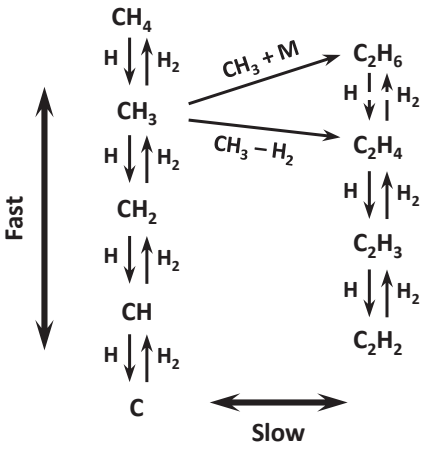

Figure 20. The principal gas phase reactions involve the rapid hydrogen transfer reactions amongst the C_1 and C_2 species, and to a lesser degree, the bimolecular hydrocarbon reactions forming C_2 and higher species. [Modified after Butler and Woodin (1993), *Philosophical Transactions: Physical Sciences and Engineering*, Vol. 342, Fig. 2, p. 211.]

The composition of the gas near the hot filaments or in the plasma (>2400 °C) is very different than the flux of gaseous species colliding with the growing diamond surface. This is because the stagnant gas at or near the growing surface has (nearly) the same temperature as the growing surface (800–1200 °C). Thermal and compositional boundary layers form with sharp gradients between the bulk gas and the surface.

Since diamond growth occurs on the surface of the diamond substrates, the critical chemical species causing growth must collide with the surface at a rate at least as fast as carbon is incorporated in diamond. Extensive experimental measurement and kinetic modeling have determined that the only species meeting this criterion in the CVD environment are H_2, H, CH_4, CH_3, and C_2H_2, and that the dominant carbon contributor is the CH_3 radical. Goodwin and Butler (1997) provide a detailed review and discussion.

The surface of the growing diamond is terminated by hydrogen, forming C-H bonds, very strong single bonds with strengths ~ 96 to 102 kcal/mole (Calvert and Pitts 1966). Temperatures above 850 °C are sufficient to slowly break these strong bonds and desorb hydrogen (Koleske et al. 1994, 1995). In ultra-high vacuum, "clean" non-hydrogenated surfaces can be produced by annealing to over 850 °C (Pate 1986; Thomas et al. 1992), but in a gas containing atomic and molecular hydrogen and hydrocarbon species, the surfaces are partially hydrogenated by the balance of desorption and reactive adsorption. The limitations on the surface temperatures for CVD diamond growth are set by the hydrogen termination of the surface: for complete hydrogen coverage there are no reactive sites, and when there are no terminating hydrogen atoms, the surface reverts to sp^2 bonding and converts to graphite.

Given the shortness of the C-C bond in diamond, the surfaces have an extremely high areal density of surface carbon atoms (1 to 3×10^{15} cm^{-2}). Termination of all the carbon surface bonds with any non-carbon atom except H(D) is impossible. Even H is too large to terminate all the bonds on the (100) surface. This surface undergoes a (2 × 1) surface reconstruction to form carbon dimer chains on the surface (Hamza et al. 1990). Growth surfaces are not necessarily flat low index planes, but contain many steps and local geometric environments. Figure 21 displays ball and stick models of steps on the (111), (110), and (100) 2 × 1 surfaces.

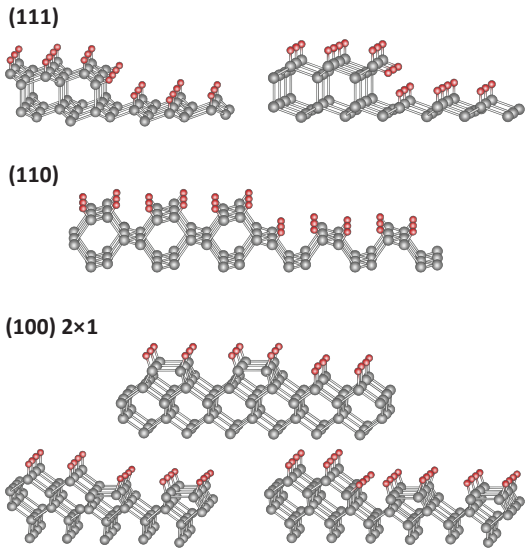

Figure 21. Idealized structures for steps on the indicated low index hydrogen-terminated diamond surfaces. The **large gray balls** represent carbon atoms and the **small red balls** represent the surface bound hydrogen atoms. [Modified after Butler et al. (2009b), *Journal of Physics: Condensed Matter*, Vol. 21, Fig. 4, p. 364201-9.]

A "standard mode" of diamond CVD has evolved over the years with many contributors and is summarized in (Butler and Woodin 1993; Goodwin and Butler 1997; Butler et al. 2009a,b). The key elements of the model are:

The diamond lattice is stabilized and prevented from rearrangement to graphitic carbon by termination with hydrogen atoms (or a similar chemical species), while the temperature is too low for spontaneous bulk rearrangement to occur (i.e., below the Debye temperature of diamond)

The gaseous activation process dissociates molecular hydrogen into atomic hydrogen which reacts with the source hydrocarbon to create a complex mixture of hydrocarbon species including reactive carbon-containing radicals. The H atoms created by the gaseous activation

process also abstract hydrogen from the surface C-H bonds, thereby creating surface radical sites. These radical sites will occasionally react with gas phase carbon-containing radicals such as methyl radicals (as discussed above), resulting in a strongly bound adsorbed carbon species. Much more frequently, however, the radical sites are simply refilled by recombining with gaseous H atoms. This constant turnover of the surface-terminating species (hydrogen) drives the surface chemistry to dehydrogenate the adsorbed carbon species and to incorporate carbon into the lattice by creating multiple bonds to the lattice

The atomic hydrogen, and, to a lesser extent, other gaseous species, react with any *sp* or sp^2 carbon sites on the surface, converting them into sp^3 bonded carbon

Single crystal diamond growth

CVD epitaxial growth of single crystal begins with a single crystal diamond substrate, usually in the form of a thin plate (ca. 200 to 500 µm thick). The surfaces of the plate may be polished, laser cut, or cleaved. The most popular orientation of the upper surface is near or on-axis (100). Other orientations like (110), (111), and (113) are less frequently used. The quality and orientation of the seed crystal may be important for some applications. For example, dislocations in the seed generally propagate in the epitaxial layer, and impurities or dopants tend to incorporate preferentially on certain crystal faces and local structures (Martineau et al. 2004; Gaukroger et al. 2008; Friel et al. 2009; Tallaire et al. 2017a). An example of CVD diamond growth on a yellow Type Ib seed is shown in Figure 22, where the epitaxial growth was performed in two sequential growth runs. When viewed from the growth side to the seed, the color is dominated by that of the seed. Dark polycrystalline diamond rims readily grow on the sample edges, potentially encroaching on the growing diamond and shrinking the top surface, unless precautions are taken to minimize their formation (Mokuno et al. 2005; Nad et al. 2015, 2016). Such blocks are often cored with a laser machining system to remove the outer rim and the initial seed. Figure 23 shows the result after coring. Figures 22 and 23 display a common result, however with the proper recipe and conditions, it is possible to expand the sides of the seed crystal without the polycrystalline rim (e.g., Tallaire et al. 2017b).

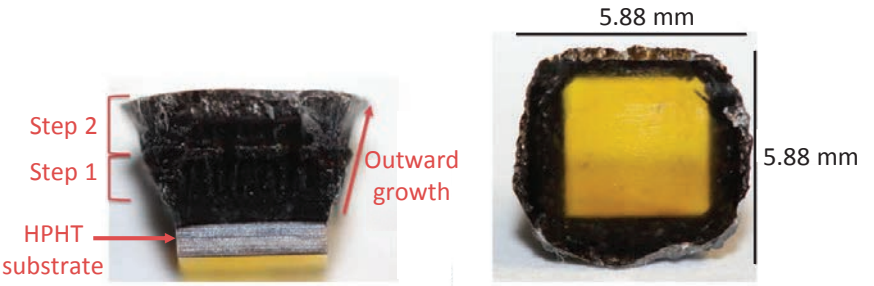

Figure 22. As-grown CVD diamonds are typically thick films with dark polycrystalline diamond rims along the edges. During sample processing, the substrate is removed and the central gem-quality portion is laser cut into a cylinder or cuboid shape which can then be faceted into a gemstone. Treatments may be used to change CVD diamond color. In this example, a colorless CVD layer was grown in a two-step process to maximize thickness. The yellow color observed is from the underlying Type Ib HPHT substrate. [Modified after Nad et al. (2015) *Diamond Related Materials*, Vol 60, Fig. 16, p. 32.]

Since sizable natural and HPHT-grown crystals are rare or expensive, larger areas of quasi single crystal material are generated either by tiling multiple plates of well oriented single crystals and growing them together (Yamada et al. 2011, 2013, 2014; Tallaire et al. 2013), or by nucleating highly oriented diamonds seeds on uniquely prepared non-diamond substrates and growing them to a thickness where they appear as single crystal material with a high dislocation density (Gallheber et al. 2018).

Figure 23. The polycrystalline rim of a CVD-grown single crystal after laser coring. [Photograph by JEB.]

Twinning

Crystal twinning occurs in all forms of crystalline diamond (Kohn 1958; Varma 1970; Walmsley and Lang 1983; Angus et al. 1992). It is particularly common to CVD-grown material and material grown at very high growth rates, e.g., HPHT diamonds. It may occur at the pressures and temperatures of natural diamond or HPHT diamond synthesis by atomic rearrangement of the lattice (annealing) to relieve stress due to plastic deformation of the crystal after growth, or as part of the growth of the crystal (Lang 1979; Palyanov et al. 2015a). During growth by CVD where there is little or no motion of the atoms in the lattice, only one model has been proposed for how a twin is formed during growth (Butler and Oleynik 2008). In this model a twin can only form on a local part of the diamond surface with an exposed {111} plane by the building of a three-atom bridge between adjacent surface carbon atoms to form a four-atom island nucleating the next layer of growth. Due to rapid isomerization of the three-atom bridge at the growth temperature, the result is a nearly 50:50 chance that the four-atom island will be twinned relative to the underlying crystal structure.

Doping

In the CVD growth of diamond, intentional doping is accomplished by adding volatile compounds of the intended dopant to the gaseous reactants, for example N_2, B_2H_6, SiH_4 or PH_3, or by placing a solid compound containing the intended dopant in the reactor and exposing it to the plasma, such as solid Si or B. Both "p-type" and "n-type" electrical conduction is observed with B and P doping, respectively (Lightowlers and Collins 1976; Koizumi et al. 1998). A dopant of particular note is nitrogen, which is known to have a catalytic effect on the growth rate (Chayahara et al. 2004; Tallaire et al. 2006; Achard et al. 2007; Butler and Oleynik 2008). Nitrogen contamination can occur from gases, leaks or desorption from reactor components, but careful growth can produce high purity CVD diamonds with nitrogen concentrations below 1 ppb (parts per billion carbon atoms, 10^{14} cm^{-3}), which are attractive for electronic applications (Isberg et al. 2002; Tallaire et al. 2006; Edmonds et al. 2012). Intentional doping using N_2 can result in the incorporation of up to tens of ppm (parts per million) of nitrogen (Edmonds et al. 2012). For the growth of optically transparent material or larger samples, nitrogen-doping can be beneficial, with even low concentrations of nitrogen in the gas phase (~10 ppm) resulting in nearly a tripling of the growth rate (Tallaire et al. 2006). However, a balance must be struck as high concentrations of nitrogen introduce brown color in the material, attributed to the formation of vacancy clusters and/or nitrogen-related defects (Barnes et al. 2006; Jones et al. 2007; Mäki et al. 2007; Khan et al. 2013; Zaitsev et al. 2020). The presence of nitrogen in the growth gases also has a pronounced effect on the growth mode, transitioning from layer-by-layer growth

to step-flow with macroscopic step-bunching (Yamada et al. 2016). Unlike natural diamonds, nitrogen in CVD diamonds is found primarily as isolated substitutional nitrogen (N_S), nitrogen-vacancy (NV), or nitrogen-vacancy-hydrogen (NVH) forms (Edmonds et al. 2012). Since CVD diamond is grown at low temperatures (well below its Debye temperature), is produced in relatively short time scales (~ days to months, not years), and has a comparatively low nitrogen concentration, there is little opportunity to form the more complicated nitrogen-related defects common to natural diamonds, such as the A- (nitrogen pairs), B- (N_4V^0) aggregates, or N3 (N_3V^0) centers, unless subjected to post-growth annealing at high temperatures.

Technology of growth

A source of atomic hydrogen is a critical component in the CVD growth of diamond materials. In the commercial production of CVD diamond, two general sources of atomic hydrogen are employed: plasmas and hot wires or surfaces (at over 1800 °C). Each approach has technical advantages and disadvantages, as well as economic and intellectual property concerns. Almost all growth of single crystal and high purity material is done with plasma assisted CVD, generally driven by microwave sources (primarily at 2.45 GHz or 915 MHz), although some manufacturers use lower frequencies and even DC driven plasmas. Figure 3 shows a schematic of a microwave CVD reactor, while Figure 24 displays a picture of a single seed diamond growth in a typical commercial reactor operating at 2.45 GHz. Figure 25 displays a multiple seed diamond growth run in a different CVD reactor. Hot wire (tungsten, tantalum, etc.) methods of dissociating hydrogen are used mostly for growth covering larger areas (up to 1 m^2), thin film, and polycrystalline coatings. CVD diamond growth has also been demonstrated in combustion flames and molecular beams (Hansen et al. 1988; Lee et al. 1994), but neither of these is currently used in commercial production.

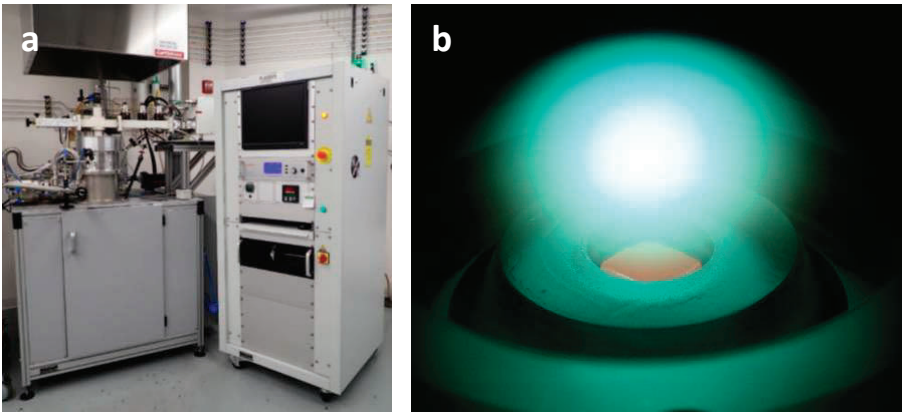

Figure 24. (**a**) A commercially available plasma tool (PLASSYS) for the growth of CVD diamond operating at 2.45 GHz. (**b**) CVD diamond synthesis showing the growing diamond in a pocket substrate holder beneath the plasma. [Photographs by Adrian Chan for GIA.]

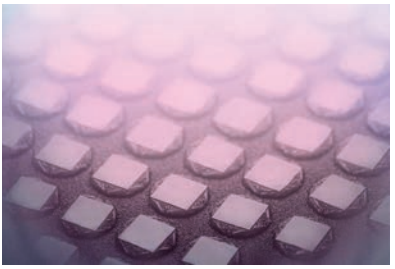

Figure 25. Multiple single crystal seeds growing in a CVD diamond reactor. [Used by permission of Element Six (UK), Ltd. and Lightbox Jewelry, Inc.]

Applications and commercial production of CVD diamond

Many companies are involved in the commercial production of CVD diamond products. Due to the competitive nature of the business, it is difficult to determine the exact size and nature of the production factories and few detailed images are available. Figure 26 displays two examples of parts of CVD diamond materials growth facilities.

Figure 26. (**a**) A CVD diamond growth facility based on commercially available tools; and (**b**) A CVD diamond growth facility based on proprietary designed tools. [Used by permission of (**a**) ABD Diamonds Pvt. Ltd. and (**b**) Diamond Foundry, Inc.]

There are a wide range of applications for diamond materials in technology due to its many extreme properties (thermal, mechanical, optical, etc.). Figure 27 displays images of many of the applications of CVD diamond materials. A unique advantage of CVD diamond is the ability to control and monitor the growth process, to "engineer" the material to the application. This can be done by controlling the purity, grain size, thermal diffusivity, optical transparency, toughness, where and what dopants are introduced, surface termination, isotopic purity, etc. The diverse array of applications of CVD diamond span the fields of mechanical, optical, electronic, medical, quantum, electrochemical, communications, and high-power electronics, to name a few. These have been reviewed in many places such as (Prelas et al. 1997; Butler and Windischmann 1998; Wort and Balmer 2008; Balmer et al. 2009; Auciello and Sumant 2010; Nemanich et al. 2014; Awschalom et al. 2018; Yang et al. 2019; Achard et al. 2020).

Figure 27. Composite image demonstrating innovative applications derived from CVD diamonds, including ultra-precision machining, drilling, thermal management, optics, wastewater management and quantum-enabled sensing. [Used by permission of Element Six (UK) Ltd.]

The largest widely publicized initial commercial application for blocks of single crystal diamond grown by CVD methods is for gems. Figure 28 displays a 9.04 ct round brilliant cut CVD diamond, while Figure 29 shows a unique all-diamond ring fabricated from a single block of CVD diamond. As of early 2022, a 16.41 ct (G color, VVS_2 clarity) princess-cut specimen is the largest reported gem CVD diamond (Wang et al. 2022). Major players in CVD diamond gem production can be found in the United States, United Kingdom, India, Singapore and China (Linde et al. 2021).

Figure 28. A ring containing a 9.04 ct round brilliant CVD gem diamond. [Used by permission of WD Lab Grown Diamonds.]

Figure 29. A unique single crystal CVD diamond ring created for a charity auction which raised $461,250 for the fight against AIDS. [Used by permission of Diamond Foundry, Inc.]

SEPARATION OF NATURAL AND LABORATORY-GROWN DIAMONDS

Background

As the quality and purity of laboratory-grown diamonds have improved over the years, visual inspection of polished diamonds—in particular if colorless or near-colorless—is rarely sufficient for their identification as to origin. Instead, conclusive identification is largely based on the presence, absence, relative concentrations and distributions of point defects in the diamond lattice, detected by advanced microscopic and spectroscopic means. The formation of these defects are a result of the growth environment and associated processes as well as any subsequent residence at elevated temperatures and/or treatment conditions, consequently providing an insight into the diamond in question's history. It is important to note that most point defects are not unique to either natural or laboratory-grown diamonds. Laboratory-grown diamonds may also be treated to further expand the types of possible defects. Thus care needs to be taken when combining several pieces of evidence to reach a conclusion on a diamond's natural or laboratory-grown origin.

Certain defects, termed color centers, absorb electromagnetic radiation in the visible range, influencing the color of the diamond material if present in sufficiently high concentrations. Both natural and laboratory-grown diamonds exist in the full rainbow spectrum of colors. Collins (1982, 1992, 1993a, 2001), Ashfold et al. (2020), and Green et al. (2022, this volume) review some of the main color-producing defects in diamonds. Defects in natural and laboratory-grown diamonds may be as-grown or produced through treatments such as HPHT or low pressure high temperature (LPHT) annealing, irradiation, or combinations thereof. In the gem trade natural diamonds are most commonly found in hues ranging from colorless to light yellow, and are typically characterized by letter color grades ranging from D-to-Z, respectively, based on the diamond color grading system invented by the GIA (King et al. 2008). Brown and gray diamonds that are more colorless than a K color reference master stone are also assigned letter grades. For color saturations equivalent to the grades K-to-Z, brown-hued diamonds are given a letter grade as well as a color word description (K–M = "Faint," N–R = "Very Light," and S–Z = "Light"), whereas gray diamonds are only given word descriptions. Diamonds with stronger yellow color saturation than the letter grade Z, or other color hues, are known as "fancy color" diamonds and are described using the fancy color grade terminology as explained by King et al. (1994). Certain gemological laboratories offer laboratory-grown diamond reports, characterizing the materials using conventional diamond grading boundaries and terminology.

In the following sections, the identification tools used by gemologist and scientists for diamond analysis will be summarized. Subsequently, the signature characteristics of both HPHT- and CVD-grown diamonds will be reviewed, highlighting the features that can be used for their identification.

Identification tools

The identification of natural and laboratory-grown diamonds relies on a range of different observations, with gemological laboratories developing confidential testing protocols to protect the gem and jewelry buying public from deceptive or unintentional misrepresentation of laboratory-grown diamonds as natural. The tools used for identification can be separated into observational and spectroscopic tools, with many of the former being the building blocks of standard gemological studies. Foremost amongst them is a microscope allowing visual inspection of samples under magnification (10–64× for most gemological applications) with reflected, bright field and dark field illumination capabilities (Renfro 2015). Coupled with crossed-polarized filter plates, birefringence patterns related to crystallographic strain in the diamond can be revealed, which may be indicative of certain growth or post-growth processes. These patterns are also sometimes referred to as anomalous double refraction patterns (Kane 1980). Howell (2012) presents a comprehensive review on strain birefringence in natural diamonds.

Defects in diamond can interact with incident light through a variety of processes which can allow their detection (Collins 1982, 1992, 1993a; Ashfold et al. 2020; Green et al. 2022, this volume). Zaitsev (2001) and the references therein catalog several hundred features associated with defects in diamond materials, with numerous defect structures identified. Table 1 provides a brief summary of some of the key features discussed in this chapter. Many defects absorb light at characteristic wavelengths in the ultraviolet (UV) to visible and infrared (IR) range, and can be detected using absorption spectroscopy. Once appropriately normalized, the integrated intensity of the absorption spectrum for a specific defect is proportional to its concentration, with defect-dependent detection limits that may be as low as a few parts per billion carbon atoms (Collins and Williams 1971; Davies 1981; Kiflawi et al. 1994; Boyd et al. 1994, 1995; Lawson et al. 1998; Howell et al. 2019). Typically, fast Fourier transform infrared (FTIR) absorption spectra are collected at room temperature. The sensitivity of UV-visible absorption is greatly improved by cooling the samples to liquid nitrogen temperature (77 K).

Defect absorptions from nitrogen- and boron-related defects in the IR range are the basis for a diamond classification system (Robertson et al. 1934), where Type I diamonds contain detectable nitrogen, in either the aggregated (Type Ia) or isolated (Type Ib) forms. The aggregated nitrogen in Type Ia diamonds may be in the A- or B-center forms (nearest neighbor nitrogen pairs or N_4V^0, respectively) with the type refined into Type IaA, IaB or IaAB (Davies 1976, 1981; Jones et al. 1992; Boyd et al. 1994, 1995). Isolated substitutional nitrogen is also referred to as the C-center (Type Ib) (Dyer et al. 1965). If nitrogen is below the detection limit, it is a Type II diamond, further divided into those that do (Type IIb) or do not (Type IIa) contain detectable boron. The IR features associated with these defects are listed in Table 1. For more on the diamond classification system and its use in diamond gemology, refer to Collins (1993a), Breeding and Shigley (2009), Ashfold et al. (2020), and Green et al. (2022, this volume).

The absorption of light may also stimulate luminescence, the emission of light from defects in the material (Collins 1993a; Eaton-Magaña and Breeding 2016; Green et al. 2022, this volume). Conventionally, diamond luminescence is evaluated by observing the sample using a shortwave (254 nm) and longwave (365 nm) UV combination gem lamp, preferably in a dark room (Luo and Breeding 2013). The luminescence color (wavelength and energy) is related to the defect species that are effectively stimulated, and their distribution through the sample may also be observed. Luminescence detected while the sample is under illumination is known as fluorescence or photoluminescence, whereas phosphorescence is the emission of light after the excitation source is turned off. The fluorescence and phosphorescence response of diamonds depend upon the defects present in the material, and as such vary for the different synthesis chemistries, potential treatments, diamond types, and colors. Further detail can be recognized

using an instrument such as the DiamondView, where deep-UV illumination with energies greater than the diamond bandgap (i.e., wavelengths <225 nm, energies >5.5 eV) is coupled with video imaging under magnification. Nearly all diamonds will fluoresce under these conditions, and the resulting patterns will be sharp and surface-specific (Welbourn et al. 1996). These patterns are primarily associated with changes in the defect concentrations as the diamonds grow, whether naturally or in a laboratory, and as such are excellent features for their distinction. Importantly, although treatments may modify the fluorescent defect concentrations, and thus potentially the colors and distributions observed, the fundamental growth pattern will remain. Several viewing angles should be used when attempting to observe fluorescence patterns.

Additionally, gemological laboratories often use photoluminescence (PL) spectroscopy at 77 K to confirm the presence of specific luminescent defects in diamond, allowing sensitivities which may be of the order of parts per trillion. This is particularly useful for defect analysis of colorless diamonds, which have low concentrations of color centers. Unlike absorption spectroscopy, the relationship between the intensity of luminescent features and their concentration is complex, with the presence of certain defects (e.g., A-centers) potentially quenching the luminescence of others (e.g., Vasil'ev et al. 2004). A color center's excitation efficiency also depends upon the illuminating laser wavelength, so spectra are typically collected using a suite of different lasers with wavelengths such as 325, 488, 514, 532, 633, 830 nm. More rarely, cathodoluminescence imaging and spectroscopy, where incident electrons are used to excite luminescence, can also be used for defect analysis.

Identification of HPHT diamonds

External morphology. Gem quality HPHT diamonds are grown using the temperature gradient method, where the morphology is sensitive to growth conditions such as the temperature, pressure, and metal solvent/catalyst, dictating which crystallographic faces will dominate (Strong and Chrenko 1971; Kanda et al. 1980, 1989; Burns et al. 1999). HPHT diamond growth originates at a diamond seed crystal, simultaneously growing upwards and outwards along several crystallographic directions, dominated by growth along the cube ⟨100⟩ and octahedral ⟨111⟩ directions. Consequently HPHT diamonds typically exhibit well-developed octahedral {111} and cube {100} growth faces, along with minor dodecahedral {110} and trapezohedral {113} faces, as shown in Figures 6 (Strong and Chrenko 1971; Kanda et al. 1980, 1989; Sunagawa 1984, 1995; Shigley et al. 1986, 1987, 1992, 1993a,b; Burns et al. 1999). {115} and {117} faces have also been reported (Strong and Chrenko 1971; Rooney 1992; Shigley et al. 1992). The distinctive cuboctahedral morphology can be used to distinguish HPHT crystals from natural diamonds, which generally have octahedral, resorbed, or irregular shapes (Sunagawa 1995; Harris et al. 2022, this volume). However, occasionally HPHT diamonds can also be irregularly shaped.

Dendritic, vein-like, spiral, and lamellar or striated surface patterns can be observed on the external faces (Tolansky and Sunagawa 1959; Kanda et al. 1980; Koivula and Fryer 1984; Shigley et al. 1986, 1987, 1992, 1997; Sunagawa 1995). In particular, the dendritic surface patterns are considered to be indicative of HPHT diamonds. Unlike many natural rough diamonds these crystals do not show significant mechanical abrasion or chemical etching. Though rarely seen, triangular depressions (commonly known as "trigons") or triangular pyramids may be present on octahedral {111} faces and are thus not exclusive to natural diamonds (Kanda et al. 1980; Koivula and Fryer 1984; Shigley et al. 1987, 1993a, 1997; Rooney 1992). The surface patterns on HPHT diamonds have been attributed to phase transformations and the microstructure of the metal solvent/catalyst during the final quenching stages of synthesis (Kanda et al. 1980; Burns et al. 1999). The bottom growth surface of the crystal may bear the imprint of the seed.

Table 1. Summary of key defects observed in natural and laboratory-grown diamonds. Listed references pertain to descriptions of spectral features and associated defect structures. See main text for details about their observation in laboratory-grown diamonds. Collins (1982, 1992, 1993a), Zaitsev (2001), Ashfold et al. (2020) and Green et al. (2022, this volume) present reviews on defects in diamonds.

Feature	Spectroscopic technique	Details	References
λ^{-3} ramp	UV-visible-NIR absorption	Absorption ramp rising from ~1200 nm to 225 nm with a profile ~λ^{-3} seen in as-grown CVD diamonds. Structure still under debate. Correlates with the 360 nm band. Can be removed by high temperature annealing.	Barnes et al. 2006; Mäki et al. 2007; Jones 2009; Khan et al. 2013
270 nm 4.6 eV	UV-visible-NIR absorption	Neutral substitutional nitrogen, N_S^0. Also known as the C-center. Broad peak at 270 nm overlapping a rise in absorption from ~560 nm to the intrinsic diamond absorption edge. Observed in both natural and laboratory-grown diamonds.	Dyer et al. 1965; Chrenko et al. 1971
360 nm 3.49 eV	UV-visible-NIR absorption	Broad band seen in as-grown CVD diamonds. Can be removed by high temperature annealing. Correlates with the λ^{-3} ramp.	Martineau et al. 2004; Khan et al. 2009, 2010, 2013
389 nm 3.188 eV	PL	Possibly nitrogen-related. Seen in as-grown CVD diamonds, but can be removed by high temperature annealing. Rarely observed in HPHT and irradiated natural diamonds.	Collins and Woods 1987; Collins and Lawson 1989; Robins et al. 1989; Zaitsev 2000; Martineau et al. 2004
390 nm 3.18 eV	UV-visible-NIR absorption	Broad band associated with pink color in natural diamonds. Seen in conjunction with 550 nm band. Defect responsible is unidentified, but linked to plastic deformation.	Collins 1982; King et al. 2002; Fisher et al. 2009; Byrne et al. 2012, 2014a,b; Howell et al. 2015; Eaton-Magaña et al. 2018a
393.3 nm 3.15 eV	UV-visible-NIR absorption	Negatively charged vacancy defect, V^-, also known as ND1. Observed in some natural diamonds. Can be produced in laboratory-grown diamonds through treatment.	Dyer and Du Preez 1965; Davies 1977; Twitchen et al. 1999
415 nm 2.985 eV	UV-visible-NIR absorption, PL	N_3V^0 defect, known as N3. In absorption it is also referred to as the "Cape series." Common in natural diamonds. Can be produced in HPHT diamonds synthesized or annealed at high temperatures, and in CVD diamonds by high temperature annealing.	Davies et al. 1978; Collins 1982

Feature	Spectroscopic technique	Details	References
451–459 nm 2.70–2.75 eV	PL	Series of unidentified peaks introduced by high temperature annealing in CVD diamonds.	Martineau et al. 2004; Wang et al. 2012
468 nm 2.65 eV	PL	Also reported at 467 nm. Sometimes referred to as TR12'. Possibly related to nitrogen, interstitials, or vacancy-clusters. Observed in as-grown CVD diamonds, but can be removed by high temperature annealing.	Iakoubovskii and Adriaenssens 2000a,b; Iakoubovskii et al. 2000; Rzepka et al. 2001; Iakoubovskii and Stesmans 2002; Zaitsev et al. 2021
478 nm 2.596 eV	UV-visible-NIR absorption	A transition at the N3 (N_3V^0) defect, known as the N2 band. Part of the "Cape series" of peaks.	Davies et al. 1978; Collins 1982
484 nm 2.56 eV	UV-visible-NIR absorption, PL	Complex multiplet with four thermalized components (483.67/483.97/484.28/484.56 nm), each with a fine doublet structure. Nickel-related defect, possibly including a negatively charged substitutional ion. Seen in nickel-containing HPHT diamonds. Rare in natural diamonds.	Collins and Spear 1983; Collins et al. 1990; Lawson and Kanda 1993a,b; Pereira et al. 1994, 1995; Nazaré et al. 1995; Collins 2000
489.2 nm 2.534 eV	UV-visible-NIR absorption, PL	Known as the S2 or NE2 center. Has additional peaks at 477.8, 472.6, and 470.6 nm. Nickel ion in a divacancy position surrounded by three nitrogen atoms $(C_2–N–Ni–N_2–C)^0$ with a triclinic symmetry. Can be observed in HPHT and natural diamonds.	Nadolinny and Yelisseyev 1993; Yelisseyev and Nadolinny 1995; Yelisseyev et al. 1996, 2002; Nadolinny et al. 1997, 1998, 1999; Kanda and Watanabe 1999; Yelisseyev and Kanda 2007
494 nm 2.51 eV	UV-visible-NIR absorption	Possibly the negatively charged substitutional nickel defect, Ni_S^-. Seen in some nickel- and nitrogen-containing HPHT diamonds. Reported in some natural diamonds.	Collins and Spear 1982; Collins et al. 1990; Lawson and Kanda 1993a,b; Nazaré et al. 2001; Yelisseyev and Kanda 2007
495.9 nm 2.498 eV	UV-visible-NIR absorption, PL	N_4V^0 defect, known as H4. Seen in natural diamonds. Can be introduced by treatments in laboratory-grown diamonds.	Clark et al. 1956; de Sa and Davies 1977; Jones et al. 1994; van Wyk and Woods 1995

Feature	Spectroscopic technique	Details	References
496.7 nm 2.495 eV	UV-visible-NIR absorption, PL	Known as the S3 or NE1 defect. Nickel ion in a divacancy position surrounded by two nitrogen atoms $(C_2–N–Ni–N_2–C)^-$. Can be observed in HPHT-grown and natural diamonds.	Nadolinny and Yelisseyev 1993; Yelisseyev et al. 1996, 2006; Nadolinny et al. 1997, 1998, 1999; Yelisseyev and Kanda 2007
503.2 nm 2.463 eV	UV-visible-NIR absorption, PL	N_2V^0 defect, known as H3. Common in natural diamonds. Occasionally observed in as-grown CVD diamonds and Type Ib HPHT diamonds. Can be produced by treatment in CVD and HPHT diamonds.	Clark et al. 1956; Davies 1976; Davies et al. 1976, 1992; Mita et al. 1990; Jones et al. 1994; van Wyk and Woods 1995
503.5 nm 2.462 eV	UV-visible-NIR absorption, PL	Known as the 3H defect. Possibly the ⟨100⟩ split self-interstitial (also called the di-interstitial) in diamond. Rarely observed in natural diamonds. Can be introduced in natural and laboratory-grown diamonds by treatments.	Walker 1977; Steeds et al. 1999a,b; Iakoubovskii et al. 2001, 2003
520 nm 2.39 eV	UV-visible-NIR absorption	Broad band, sometime referred to as the 515 nm band. Possibly related to NVH^0. Seen in CVD diamonds, but be removed by high temperature annealing.	Martineau et al. 2004; Khan et al. 2009, 2010, 2013
520–580 nm 2.14–2.38 eV	PL	Unidentified series of peaks introduced by high temperature annealing in CVD diamonds.	Wang et al. 2012
523.3 nm 2.326 eV	UV-visible-NIR absorption, PL	Known as the NE3 defect. Nickel ion in a di-vacancy position surrounded by three nitrogen atoms $(C_2–N–Ni–N_2–C)^0$ with a monoclinic symmetry. Observed in natural and HPHT diamonds.	Nadolinny and Yelisseyev 1993; Yelisseyev et al. 1996; Nadolinny et al. 1997, 1998, 1999; Yelisseyev and Kanda 2007
533 nm 2.326 eV	PL	Also reported at 534 nm. Stress can split line into a doublet. Possibly a nitrogen-vacancy type complex. Observed in CVD diamonds, but can be removed by high temperature annealing.	Ruan et al. 1991; Burton et al. 1995; Charles et al. 2004; Martineau et al. 2004
550 nm 2.25 eV	UV-visible-NIR absorption	Broad band associated with pink color in natural diamonds. Often seen in conjunction with 390 nm band. Unidentified defect linked to plastic deformation.	Collins 1982; King et al. 2002; Fisher et al. 2009; Gaillou et al. 2010; Byrne et al. 2012, 2014a,b; Eaton-Magaña et al. 2018a, 2020

Feature	Spectroscopic technique	Details	References
575 nm 2.156 eV	UV-visible-NIR absorption, PL	The neutral nitrogen-vacancy defect, NV^0. Observed in natural and laboratory-grown diamonds.	Davies 1979; Collins and Lawson 1989; Mita 1996, Doherty et al. 2013
594.3 nm 2.086 eV	UV-visible-NIR absorption	Sometimes referred to as the 594 or 595 nm defect. Unidentified defect, possibly nitrogen-related. Can be introduced by treatment in natural and laboratory-grown diamonds.	Collins 1978, 1982; Davies and Nazaré 1980
596 nm 2.08 eV	UV-visible-NIR absorption	Unidentified defect seen in CVD diamonds. Not the same defect as that responsible for the 596/597 nm doublet in PL. Can be removed by high temperature annealing.	Wang et al. 2003; Martineau et al. 2004
596/597 nm 2.077/2.080 eV	PL	Unidentified defect seen in CVD diamonds. Not the same defect as that observed at 596 nm in absorption. Can be removed by high temperature annealing.	Wang et al. 2003; Martineau et al. 2004
637 nm 1.945 eV	UV-visible-NIR absorption, PL	Negatively charged nitrogen-vacancy defect, NV^-. Can be observed in natural and laboratory-grown diamonds.	Davies and Hamer 1976; Loubser and van Wky 1977; Mita 1996; Doherty et al. 2013
658 nm 1.883 eV	UV-visible-NIR absorption, PL	System includes peaks at 658.4 (dominant), 650.8 and 648.1 nm, as well as a vibronic band at ~638 nm in absorption (~682 nm in PL). Sometimes reported at 659 nm. Detected in nickel- and nitrogen-containing HPHT diamonds and thought to involve both elements. Has been observed in natural diamonds.	Collins and Spear 1982; Collins et al. 1990; Lawson and Kanda 1993a,b; Nazaré and Rino 1993; Nazaré et al. 1996; Yelisseyev and Kanda 2007
694 nm 1.787 eV	PL	Doublet (~692.9/691.5 nm) that has been attributed to nickel-, iron-, nitrogen- and hydrogen-related defects. Can be observed in natural and HPHT diamonds.	Nadolinny et al. 1999; Iakoubovskii and Adriaenssens 2002; Yelisseyev and Kanda 2007; Kupriyanov et al. 2016
736.7/736.9 nm 1.682 eV	UV-visible-NIR absorption, PL	The negatively charged silicon-vacancy defect, SiV^-. Common in CVD diamonds, and rare in natural and HPHT diamonds.	Clark and Dickerson 1991; Clark et al. 1995; Goss et al. 1996; Hepp et al. 2014; Rogers et al 2014; Breeze et al. 2020

Feature	Spectroscopic technique	Details	References
741 nm 2.673 eV	UV-visible-NIR absorption, PL	The neutral vacancy defect, V^0, also known as GR1. In absorption has associated transitions labeled GR2–GR8. Present in some natural diamonds. Can be introduced in laboratory-grown diamonds by treatment.	Coulson and Larkins 1971; Clark and Walker 1973; Davies 1977; Collins 1982; Lowther 1993; Twitchen et al. 1999
793.5 nm 1.563 eV	UV-visible-NIR absorption, PL	Known as the NE8 defect. A nickel atom surrounded by four nitrogen atoms. In absorption shows vibronic structure at ~700 nm. Can be observed in HPHT and natural diamonds.	Lawson and Kanda 1993b; Nadolinny et al. 1999; Yelisseyev and Kanda 2007
796.9 nm 1.56 eV	PL	Unidentified defect. Observed in some treated CVD diamonds.	Wang et al. 2010
806.4 nm 1.54 eV	PL	Unidentified defect. Observed in some treated CVD diamonds.	Wang et al. 2010
850 nm 1.46 eV	PL	Unidentified defect. Observed in some high temperature annealed CVD diamonds	Wang et al. 2012
875.5 nm 1.42 eV	PL	Unidentified defect. Observed in some high temperature annealed CVD diamonds	Wang et al. 2012
884 nm 1.40 eV	UV-visible-NIR absorption, PL	Doublet split at ~885.1/883.4 nm with an associated broad absorption band at ~685 nm. Nickel-related, possibly described by a trigonally distorted Ni^+ ion or a Ni–B complex. The dominant feature seen in nickel-containing HPHT diamonds. Occasionally observed in natural and CVD diamonds.	Collins and Spear 1983; Collins 1989; Davies et al. 1989; Collins et al. 1990; Isoya et al. 1990; Nazaré et al. 1991; Lawson and Kanda 1993a,b; Goss et al. 2004; Yelisseyev and Kanda 2007
946 nm 1.31 eV	UV-visible-NIR absorption, PL	The neutral silicon-vacancy defect, SiV^0. Only reported in CVD diamonds, but may be present in rare HPHT and naturals as the negative charge state of the defect has been observed.	D'Haenens-Johansson et al. 2010, 2011; Green et al. 2017, 2019; Rose et al. 2018; Breeze et al. 2020; Zhang et al. 2020
949 nm 1.31 eV	PL	Unidentified defect. Observed in some treated CVD diamonds.	Wang et al. 2010
986 nm 1.257 eV	UV-visible-NIR absorption, PL	N_2V^- defect, known as H2. Observed in some natural and HPHT diamonds. Can be produced in CVD diamonds by HPHT annealing.	Mita et al. 1990; Lawson et al. 1992

Feature	Spectroscopic technique	Details	References
7354 cm^{-1}	FTIR absorption	Hydrogen-related defect. Associated peaks reported at 6428, 6524, 6525, and 8753 cm^{-1}. Observed in CVD diamonds, but can be removed by high temperature annealing.	Fuchs et al. 1995a,b; Glover 2003; Charles et al. 2004; Martineau et al. 2004; Cruddace 2007
6856 cm^{-1}	FTIR absorption	Hydrogen-related defect. Observed in CVD diamonds, but can be removed by high temperature annealing.	Fuchs et al. 1995a,b; Martineau et al. 2004
5564 cm^{-1}	FTIR absorption	Hydrogen-related defect. Observed in CVD diamonds, but can be removed by high temperature annealing.	Fuchs et al. 1995a,b; Martineau et al. 2004
3323 cm^{-1}	FTIR absorption	Also reported at 3324 cm^{-1}. Attributed to a N–H–C defect. Observed in CVD diamonds, but can be removed by high temperature annealing.	Fuchs et al. 1995a,b; Charles et al. 2004; Martineau et al. 2004; Cruddace 2007; Liggins 2010; Goss et al. 2014
3123 cm^{-1}	FTIR absorption	The neutral nitrogen-vacancy-hydrogen defect, NVH^0. Common in as-grown CVD diamonds. Removed by high temperature annealing. Rare in natural diamonds, but a peak at this position has been reported in Type Ia natural diamonds with strong N_3VH^0 (3107 cm^{-1}) absorption.	Fuchs et al. 1995a,b; Cruddace 2007; Khan et al. 2013; Lai et al. 2020
3107 cm^{-1}	FTIR absorption	The N_3VH^0. Associated peak at 1405 cm^{-1}. Common in natural diamonds. Present in some HPHT diamonds that have been grown or annealed at high temperatures. Can be produced in CVD diamonds by high temperature annealing.	Woods and Collins 1983; Goss et al. 2014
~2803 cm^{-1}	FTIR absorption	The uncompensated substitutional boron defect, B_S^0. The most easily identifiable feature is a broad peak at 2803 cm^{-1} peak. Spectrum also includes bands at 2458 and 2930 cm^{-1}, as well as a rise in absorption from the 2930 cm^{-1} feature through the infrared into the red region of the visible spectrum. Can be observed in natural and laboratory-grown diamonds.	Collins and Williams 1971; Collins 1993b; Howell et al. 2019; Green et al. 2022, this volume

Feature	Spectroscopic technique	Details	References
1502 cm^{-1}	FTIR absorption	Possibly a stretching mode vibration of a C–N bond. Can be introduced by treatment in natural and laboratory-grown diamond.	Woods 1984; Collins et al. 1988
1450 cm^{-1}	FTIR absorption	The dinitrogen ⟨001⟩ split-interstitial defect, known as H1a. Can be introduced by treatment in natural and laboratory-grown diamonds	Clark et al. 1956; Collins 1980; Wood and Collins 1982; Woods 1984; Collins et al. 1988; Liggins et al. 2010
1344 cm^{-1}	FTIR absorption	The neutral substitutional nitrogen defect, N_S^0, also known as the C-center. Spectrum includes a broad band at 1130 cm^{-1}. Also produces absorption in the visible range (270 nm peak). Observed in natural and laboratory-grown diamonds, though more common in the latter.	Dyer et al. 1965; Chrenko et al. 1971; Collins 1980; Collins and Woods 1982; Kiflawi et al. 1994; Lawson et al. 1998
1332 cm^{-1}	FTIR absorption	The positively-charged substitutional nitrogen defect, N_S^+. Other defects can produce absorption at 1332 cm^{-1}, but the N_S^+ spectrum also shows bands at 950 and 1046 cm^{-1}. Can be seen in natural and laboratory-grown diamonds.	Lawson et al. 1998
~1282 cm^{-1}	FTIR absorption	Neutral nearest-neighbor substitutional nitrogen pairs, N_2^0, known as A-centers. Common in natural diamonds. Present in some as-grown yellow- or orange-hued HPHT diamonds that have been grown or annealed at high temperatures.	Davies 1976, 1981; Jones et al. 1992; Boyd et al. 1994
~1175 cm^{-1}	FTIR absorption	The N_4V^0 defect, known as the B-center. Common in natural diamonds. Present in some as-grown yellow- or orange-hued HPHT diamonds that have been grown or annealed at high temperatures.	Davies 1981; Jones et al. 1992; Boyd et al. 1994, 1995

Note: "Annealing" refers to high temperature treatment, typically done at atmospheric pressure. "Treatment" refers to some combination of annealing at low (LPHT) and/or high (HPHT) pressures, and irradiation. Some treatment sequences are disclosed in the literature, whereas others are not. Diamonds (either natural or laboratory-grown) treated at HPHT conditions should not be confused for those that are grown by HPHT methods.

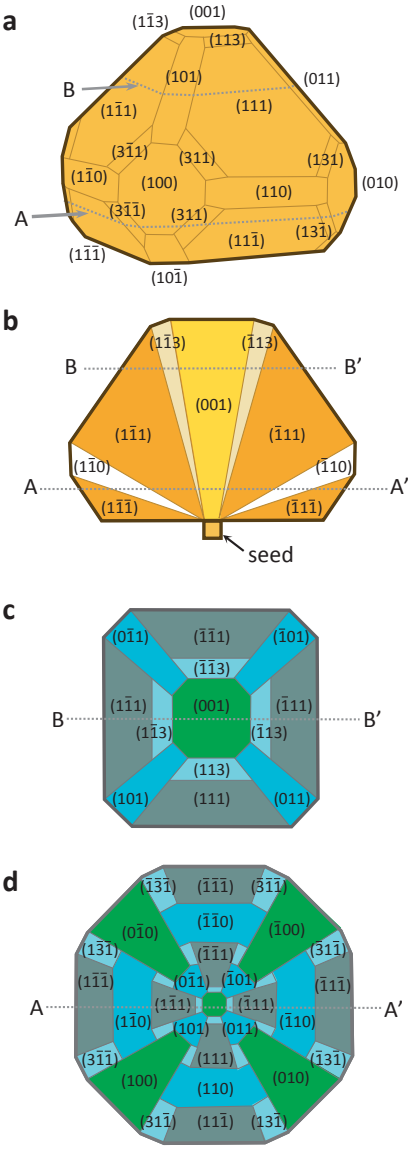

Figure 30 (**a**) A classic HPHT diamond showing the dominant octahedral {111} and cube {100} growth faces, and the minor dodecahedral {110} and trapezohedral {113} faces. (**b**) A cross-sectional view of the crystal parallel to the (110) plane, revealing the growth sectors and seed. The saturation of the yellow color correlates with the nitrogen concentration. (**c**) and (**d**) illustrate the growth patterns that could be observed by fluorescence techniques if the sample was sectioned in the (001) cube planes labelled **A** or **B**. The cross-like pattern is often referred to as a "Maltese cross." [Modified after Welbourn et al. (1996) *Gems and Gemology*, Vol. 32, Fig. 5, p. 162.]

Growth sectors. A growth sector is defined as the region of the sample that was grown with a common crystallographic growth plane (Burns et al. 1990), as illustrated in Figure 30. The incorporation efficiency for impurities differs for the growth sectors, leading to sector-dependent distributions throughout the crystal (Strong and Chrenko 1971; Burns et al. 1990, 1999; Collins et al. 1990; Satoh et al. 1990; Lawson et al. 1996). For instance, for most as-grown HPHT diamonds isolated nitrogen defect concentrations in the sectors can be arranged from highest to lowest as {111} > {100} > {113} > {110} (Burns et al. 1990). The behavior may be reversed for {100} and {111} sectors when grown at low temperatures (Satoh et al. 1990). Meanwhile for boron, another common contaminant or dopant of HPHT diamonds, the highest concentrations are found in the {111} sectors, followed by the {110} sectors (Burns et al. 1990). The distribution of nickel- and cobalt-related defects have also been found to be sector-dependent (Collins et al. 1990; Lawson et al. 1996). Importantly, as this distribution is the result of the intrinsic growth structure, it can still be perceived if the sample has been cut and polished to remove the distinctive external morphology. Furthermore, although defect species may be modified through treatment, the growth pattern will remain (Shigley et al. 1993a, 2004a; Moses et al. 1993). Consequently, the positive identification of HPHT origin is often based on techniques that can reveal the distinguishing growth pattern.

HPHT diamonds with sufficiently high concentrations of color-producing defects can show distinct color zoning (Figs. 16 and 31). For cut samples, the appearance will depend not only on the defect concentrations of the growth sectors, but also on their distribution relative to the faceting arrangements. The zoning may be more obvious by viewing samples under magnification and diffuse lighting while immersed in methylene iodide, water, or colorless alcohol to minimize reflections. There are many examples of brown-to-yellow-to-orange color zoning due to single substitutional nitrogen, and blue

due to boron, documented in the literature (Crowningshield 1971; Strong and Chrenko 1971; Koivula and Fryer 1984; Shigley et al. 1986, 1987, 1992, 1993a, 2002, 2004a,b; Burns et al. 1990; Fritsch and Shigley 1993; Rooney et al. 1993; Howell et al. 2019). Mixed Type Ib + IIb HPHT diamonds may show both yellow and blue color zoning, and may have a green face-up appearance if faceted (Shigley et al. 1992, 2004a; Fritsch and Shigley 1993; Rooney et al. 1993; Hainschwang and Katrusha 2003). Rarely, the concentration of nickel-related defects in HPHT diamonds can be sufficiently high to produce green color, preferentially incorporating into the {111} growth sectors (Collins and Spear 1982; Collins et al. 1990; Johnson and Myagkaya 2017; Eaton-Magaña 2019). Red or pink hued HPHT diamonds can be created by irradiation followed by annealing of Type Ib or Ib + IaA HPHT material, producing high concentrations of nitrogen-vacancy (NV) centers responsible for the color (Moses et al. 1993; Shigley et al. 2004a). Color zoning is not exclusive to HPHT diamonds. For instance, ~8% of natural yellow diamonds have a patchy "scotch and water" color distribution (King et al. 2005), while pink diamonds often show pink lamellae (Hofer 1985; King et al. 2002; Gaillou et al. 2010; Eaton-Magaña et al. 2018a), and subtle blue parallel bands may be observed in blue diamonds (King et al. 1998). Treatments that include irradiation can also produce regional color concentrations in both natural and laboratory-grown samples (Fritsch and Shigley 1989; Wang et al. 2005a). However, sharp geometric patterns—in particular squares, octagonal "stop signs," and the "Maltese Cross" (Figs. 30c,d)—are rarely observed in natural diamonds and should be treated as suspicious.

Figure 31. Distinctive color zoning in faceted HPHT diamonds stemming from growth sector dependent impurity distributions. [Used by permission of the Gemological Institute of America, from Shigley et al. (2004b) *Gems and Gemology*, Vol. 40, Fig. 5, p. 307.]

In addition to color zoning, "color graining" may be observed at the growth sector boundaries in the interior of the diamond or on its surface (Fig. 32). As with color zoning, graining may reveal a stop-sign, Maltese Cross, funnel, or hourglass patterns (Shigley et al. 1986, 1987, 1992, 1993a, 2004a; Fritsch and Shigley 1993). Grain lines may also be found in the {100} sectors in planes aligned parallel to the cube crystal faces (Shigley et al. 1987, 1992). In contrast, grain lines in natural diamonds are usually parallel to octagonal planes (Kane 1980). For brown-to-yellow-to-orange HPHT diamonds, this distinctive graining is attributed to variations in the index of refraction from the changing nitrogen content (Burns et al. 1990; Frank et al. 1990). For a review on graining in natural diamonds see Kane (1980).

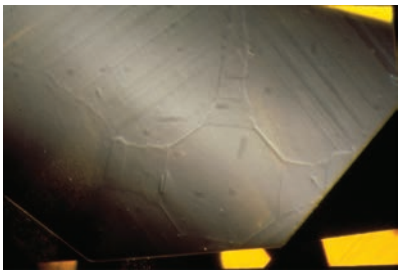

Figure 32. Octagonal stop-sign shaped graining on the polished surface of an HPHT diamond (field of view 3.5 mm). [Photomicrograph by John I. Koivula for GIA.]

By definition, near-colorless, and colorless HPHT diamonds cannot show color zoning. However, the underlying growth sectors are still present, and can be detected using techniques that are more sensitive to minute defect concentrations, such as deep UV fluorescence imaging. The application of fluorescence methods to reveal growth zoning in both colored and colorless HPHT diamonds will be detailed below in *Luminescence behavior*.

***Inclusions*.** Like natural diamonds, HPHT diamonds are susceptible to trapping materials from their environment during growth. Traces of the metal solvent/catalyst can be encapsulated in the crystal, often having elongated, triangular tabular, or irregular shapes, as shown in Figures 33a,b (Crowningshield 1971; Strong and Chrenko 1971; Koivula and Fryer 1984; Shigley et al. 1986, 1987, 1992, 1993a,b, 1997, 2002, 2004a,b; Burns et al. 1990, 1999; Fritsch and Shigley 1993; Moses et al. 1993; Lang et al. 1995; Sumiya and Satoh 1996; Sumiya et al. 2002; D'Haenens-Johansson et al. 2014, 2015a). Using transmitted light, they are black and opaque, while reflected light reveals a gray and metallic appearance. The metal solvent/catalyst composition, growth rate, temperature, and pressure can affect the number, size, and shapes of

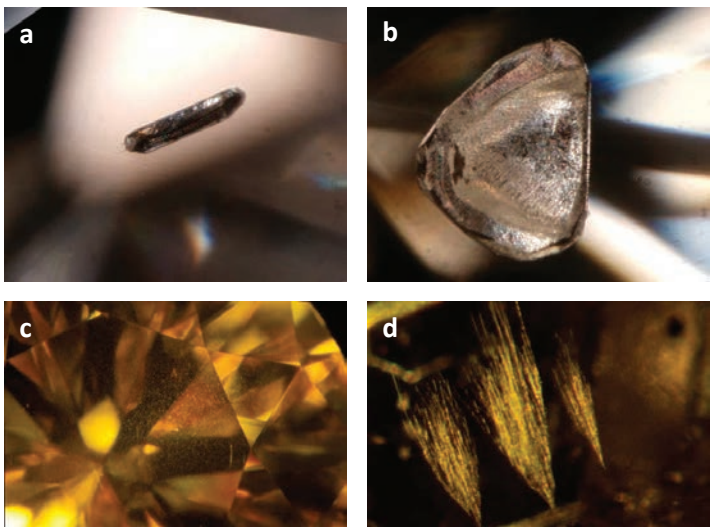

Figure 33. The metal solvent/catalyst used for HPHT diamond growth may be trapped in the crystal, resulting in dark, metallic inclusions which can be (**a**) rod, (**b**) triangular planar, or irregularly shaped. (**c**) Sparse pinpoint inclusions may be dispersed through the crystal, as in this yellow Type Ib HPHT diamond. (**d**) Horsetail or broom-like inclusions of unknown origin have also been reported in HPHT diamonds. Image widths are (**a** and **b**) 1.26, (**c**) 7.19, and (**d**) 2.85 mm. [Used by permission of the Gemological Institute of America, (**a, b**) from D'Haenens-Johansson et al. (2015a) *Gems and Gemology*, Vol. 51, Fig. 6, p. 267, (**c**) from Shigley et al. (2002) *Gems and Gemology*, Vol. 38, Fig. 6, p. 305, and (**d**) from Koivula and Fryer (1984) *Gems and Gemology*, Vol. 20, Fig. 12, p. 153.]

the inclusions. The addition of nitrogen getters to exclude nitrogen from the growing diamond by forming stable nitrides can further increase the uptake of inclusions (Sumiya and Satoh 1996; Burns et al. 1999, 2009; Sumiya et al. 2002). Due to their ferrous origin, an inclusion-containing HPHT diamond may be attracted to a strong magnet (Koivula and Fryer 1984; Rossman and Kirschvink 1984; Shigley et al. 1986, 1987, 1993a,b, 1997, 2004a,b; D'Haenens-Johansson et al. 2014, 2015a; Eaton-Magaña et al. 2017). For example, D'Haenens-Johansson et al. (2014, 2015a) found that faceted HPHT diamonds with clarities of VS_2 or poorer were weakly magnetic. Rare metallic inclusions have been observed in Type IIa, IaB, and IIb natural diamonds, but differ in appearance, with natural inclusions found adjacent to graphitic decompression cracks unlike those in the laboratory-grown samples (Sharp 1966; Rossman and Kirschvink 1984; Jacob et al. 2004; Kaminsky and Wirth 2011; Mikhail et al. 2014; Smith et al. 2016, 2018a,b).

Dilutely dispersed whitish pinpoint inclusions, as shown in Figure 33c, are frequently seen in fancy colored HPHT diamonds (Crowningshield 1971; Koivula and Fryer 1984; Shigley et al. 1986, 1987, 1993a,b, 1997, 2002, 2004a). Their sparse, even distribution is distinct from that of pinpoints in natural diamonds, which are typically concentrated in wispy clouds or associated with growth zones. Pinpoints in HPHT diamonds may consist of metallic and silicate phases (Lang et al. 1995). In diamonds grown using nitrogen getters, pinpoints have been attributed to the formation of stable carbides associated with the nitrogen getter element (Sumiya and Satoh 1996; Burns et al. 1999). The addition of copper to the growth capsule can suppress carbide formation.

Figure 33d presents another unusual inclusion seen in HPHT diamonds, described as a "horsetail" (Crowningshield 1971; Koivula and Fryer 1984). They form near the crystal surfaces and are typically lost during faceting.

Strain birefringence patterns. Examination of untreated near-colorless, colorless, and blue HPHT diamonds (which are always Type II, see the *Absorption spectroscopy and color* section) between crossed-polarized filters has been shown to be a simple method to alert the viewer of their laboratory-grown nature. Their low concentration of impurities, coupled with the even pressure that they are subjected to during growth, result in high crystalline perfection and few extended defects such as dislocations (Sumiya et al. 1997; Burns et al. 2009; Sumiya and Tamasaku 2012; Tran Thi et al. 2017). Consequently, they have low internal strain levels and only show extremely weak (black, gray or blue interference colors)—or more typically no—strain birefringence patterns, except adjacent to inclusions and cracks (Fig. 34) (Crowningshield 1971; Lang et al. 1991; Fritsch and Shigley 1993; Rooney et al. 1993; Shigley et al. 1993b; D'Haenens-Johansson 2014, 2015a). Natural diamonds commonly show mottled, banded, radial, or tatami (cross-hatched) birefringence patterns originating from the presence of defects, inclusions, and deformation events from their growth and mantle residency history (Tolansky 1966; Lang 1967; Kane 1980; Sumiya et al. 1997; Howell 2012). Natural Type II diamonds are characterized by high levels of strain and dislocations, forming distinctive tatami patterns. Conversely, natural Type I diamonds occasionally do not show clear strain patterns, so the absence of a pattern in an unknown diamond is not conclusive proof that it is HPHT-grown, and should thus be analyzed using another complementary method for confirmation (e.g., FTIR for diamond type) (Koivula and Fryer 1984). Radial, cross-hatched, and banded strain birefringence patterns have been reported for Type I HPHT diamonds due to variations in the lattice parameters from the inhomogeneous distribution of nitrogen defects, as well as surrounding both pinpoint and larger inclusions (Koivula and Fryer 1984; Shigley et al. 1986, 1987, 1992, 1993a, 2004b; Frank et al. 1990; Lang et al. 1991; Fritsch and Shigley 1993; Sumiya et al. 1997; Palyanov et al. 2010). Many note that the patterns are nevertheless weaker compared to those for natural diamonds.

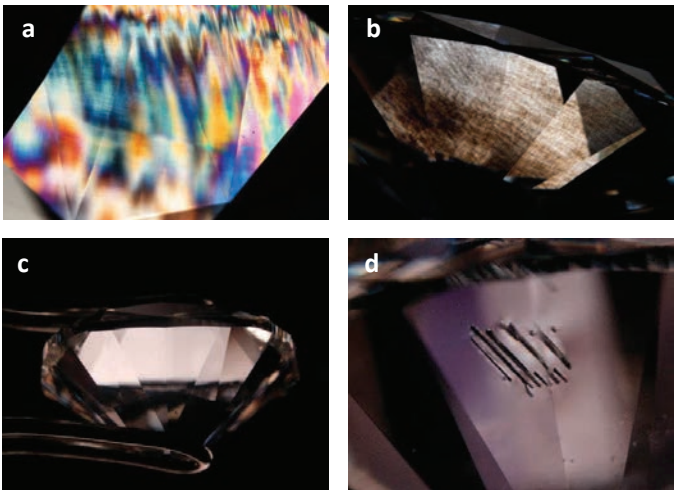

Figure 34. Strain birefringence patterns produced when viewing a diamond sample between crossed polarizing filters can help alert the operator of potential HPHT diamonds. Natural diamonds [(**a**) and (**b**)], as well as those grown by CVD methods (see Fig. 38), show a range of patterns including patchy/mottled, tatami-like/cross-hatched, or banded. On the other hand, HPHT diamonds that fall in the D–Z color range [(**c**) and (**d**)] are characterized by extremely low strain levels and the absence of patterns, except adjacent to clarity features such as inclusions. Sample details: (**a**) 4.59 ct, Fancy Intense pink, VS_2 clarity (field of view 4.77 mm), (**b**) 6.92 ct, D color, IF clarity (field of view 9.61 mm), (**c**) 2.30 ct, E color, SI_1 clarity (field of view 14.48 mm), and (**d**) 0.54 ct, E color, SI_1 clarity (field of view 3.57 mm). [Photomicrographs by UFSDJ.]

Luminescence behavior. Table 2 summarizes common fluorescence and phosphorescence colors and intensities for as-grown and treated HPHT diamonds analyzed using shortwave and longwave UV (Shigley et al. 2004b). Representative data for individual samples can be found in Crowningshield (1971), Koivula and Fryer (1984), Shigley et al. (1986, 1987, 1992, 1993a,b, 1997, 2002, 2004a), Moses et al. (1993), Rooney et al. (1993), and D'Haenens-Johansson et al. (2014, 2015a), while Eaton-Magaña et al. (2017) present statistical analysis of several thousand HPHT diamonds submitted to GIA. Most HPHT diamonds show a stronger fluorescence response to the shortwave rather than the longwave UV light produced by a gem lamp, a useful quality as it is opposite to that typical to natural diamonds (e.g., Moses et al. 1997; King et al. 1998, 2002, 2005). It is important to note that there are exceptions to this behavior for both HPHT and natural diamonds. The sector-dependent impurity incorporation in HPHT diamonds can lead to zonation in the fluorescence patterns, often taking distinctive square or cross shapes which may be perceived in fancy colored specimens (Fig. 35a). Cuboctahedral patterns are extremely rare for natural diamonds.

Colorless to near-colorless HPHT diamond are typically inert to longwave UV light, with Eaton-Magaña et al. (2017) reporting only ~2% of colorless HPHT diamonds showing fluorescence, which was orange or yellow in color. Yet among natural diamonds, 35% show longwave UV fluorescence, and of those 99% fluoresce blue due to the presence of N3 (N_3V^0) centers (Moses et al. 1997). The strong, persistent phosphorescence observed for colorless to near-colorless HPHT Type IIa and IIb diamonds is also particularly useful for their detection due to the rarity of phosphorescence in similarly colored natural diamonds (Fig. 35b) (Crowningshield 1971; Koivula and Fryer 1984; Rooney et al. 1993; Shigley et al. 1993b, 1997; D'Haenens-Johansson et al. 2014, 2015a). The phosphorescence, associated with boron (Watanabe et al. 1997), indicates the presence of this element even in nominally Type IIa HPHT diamonds. This behavior is the basis for certain diamond screening equipment used by gemologists. However, this useful property can be removed by irradiation treatments (Robinson 2018).

Table 2. Fluorescence and phosphorescence behavior of as-grown and treated HPHT diamonds stimulated by longwave (LWUV, 365 nm) and shortwave (SWUV, 254 nm) ultraviolet light from a combination gem lamp. [Adapted from the fold-out chart accompanying Shigley et al. (2004b) *Gems and Gemology*, Vol. 40, p. 303–313.]

HPHT diamond	LWUV fluorescence	SWUV fluorescence	Fluorescence intensities	Phosphorescence to SWUV
yellow/brown Ib (+ IIa), as-grown	usually inert	weak to moderate green-yellow, yellow-green, green, or inert	typically SWUV > LWUV	occasionally weak yellow or greenish yellow
green Ib + IIb, as-grown	usually inert or weak orange	weak to moderate yellow, green-yellow, or orange	typically SWUV > LWUV	weak to moderate yellow, often persistent
blue IIb (+ IIa), as-grown	usually inert or weak orange	weak to moderate green, yellow, or orange	typically SWUV > LWUV	moderate to strong yellow or blue, often persistent
colorless IIa (+ IIb*), as-grown	usually inert	weak to moderate green, yellow, blue, or orange	typically SWUV > LWUV	weak to moderate blue, yellow, or green-yellow, often persistent
yellow/brown IaA +Ib, HPHT annealed	moderate to strong green, yellow-green, green-yellow, yellow, or orange	moderate to strong green, yellow-green, green-yellow, yellow, or orange	SWUV > LWUV, SWUV = LWUV, LWUV > SWUV	occasionally weak to moderate yellow or yellow-green, often persistent
pink Ib, irradiated + annealed	moderate to strong orange or orange-red	weak to moderate orange	often LWUV > SWUV	occasionally weak orange or orange-red
red/purple Ib + IaA, irradiated + annealed	inert or weak to moderate orange or orange-red	weak to moderate orange or orange-red	SWUV > LWUV, SWUV = LWUV, LWUV > SWUV	weak green
green IIa or Ib, irradiated	very weak to weak red-orange or orange-red	weak to moderate green-yellow, yellow-green, green, or inert	SWUV > LWUV, SWUV = LWUV, LWUV > SWUV	rarely observed

Note: * Colorless HPHT diamonds can contain low concentrations of boron (D'Haenens-Johansson et al. 2014, 2015a).

Inspection under deep-UV (wavelength <225 nm) can reveal further detail in the growth patterns, stimulating sufficient contrast even in near-colorless to colorless Type IIa or weak Type IIb HPHT diamonds such as those shown in Figure 36 (Welbourn et al. 1996; Shigley et al. 1997, 2002, 2004b; D'Haenens-Johansson et al. 2014, 2015a; Eaton-Magaña et al. 2017). The majority of natural diamonds show octahedral, or occasionally cubic, growth patterns which may also reveal a complex sequence of dissolution and growth events (Welbourn et al. 1996; Harris et al. 2022, this volume). In contrast, cuboctahedral patterns such as those seen for HPHT diamonds are unusual. Growth zones are rarely detected for natural Type II diamonds, whose fluorescence patterns are instead dominated by polygonized dislocation networks (Fig. 36d) and can thus be clearly separated from HPHT diamonds (Sumida and Lang 1981; Martineau et al. 2004). The fluorescence colors depend upon the defect compositions of individual samples. When considering colorless and near-colorless natural and HPHT-grown Type II diamonds it is common for naturals to show clear blue "Band A" fluorescence associated with dislocations or N3 centers (Dean 1965; Ruan et al. 1992; Takeuchi et al. 2001; Martineau et al. 2004), whereas HPHT diamonds show blue-green or green-blue fluorescence colors (D'Haenens-Johansson et al. 2014, 2015a). Furthermore, deep-UV light stimulates strong, long-lived green-blue phosphorescence centered about 500 nm and may also show yellow

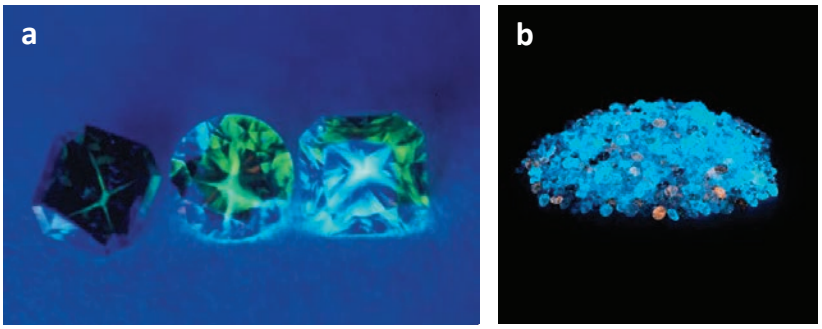

Figure 35. Analysis of HPHT diamonds under UV illumination may reveal their laboratory-grown origin. (**a**) These yellow diamonds display characteristic cross- and square-shaped green fluorescence patterns under longwave UV, indicative of HPHT growth. The fluorescence colors in HPHT diamonds may include green, yellow-green, green-yellow, yellow, orange, or orange-red, depending on the diamond type and treatment history (Table 2). It is typical for them to show a stronger response to shortwave (254 nm) rather than longwave (365 nm) excitation. For comparison, 99% of natural fluorescing diamonds emit blue light and most have a stronger response to longwave UV. (b) Colorless and blue HPHT diamonds display long-lived phosphorescence to shortwave UV due to the presence of boron impurities, a feature that is seldom seen for natural diamonds. [Used by permission of the Gemological Institute of America. (**a**) Kammerling et al. (1995) *Gems and Gemology*, Vol. 31, Fig. 7, p. 123. (**b**) Persaud et al. (2018) *Gems and Gemology*, Vol. 54, Fig. 10, p. 209.]

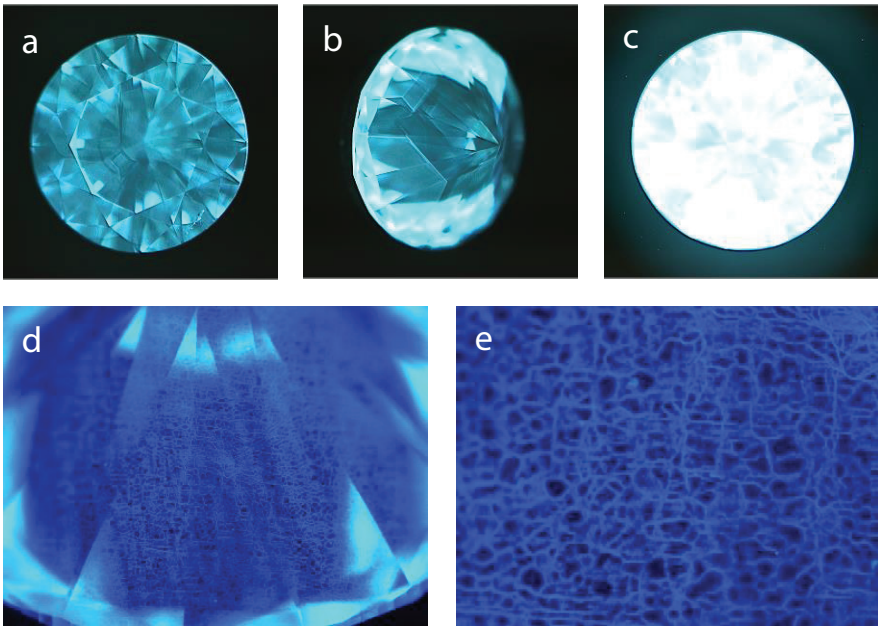

Figure 36. Cuboctahedral growth patterns revealed using a DiamondView deep-UV imaging system for a 0.41 ct G color HPHT diamond. (**a**) and (**b**) are fluorescence images collected under illumination, whereas (**c**) demonstrates the strong, long-lived phosphorescence that is characteristic of untreated Type IIa (generally contaminated with traces of boron) or IIb HPHT diamonds. In contrast, natural Type IIa or IIb diamonds rarely show growth zones, with fluorescence patterns dominated by polygonized dislocation networks as shown in (**d**) and (**e**) for a 2.09 ct D color diamond. Phosphorescence observed for natural Type IIb diamonds typically decay more rapidly than for HPHT diamonds. [Images (**a–c**) used by permission of the Gemological Institute of America, D'Haenens-Johansson et al. (2014) *Gems and Gemology*, Vol. 50, Fig. 4, p. 36. Images (**d**) and (**e**) by UFSDJ.]

emission at 575 nm (Watanabe et al. 1997; Eaton-Magaña et al. 2008; Eaton-Magaña and Lu 2011; D'Haenens-Johansson et al. 2014, 2015a). Under deep-UV, the overall phosphorescence of natural Type IIb diamonds may appear blue, gray, violet, or red due to emission bands centered about 500 nm and/or 660 nm, decaying more rapidly than that of laboratory-grown diamonds (Eaton-Magaña et al. 2008; Eaton-Magaña and Lu 2011).

Largely superseded by the comparatively user-friendly DiamondView deep-UV imaging system, cathodoluminescence has also been shown to be a powerful technique for detailed analysis of HPHT diamond growth patterns and their luminescent defects (Woods and Lang 1975; Shigley et al. 1987, 1992, 1993a,b; Collins et al. 1990; Ponahlo 1992; Fritsch and Shigley 1993; Rooney et al. 1993; Burns et al. 2009).

Absorption spectroscopy and color. HPHT diamonds belonging to several classification types can be produced (Table 2). The different impurity uptakes of growth sectors mean that oftentimes a single crystal will contain minor sectors belonging to different diamond types. Unless steps are taken to minimize nitrogen incorporation standard HPHT synthesis results in predominantly Type Ib material, similar to that mass-produced for diamond grit (Dyer et al. 1965; Chrenko et al. 1971; Crowningshield 1971; Strong and Chrenko 1971; Koivula and Fryer 1984; Shigley et al. 1986, 1987, 1992, 1993a, 2002, 2004a,b; Burns et al. 1990; Fritsch and Shigley 1993; Rooney et al. 1993). They may have yellow, to greenish or orangy or brownish yellow, to orange-yellow color. Type Ib diamonds contain single substitutional nitrogen dispersed through the crystal lattice. This color center produces absorption both in the IR and visible regions. IR absorption spectra show a peak at 1344 cm^{-1} and a broad band at 1130 cm^{-1} (Dyer et al. 1965; Chrenko et al. 1971; Collins 1980; Collins and Woods 1982; Kiflawi et al. 1994; Lawson et al. 1998), while UV-visible spectra show a rise in absorption from ~560 nm toward the intrinsic diamond absorption edge at 225 nm, with a broad peak at 270 nm, responsible for the yellow-to-orange-to-brown color (e.g., Fig. 12) (Dyer et al. 1965; Chrenko et al. 1971; Collins 1982, 1993a, 2001). Nickel-related defects introduced by the metal solvent/catalyst may produce additional absorption features at 494, 658, 793.5 (with vibronic structure at ~700 nm), and a doublet about 884 nm (broad band at ~685 nm), imparting a green hue (Collins and Spear 1982; Shigley et al. 1987, 1993a, 2004a; Collins et al. 1990; Lawson and Kanda 1993a,b; Yelisseyev and Nadolinny 1995; Yelisseyev et al. 1996, 2002; Yelisseyev and Kanda 2007; Johnson and Myagkaya 2017; Eaton-Magaña 2019). These peaks are not exclusive to HPHT diamonds, but may indicate a laboratory-grown diamond that needs further inspection (e.g., Chalain 2003; Lang et al. 2004; Wang and Moses 2007; Wang et al. 2007a; Breeding et al. 2018). Figure 37a illustrates a representative UV-visible absorption spectrum for a Type Ib yellow HPHT diamond. In nature, Type Ib diamonds are very rare, accounting for ~0.1% of diamonds, and often contain natural needle-like inclusions to help in their identification (Dyer et al. 1965; Shigley et al. 1986; Breeding and Shigley 2009). Most yellow-hued natural diamonds are Type Ia and are instead colored by the "Cape series" of peaks that include the N3 (N_3V^0) zero phonon line at 415 nm, vibronic structure to shorter wavelengths, as well as the N2 transition at the same defect at 478 nm (Davies et al. 1978; Collins 1982, 2001; King et al. 2005; Green et al. 2022, this volume).

Isolated nitrogen atoms may aggregate to A-centers (nitrogen pairs) if synthesis times and temperatures are elevated, resulting in Type IaA material, and may also progress further to form B-centers (N_4V^0) (Kanda et al. 1990; Vins et al. 1991; Kanda and Yamaoka 1993; Shigley et al. 1993a, 2002; Babich et al. 2000, 2004; Yelisseyev et al. 2002). HPHT or LPHT annealing of as-grown Type Ib diamond is an alternative route for nitrogen aggregation (Chrenko et al. 1977; Evans et al. 1981; Evans and Qi 1982; Shigley et al. 1993a; Kiflawi et al. 1994, 1998; Kim et al. 2011; Kazuchits et al. 2016; Chen et al. 2018). For both the as-grown and treated cases, a portion of the isolated nitrogen centers will remain (e.g., they are mixed Type Ib + IaA) as the nitrogen aggregates cycle through formation and dissociation (Brozel et al. 1978).

A- and B-centers show characteristic IR spectra with absorption features at 1282 and 1175 cm^{-1}, respectively (Davies 1981; Boyd et al. 1994, 1995). They do not produce diamond color as they do not absorb light in the visible range. However, the isolated nitrogen present will contribute, resulting in similarly hued material as the Type Ib HPHT diamonds (Fig. 37a) (Shigley et al. 1993a, 2002; Yelisseyev et al. 2002; Kim et al. 2011; Kazuchits et al. 2016; Chen et al. 2018). Unlike natural diamonds, there are no Type Ia colorless or near-colorless HPHT diamonds. This is significant as ~98% of natural diamonds are Type Ia (Dyer et al. 1965), making diamond typing a useful tool for screening out colorless to near-colorless HPHT diamonds. Nitrogen-containing HPHT diamonds that have been annealed or grown at temperatures sufficiently high to induce nitrogen aggregation can also form the N3 and N_3VH^0 (3107 cm^{-1}) centers (Chrenko et al. 1977; Evans and Qi, 1982; Kiflawi et al. 1996; Goss et al. 2014). These centers are common in natural Type Ia diamonds, and occasionally observed in Type IIa diamonds.

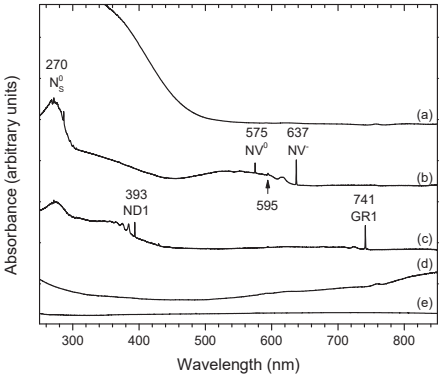

Figure 37. UV-visible-NIR absorption spectra collected at 77 K for HPHT diamonds reveal the defects responsible for their color. (**a**) This 1.25 ct Fancy Vivid orange yellow diamond is colored by isolated nitrogen, producing strong absorption at wavelengths below 350 nm. (**b**) This 0.30 ct Fancy Vivid purplish pink diamond owes its color from nitrogen-vacancy centers that were produced by irradiation and annealing of Type Ib diamond. The spectrum includes isolated nitrogen absorption at 270 nm, as well as the treatment-related 595 nm center and neutral vacancy (GR1, too weak to observed at this scale). (**c**) HPHT diamonds that are irradiated to a blue-to-green color, as this 0.41 ct Fancy bluish green sample, contain high concentrations of vacancies in the neutral (GR1) and negatively charged (ND1) states. This sample also has detectable isolated nitrogen. (**d**) Boron in this 0.55 ct Fancy Intense blue HPHT diamond results in featureless absorption from the infrared to red region of the spectrum. (**e**) Colorless HPHT diamonds like this D color 0.71 ct have defect concentrations that are too low to produce detectable absorption in the visible range.

Type Ib and Ib + IaA HPHT diamonds are candidates for irradiation and annealing to form pink/red to orangy or brownish pink/red to purplish pink or purple material, as show in Figure 15 (Moses et al. 1993; Shigley et al. 2004a,b). This treatment sequence combines vacancies produced by the irradiation with the resident isolated nitrogen centers to form nitrogen-vacancy (NV) centers. NV centers in the neutral and negative charge states absorb in the visible, with zero phonon lines at 575 and 637 nm, respectively (Collins 1982, 2001). Due to the high isolated nitrogen content in Type Ib and Ib + IaA, which acts as an electron donor, a majority of the NV centers will be negatively charged, resulting in absorption from its associated vibronic structure between 500 and 600 nm, producing the pink-to-red hued color component (Fig. 37b). This, combined with the yellow-to-brown component of the isolated nitrogen absorption produces the characteristic color range of these treated HPHT diamonds. The treatment may also introduce features including GR1 (neutral vacancy, V^0, 741 nm), H3 (N_2V^0, 503.2 nm), and 595 nm peaks as tabulated by Moses et al. (1993) and Shigley et al. (2004a). In the infrared range, absorption from the dinitrogen ⟨001⟩ split-interstitial H1a (1450 cm^{-1}) and a peak at 1502 cm^{-1}, both

produced through irradiation and annealing treatment, may be detected (Clark et al. 1956; Collins 1980; Woods and Collins 1982; Woods 1984; Collins et al. 1988; Liggins 2010; Liggins et al. 2010). Increased control during growth and treatment can also be used produce weak Type Ib (nominally Type IIa) pink HPHT diamonds (Eaton-Magaña et al. 2017). The vast majority of similarly hued natural diamonds are colored by unidentified broad absorption bands at 390 and 550 nm, an underlying brown absorption continuum attributed to vacancy clusters, as well as possibly N3 (Collins 1982, 2001; King et al. 2002; Fisher et al. 2009; Gaillou et al. 2010; Byrne et al. 2012, 2014a,b; Howell et al. 2015; Eaton-Magaña et al. 2018a, 2020; Green et al. 2022, this volume), making the detection of NV centers suspicious. Untreated natural Type IIa pink diamonds colored by NV centers, known as "Golconda" diamonds, only account for ~0.6% of natural pink diamonds (Fritsch 1998; Eaton- Magaña et al. 2018a). However, note that NV centers can also be responsible for pink color in treated natural and CVD diamonds (Collins 1982, 2001; Wang et al. 2005a, 2010; Eaton-Magaña and Shigley 2016).

Blue or grayish blue HPHT diamonds containing sufficient uncompensated boron (i.e., an excess of boron compared to isolated nitrogen) to be classified as Type IIb show absorption features at ~2458, 2803, and 2930 cm^{-1}, with the latter feature having a tail which extends through the infrared into the red region of the visible spectrum (Collins and Williams 1971; Strong and Chrenko 1971; Koivula and Fryer 1984; Collins 1993b; Rooney et al. 1993; Shigley et al. 2004a,b; Howell et al. 2019; Green et al. 2022, this volume). Boron readily incorporates into the growing diamond lattice, and may be added intentionally to the growth capsule. Boron contamination may originate from the carbon source material or the metal solvent/catalyst (Sumiya and Satoh 1996). Colorless and near-colorless HPHT diamonds can be Type IIa or IIa + IIb, where the uncompensated boron concentration is insufficient to produce appreciable color (Strong and Chrenko 1971; Koivula and Fryer 1984; Rooney et al. 1993; Shigley et al. 1993b, 1997, 2004b; Sumiya and Satoh 1996; D'Haenens-Johansson et al. 2014, 2015a). Pure Type IIa diamonds only show intrinsic diamond absorption in the infrared region, and are transparent through the visible to UV range down to the diamond absorption edge at 225 nm. Figure 37 shows a representative UV-visible absorption spectrum for both blue (d) and colorless (e) HPHT diamond, demonstrating an absence of sharp features. Their absorption spectra are often indistinguishable to those of natural Type IIa and IIb diamonds, highly valuable groups that account for <1.3% and <0.02% of natural gem diamonds, respectively (King et al. 1998; Smith et al. 2016, 2018a; Eaton-Magaña et al. 2018a).

Samples have also been grown containing both Type IIb and Ib sectors (Shigley et al. 1992, 2004a,b; Fritsch and Shigley 1993; Rooney et al. 1993; Hainschwang and Katrusha 2003). When faceted they may have a yellowish green to green to bluish green appearance due to the absorption contributions from boron and isolated nitrogen (Fig. 37). The authors are not aware of any reports of mixed Type Ib + IIb natural diamonds, in agreement with Shigley et al. (1992).

Type IIa and weak Ib HPHT diamonds may be irradiated to produce vacancies, introducing GR1 (V^0) absorption with a zero phonon line at 741 nm and vibronic structure in the red, and may also include sharp irradiation-related features such as ND1 (V^-, 393.5 nm), GR2–GR8 peaks (412–430 nm), and the 595 nm peak (Fig. 37c) (Davies 1977; Shigley et al. 2004a,b). The treated diamond will have a yellowish green to green to bluish green to blue color, depending on the strength of nitrogen-related absorption present in the as-grown material and the ratio of GR1 to ND1 defects. The GR1 center is also the primary defect responsible for green color in both natural and treated diamonds, complicating their distinction (Collins 1982, 2001; Shigley and Fritsch 1990; Breeding et al. 2018; Green et al. 2022, this volume). Natural diamonds colored by GR1 may be Type IIa or Ia. For a review on green color in natural diamonds, including spectroscopic and gemological features such as irradiation spots or coatings, see Breeding et al. (2018).

Photoluminescence spectroscopy. The increased detection sensitivity provided by PL is particularly useful for probing defects in colorless to near-colorless Type IIa or IIb diamonds. Nevertheless, PL spectra for such HPHT diamonds typically show very few, and oftentimes weak, emission peaks (D'Haenens-Johansson et al. 2014, 2015a). The most prominent features are nickel-related, such as the 884 nm doublet and a 4-peak multiplet at about 484 nm (Collins and Spear 1982, 1983; Davies et al. 1989; Collins et al. 1990; Nazaré et al. 1991, 1995; Lawson and Kanda 1993a,b; Collins 2000; Yelisseyev and Kanda 2007; D'Haenens-Johansson et al. 2014, 2015a), likely due to nickel contamination from the metal solvent/catalyst. Occasionally doublet emission at 736.7/736.9 nm from the negatively charged silicon-vacancy center (SiV^-) is detected (Clark et al. 1995, D'Haenens-Johansson et al. 2014, 2015a), a defect more commonly associated with CVD diamonds (Wang et al. 2003, 2005b, 2007b, 2012; Martineau et al. 2004). These centers are seldom observed for natural diamonds, and are thus useful indicators of HPHT synthesis (Chalain 2003; Noble et al. 1998; Wang and Moses 2007; Wang et al. 2007a; Breeding and Wang 2008).

Absorption spectroscopy, coupled with gemological observations and fluorescence behavior provide sufficient information to support the identification of fancy colored HPHT diamonds. Many of the features that would be observed using PL can be detected in absorption. Consequently, there are not many detailed reports presenting their PL spectra for this purpose (Shigley et al. 2002, 2004a; Kennedy and Johnson 2016; Eaton-Magaña et al. 2017). Most notable are peaks associated with nickel-related defects (484 nm; S2/NE2, 489.2 nm; S3/NE1, 496.7 nm; NE3, 523.3 nm; 658 nm; 694 nm; NE8, 793.5 nm; 884 nm), nitrogen-related defects ($H3/N_2V^0$, 503.2 nm; NV^0, 575 nm; NV^-, 637 nm; $H2/N_2V^-$, 986 nm), or the neutral vacancy defect GR1 (741 nm) if the sample had undergone irradiation treatment (Yelisseyev et al. 1996, 2002, 2003, 2006; Kanda and Watanabe 1999; Nadolinny et al. 1999; Yelisseyev and Kanda 2007). Peak details are summarized in Table 1.

Identification of CVD diamonds

External morphology. As-grown uncut CVD diamonds can be readily identified due to their unique appearance, as shown in Figure 22. CVD diamond morphology depends upon the orientation of the underlying seed and growth conditions (Silva et al. 2006, 2008, 2009; Brinza et al. 2008; Tallaire et al. 2013). Gem-quality material is usually synthesized using (100)-oriented substrates, consequently growing as cubic (001)-oriented thick films with (100) and (010) edges. Minor dodecahedral {110} faces may form along the edges, as well as octahedral {111} and trapezohedral {113} faces on the crystal corners. The {111} faces are undesirable as they are susceptible to twinning, resulting in stress buildup and crack development. The {110} faces have also been linked to higher internal stress levels and sample breakage (Tallaire et al. 2013). Uncut CVD diamonds may also show a dark polycrystalline diamond rim along the edges (Mokuno et al. 2005; Nad et al. 2015, 2016). The top surface topography of a CVD crystal is affected by many factors including the substrate orientation, misalignment angle, and crystalline quality, gas composition, and temperature, and may show macro-bunching steps that flow across the surface and/or hillocks (Janssen et al. 1992; de Theije et al. 2000; Takeuchi et al. 2000; Wang et al. 2005b; Achard et al. 2007; Martineau et al. 2009).

Visual features. CVD diamonds generally obtain high clarities. They may contain small, black, irregularly shaped amorphous carbon or disordered graphitic inclusions or pinpoints (Wang et al. 2003, 2005b, 2007b, 2012; Martineau et al. 2004; Crisci et al. 2011). Sometimes these inclusions are cloud-like or lie in planes oriented parallel to the substrate. In samples that have been HPHT treated for decolorization, inclusions may be surrounded by radial fractures stemming from high levels of localized strain (Wang et al. 2012). Inclusions in CVD diamonds are unfortunately not diagnostic since they have a similar appearance to those in some natural diamonds.

Color concentration is generally even in fancy colored pink or brown CVD diamonds, though fluctuations in growth parameters or interruptions may lead to colored bands aligned parallel to the substrate plane (Wang et al. 2003, 2005b, 2010; Martineau et al. 2004). Graining associated with threading dislocations may be apparent (Wang et al. 2007b, 2010).

Strain birefringence patterns. Threading dislocations aligned approximately perpendicular to the growing surface are known to nucleate at or near the interface between the substrate and the CVD diamonds, often forming bundles (Fujita et al. 2006; Gaukroger et al. 2008; Martineau et al. 2009; Pinto and Jones 2009). They may lead to an anisotropic strain birefringence, most easily observed parallel to the growth direction in unfaceted samples (Martineau et al. 2004). Irregular, banded, and cross-hatched (tatami-like) birefringence patterns have been seen for CVD diamonds (Fig. 38), with interference colors ranging from subdued grays and blues to vivid reds and greens (Wang et al. 2003, 2005b, 2007b, 2010, 2012). Localized strain fields may be found surrounding inclusions (Wang et al. 2003, 2005b, 2010, 2012; Pinto and Jones 2009; Crisci et al. 2011). Unlike many HPHT diamonds, strain birefringence patterns in CVD diamonds are generally difficult to distinguish from those in natural samples.

Figure 38. Strain birefringence patterns for faceted CVD diamonds can be (**a**) patchy, (**b**) tatami-like or (**c**) banded, making them difficult to separate from natural diamonds (e.g., Fig. 34a,b). These samples are characterized as follows: (**a**) 0.28 ct, H color, VS_2 clarity (field of view 3.10 mm); (**b**) 0.47 ct, G color, VVS_2 clarity (field of view 4.33 mm); and (**c**) 0.70 ct, I color, VVS_2 clarity (field of view 5.11 mm). [Photomicrographs by Wuyi Wang for GIA.]

Luminescence behavior. Most colorless and near-colorless CVD diamonds are inert to longwave UV light. Analysis of CVD diamonds submitted to GIA between 2003 and 2016 suggests only approximately 7% of samples show very faint to faint fluorescence (Eaton-Magaña and Shigley 2016). However, it was noted that the incidence of longwave UV fluorescence decreased over the years as CVD products evolved, with all samples tested since 2013 being inert. When the color of such fluorescence was noted, as-grown CVD diamonds emitted orange, orange-yellow, or yellow light originating from nitrogen-vacancy centers (Martineau et al. 2004; Wang et al. 2005b, 2007b). The brown hue common in CVD diamonds grown with intentional or unintentional nitrogen doping can be removed by high temperature annealing (usually using an HPHT press, but LPHT annealing has also been reported), resulting in a more valuable gem product (Wang et al. 2003, 2012; Charles et al. 2004; Martineau et al. 2004; Mäki et al. 2007; Meng et al. 2008; Liang et al. 2009; Eaton-Magaña and Shigley 2016; Eaton-Magaña et al. 2021). This treatment will reduce NV content, while introducing H3 (N_2V^0) centers, producing green fluorescence (Wang et al. 2012). These orange and green fluorescence colors can alert viewers of their laboratory-grown origin as 99% of natural similarly colored fluorescing diamonds emit blue light due to N3 (N_3V^0) (Moses et al. 1997). Furthermore, CVD diamonds show a stronger fluorescence response to shortwave UV, in contrast to most naturals.

The second most common color of CVD diamonds are pink-hued (Eaton-Magaña and Shigley 2016; Eaton-Magaña et al. 2021), with the vast majority colored by high concentrations of NV centers produced through treatment (see *Absorption spectroscopy and color* section below). The dominance of NV centers in pink CVD diamonds gives rise to moderate to strong

red or orange fluorescence to both longwave and shortwave UV light (Wang et al. 2010; Eaton-Magaña and Shigley 2016). Extremely rare Golconda pink natural diamonds (~0.6% of natural pink diamonds) as well as most treated pink natural-grown and HPHT diamonds (Table 2) will also fluoresce in similar hues due to their elevated NV concentrations (Eaton-Magaña and Shigley 2016; Eaton-Magaña et al. 2018a). Meanwhile, 58% and 9% of natural pink diamonds colored by the 550 nm band show blue (N3) or yellow fluorescence, respectively, with the remainder being inert (Eaton-Magaña et al. 2018a).

Inspection of CVD diamonds under magnification and deep-UV excitation (<225 nm) can reveal characteristic growth patterns and help with conclusive identification. CVD synthesis of gem-quality diamond usually proceeds through step-flow growth on (001)-oriented substrates, with riser and terrace segments oriented along [001] and [101] directions. As they present differently oriented planes of growth, the distinct impurity uptake of terraces and risers can result in the formation of a fluorescence pattern of tightly spaced lines known as "striations," illustrated in Figures 39 and 40 (Martineau et al. 2004, 2009). Additionally, deliberate or accidental growth events such as variations in deposition conditions or interruptions can

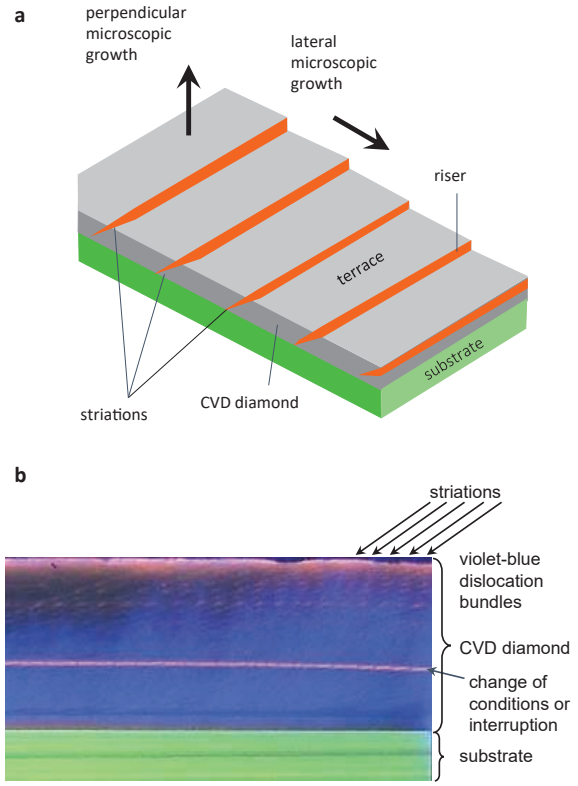

Figure 39. (**a**) The different incorporation efficiency of defects on risers and terraces during step-flow growth of CVD diamond can lead to formation of striations. (**b**) This DiamondView deep-UV fluorescence image of a cross-sectional slice of a CVD diamond layer grown on an HPHT diamond substrate displays several characteristic growth patterns. Orange striations from the differential incorporation of NV centers are inclined diagonally relative to the substrate plane. The horizontal line traversing the CVD layer indicates a change in growth conditions or potential interruption. Violet blue dislocation bundles appear to originate close to the substrate–CVD layer interface, threading upwards through the CVD material. [Image (**a**) modified after Martineau et al. (2004) *Gems and Gemology*, Vol. 40, Fig. 15, p. 13. Image (**b**) modified after Martineau et al. (2009) *Physics Status Solidi C*, Vol 6, Fig. 4, p. 1955.]

dramatically modify the impurity content, resulting in an abrupt change in fluorescence color and/or brightness (Figs. 39b and 40a,d). In a cross-sectional view this will appear as a line lying parallel to the growth plane. Evidence of these growth events, in particular in larger CVD diamonds, suggests that they are being grown in stages as a series of layers (Mokuno et al. 2005; Asmussen et al. 2008; Dieck et al. 2015; Nad et al. 2015; Law and Wang 2016). Figure 22 displays an as-grown CVD diamond crystal grown in two stages. Blue fluorescing threading dislocations, typically nucleating at or close to the boundary between the substrate and CVD diamond layer, may propagate through the CVD material aligned approximately parallel to the bulk growth direction (Martineau et al. 2004). Step-flow growth may cause the dislocations to deviate, following a zigzag path (Martineau et al. 2009). Depending on the viewing direction, dislocations may appear as threads or bundles with a clear linear habit, or may be patchy (Martineau et al. 2004, 2009; Wang et al. 2005b; Dieck et al. 2015). The anisotropy of the patterns emphasizes the importance of inspecting diamonds from multiple viewing angles.

Deep-UV fluorescence images for faceted CVD diamonds are presented in Figure 40. Variations in growth and treatment histories mean that CVD diamond fluorescence can span the full rainbow spectrum of colors (Eaton-Magaña and Shigley 2016). Importantly, treatments cannot remove the intrinsic growth patterns of diamonds, but will affect the relative concentrations of defects and thus potentially fluorescence colors. Here we review the most commonly observed

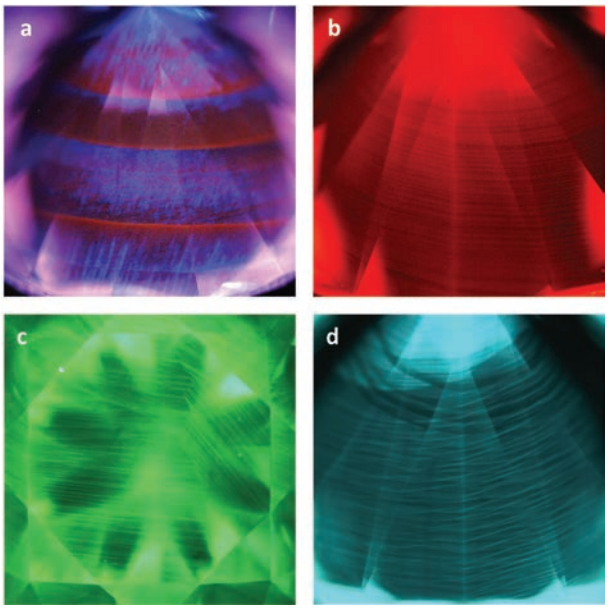

Figure 40. DiamondView deep-UV fluorescence images of CVD diamonds can help unravel their growth and treatment histories. (**a**) This 3.23 ct I color untreated CVD diamond was grown as a series of layers. Violet blue dislocation bundles are seen to propagate through the layers, with striations oriented diagonally with respect to the boundaries. The sample's overall pinkish red fluorescence originates from NV centers. Color treatments of CVD diamonds change defect concentrations and hence can modify their fluorescence colors, yet characteristic patterns such as striations and layer boundaries will remain unchanged. (**b**) This 1.23 ct Fancy Intense pink CVD diamond underwent multi-treatment to produce high concentrations of NV centers, responsible for the red fluorescence observed. HPHT decolorization treatment of these (**c**) 2.55 ct J color and (**d**) 0.41 ct G color CVD diamonds created H3 (N_2V^0) and N3 (N_3V^0) defects, producing the green to greenish blue fluorescence colors. Additionally, these two samples show green-blue phosphorescence othat may be related to N–B donor–acceptor pairs (not shown). [Image (**a**) used by permission of the Gemological Institute of America from Dieck et al. (2015) *Gems and Gemology*, Vol. 51, Fig. 23, p. 438. Images (**b**), (**c**), and (**d**) taken for GIA by Kyaw Soe Moe, Pui Lai Law, and Ellen Barrie, respectively.]

fluorescence reactions. High purity CVD diamonds with low nitrogen concentrations are characterized by low fluorescent defect content, typically only showing patchy or thread-like blue fluorescence from dislocation bundles, yet can be separated from natural Type IIa polygonized dislocation networks by careful examination (Martineau et al. 2004; Wang et al. 2005b). Such CVD diamonds are rarely grown for gem purposes due to cost. Instead, deep-UV fluorescence images of as-grown colorless, near-colorless or brown CVD diamonds usually show orange, red or pink bulk fluorescence due to NV center emission (Wang et al. 2003, 2005b, 2007b; Martineau et al. 2004; Wassell et al. 2018; McGuinness et al. 2020). They may also weakly phosphoresce orange or blue (Wang et al. 2007b; McGuinness et al. 2020). HPHT annealing for decolorization introduces H3 (N_2V^0), N3 (N_3V^0), and a series of unidentified emission peaks and bands between 430 and 500 nm (Wang et al. 2012 ; Wassell et al. 2018; McGuinness et al. 2020). Consequently, the overall fluorescence excited by deep-UV changes from the as-grown orange, red, or pink response colors to green or green-blue. Additionally, the HPHT annealed diamonds show strong green-blue phosphorescence that may be associated with N–B donor–acceptor pairs (Watanabe et al. 1997; Wang et al. 2007b, 2012; Wassell et al. 2018). Multi-treatment of CVD diamonds to produce pink body color yield high NV concentrations, resulting in intense yellowish orange, orange, reddish orange, or red fluorescence (Wang et al. 2007b, 2010).

Absorption spectroscopy and color. The vast majority of D–Z color CVD diamonds can be classified as Type IIa, although trace amounts of isolated nitrogen may be detected for poorer colors (N_S^0 peak at 1344 cm^{-1}). The rarity of this diamond type in nature, and its frequency for both HPHT- and CVD-grown diamonds emphasize that such diamonds should be treated as suspicious and undergo careful testing. FTIR spectra may aid in determining whether a CVD diamond is as-grown or treated. Hydrogen-related peaks at 8753, 7354, 6856, 6425 (also reported at 6428 cm^{-1}), 5564, and 3323 cm^{-1} (N–C–H, also reported at 3324 cm^{-1}) are exclusive to CVD diamonds, but can be reduced or removed by LPHT or HPHT decolorizing treatments (Fuchs et al. 1995a,b; Glover 2003; Charles et al. 2004; Martineau et al. 2004; Cruddace 2007; Meng et al. 2008; Liang et al. 2009; Liggins 2010). The 3123 cm^{-1} peak, identified as the neutral nitrogen-vacancy-hydrogen center (NVH^0), is also common in CVD diamonds (Fuchs et al. 1995a,b; Cruddace 2007; Khan et al. 2013). It may be useful for identification as it has not been observed for Type IIa natural diamonds, yet may be detected in some Type Ia diamonds with intense N_3VH^0 center absorption (3107 cm^{-1}) (Lai et al. 2020). NVH^0 also anneals out during HPHT treatment, but may survive LPHT treatment (Martineau et al. 2004; Cruddace 2007; Meng et al. 2008; Liang et al. 2009). The N_3VH^0 center, a common defect in natural diamonds, can be introduced by annealing at temperatures >1700 °C (Charles et al. 2004; Martineau et al. 2004; Liggins 2010; Wang et al. 2012). For more detail regarding FTIR absorption features present in as-grown and HPHT treated D–Z color CVD diamonds see the work by Martineau et al. (2004) and Wang et al. (2003, 2005b, 2007b, 2012).

UV-visible-NIR absorption spectra of CVD diamonds may have a combination of broad bands and sharper peaks contributing to their color (Fig. 41). At room temperature, colorless and near-colorless CVD diamonds are often featureless, possibly showing an absorption ramp rising from ~1200 nm to the diamond absorption edge at 225 nm. The underlying "profile" is proportional to λ^{-3} (Khan et al. 2013). The defect responsible for this gradual increase in absorption is still unclear, though it may be caused by vacancy clusters or defects with internal surfaces with sp^2-like bonding (Barnes et al. 2006; Mäki et al. 2007; Jones 2009). Thus the absorption spectra may appear similar to those of rare natural Type IIa diamonds, yet differ from those of the much more common Type Ia diamonds with Cape features. Poorer color as-grown CVD diamonds tend to have yellow, brown, or pinkish undertones, with the hue determined by the relative intensities of broad absorption features at ~270 (N_S^0), 360, 520 nm (related to NVH^0, and sometimes referred to as the 515 nm band), and the underlying profile (Martineau et al. 2004; Khan et al. 2009, 2010, 2013). Khan et al. (2009, 2010, 2013) demonstrated that these three bands are thermo- and photochromic, weakening (becoming more colorless) after heating

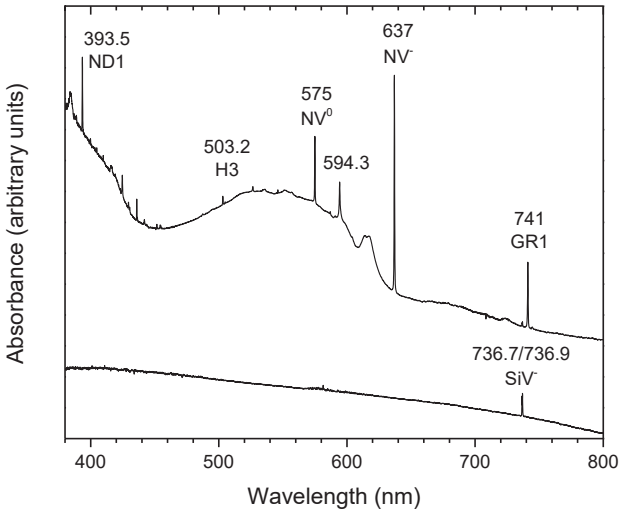

Figure 41. Representative visible-NIR absorption spectra collected at 77 K for (**bottom**) colorless and (**top**) pink CVD diamonds. The spectrum for the colorless sample (0.41 ct, F color) only shows weak absorption from the SiV^- center, transmitting most light across the visible range. A 0.48 ct Fancy Vivid purplish pink treated CVD was used for the pink example. Strongly absorbing NV centers create transmission windows around 450 nm and above 637 nm, contributing red and blue color components. Peaks at 393.5 (ND1, V^-), 594.3 (the "595 nm" center), 741 (GR1, V^0) indicate treatment. [The data for the pink CVD diamond was previously reported as sample APD-8094 in Wang et al. (2010) *Gems and Gemology*, Vol. 46, Fig. 10, p. 10.]

at 525–550 °C due to charge transfer involving $N_S^{0/+}$, $NVH^{0/-}$, and other currently unidentified defects. This effect is reversible, with UV light stimulating their increase. Annealing at temperatures greater than 1400 °C causes permanent changes to the defect structures, reducing the intensities of the featureless absorption profile, as well as the 360 and 520 nm bands, and decreasing the brown color saturation. Differences in their thermal stabilities mean that annealing at temperatures greater than 1800 °C—at which high pressures are typically used to minimize sample graphitization—results in more efficient color removal (Khan et al. 2013).

Absorption spectroscopy with cooling to liquid nitrogen temperatures may reveal the presence of additional defects, including H3 (N_2V^0, 503.2 nm), NV^0 (575 nm), NV^- (637 nm), SiV^- (736.7/736.9 nm), and an unknown CVD-specific center absorbing at 596 nm, depending on the growth and treatment history (Wang et al. 2003, 2005b, 2007b, 2012; Martineau et al. 2004). SiV^- can be detected using the more sensitive photoluminescence technique in a few natural (<1%) and HPHT diamonds (Breeding and Wang 2008; D'Haenens-Johansson et al. 2014, 2015a), but has not been reported using absorption methods, rendering it a good indicator of CVD diamond material. A peak at 946 nm has been identified as the neutral charge state of the silicon-vacancy (SiV^0), but is seldom detected (D'Haenens-Johansson et al. 2010, 2011; Breeze et al. 2020). Silicon is often unintentionally introduced into the growing CVD material by plasma etching of silicon-containing reactor components such as silica windows (Robins et al. 1989; Barjon et al. 2005). Unlike many other indicator features in CVD diamond, silicon-vacancies have excellent thermal stability and only start to anneal out at 2200 °C (Clark and Dickerson 1991). Thus SiV^- may be detected in CVD diamonds of many colors.

CVD diamonds that have been selected for irradiation and annealing treatments to produce pink color from NV centers are very weak Type Ib (sometimes referred to as "nominally Type IIa" by the gemological community), showing a sharp peak at 1344 cm^{-1} and broad band at 1130 cm^{-1} (both from N_S^0) in the IR. Their absorption features are similar to those

observed for pink treated HPHT diamonds. The UV-visible-NIR absorption spectra (Fig. 41) are dominated by NV centers, but also show other nitrogen-related features such as the 270 nm broad band from N_S^0 and the 503.2 nm peak from H3 (N_2V^0). Additionally, they include features associated with irradiation such as ND1 (V^-, 393.5 nm), GR1 (V^0, 741 nm), or irradiation and annealing such as the "595 nm" (594.3 nm) defect (Wang et al. 2010; Zaitsev et al. 2018; Song et al. 2021). FTIR spectra further indicate treatment, containing the dinitrogen ⟨001⟩ split-interstitial H1a (1450 cm^{-1}) and the 1502 cm^{-1} peak (Wang et al. 2010; Song et al. 2021). As "NV-pink" CVD samples are nitrogen-containing, the CVD-specific 3123 cm^{-1} (NVH^0) peak may be detected (Wang et al. 2010; Zaitsev et al. 2018). However, it is worth noting that this feature will be absent or weakened in samples that underwent HPHT treatment for brown color removal prior to irradiation and annealing (Wang et al. 2010; Song et al. 2021). Diamonds colored pink by NV centers are likely to be treated natural or laboratory-grown diamonds and thus should be thoroughly tested (Moses et al. 1993; Shigley et al. 2004a,b; Wang et al. 2005a,b, Eaton-Magaña et al. 2018a). Eaton-Magaña and Shigley (2016) present a succinct table comparing characteristics for such samples.

Unlike natural and HPHT diamonds, blue gem-quality CVD diamonds are rarely Type IIb crystals colored by boron. Controlled boron doping can be achieved by the addition of boron containing chemicals such as diborane (B_2H_6) to the growth gases, but synthesis is challenged by poor crystal morphology, low growth rates, and soot formation at high doping levels (Achard et al. 2012). Martineau et al. (2004) reported growing experimental boron-doped CVD diamonds with an inhomogeneous layered appearance. These samples were Fancy Light grayish blue to Fancy Deep blue in color, showed absorption spectra similar to boron-containing natural diamonds (e.g., King et al. 1998), and did not show nitrogen, hydrogen or silicon-related features to help identify their laboratory-grown origin. Boron-doped CVD overgrowth layers on natural diamonds have been observed at GIA, where 80–200 μm CVD diamond were deposited onto the stones to impart a blue color when viewed face-up. In absorption, these hybrid diamonds share properties of both the underlying natural diamond and the CVD layer, allowing identification, especially when combined with fluorescence imaging (Fritsch and Phelps 1993; Moe et al. 2017; Ardon and McElhenny 2019).

Instead of boron-doping, the most popular route to create blue colored CVD diamonds is by post-growth irradiation treatment of Type IIa samples (Ardon and Wang 2014; Moe et al. 2015; Eaton-Magaña 2018; Song et al. 2020). This introduces the GR1 (V^0) defect with a peak at 741 nm and vibronic structure absorbing in the red, as well as irradiation features such as TR12 (469.9 nm) and the 595 nm center. Irradiated CVD diamonds have a green modifier, with the color described as greenish blue or green blue, hues which account for less than 9% of blue natural diamonds (Eaton-Magaña et al. 2018b).

Unusual gray to blue color due to strong absorption from the SiV^0 center and its associated photoconductivity spectrum has also been reported for highly silicon-doped CVD diamonds (Peretti et al. 2014; D'Haenens-Johansson et al. 2015b; Eaton-Magaña and Shigley 2016; Breeze et al. 2020; Eaton-Magaña et al. 2021). SiV^0 and SiV^- are photo- and thermochromic, where the blue color can be temporarily deepened by UV illumination. Exposure to strong white light returns such diamonds to their base color, which may be gray, brownish pink or less intense blue.

Photoluminescence spectroscopy. Photoluminescence spectra collected at liquid nitrogen temperature are particularly useful for CVD diamond identification (e.g., Fig. 42), though multiple laser excitations are necessary to detect defects spanning the UV to NIR region. As-grown CVD spectra typically show emission from NV^0 (575 nm), NV^- (637 nm), often SiV^- (736.7/736.9 nm), and occasionally SiV^0 (946 nm), H3 (N_2V^0, 503.2 nm), and a peak at 389 nm (Iakoubovskii et al. 2000; Wang et al. 2003, 2005b, 2007b; Charles et al. 2004; Martineau et al. 2004; Eaton-Magaña and Shigley 2016). The latter peak, thought to be nitrogen-related, has been reported in some HPHT diamonds and in irradiated nitrogen-containing diamonds

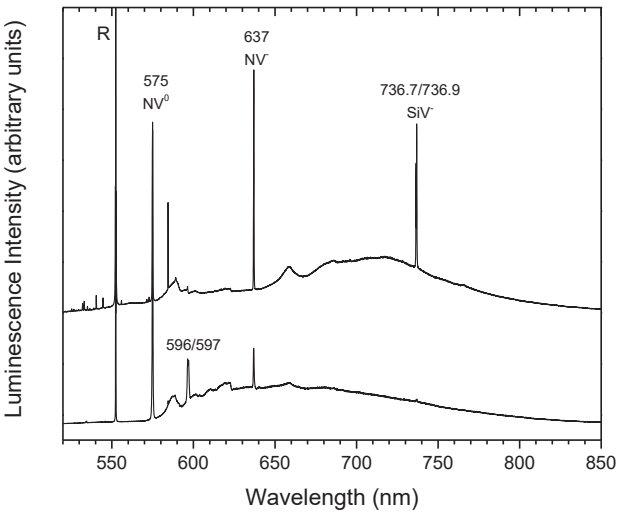

Figure 42. Photoluminescence spectra for as-grown (**bottom**) and HPHT annealed (**top**) CVD diamonds collected using 514 nm laser excitation at 77 K. Nitrogen-vacancy and silicon-vacancy centers are observed for both. SiV^- is often detected for CVD diamonds, yet extremely rare for natural diamonds (<1%), making it a good indicator for synthesis. The as-grown CVD diamond also shows a CVD-specific unassigned doublet emission at 596/597 nm. HPHT treatment removes this feature, but introduces a series of sharp peaks in the 520–580 nm region. The peak labelled R is the intrinsic diamond Raman peak.

(Collins and Woods 1987; Collins and Lawson 1989; Robins et al. 1989; Zaitsev 2000; Martineau et al. 2004). CVD-specific PL features include peaks at 468 nm (also reported at 467 nm) and 533 nm (or 534 nm), and a doublet at 596/597 nm. The center responsible for the 468 nm peak (also referred to as TR12') may involve nitrogen as the peak's intensity increases with nitrogen concentration, but has also been attributed to interstitial- or vacancy-cluster-related defects (Iakoubovskii and Adriaenssens 2000a,b; Iakoubovskii et al. 2000; Rzepka et al. 2001; Zaitsev 2001; Iakoubovskii and Stesmans 2002; Zaitsev et al. 2021). The 533 nm peak may originate from a nitrogen-vacancy type complex (Ruan et al. 1991; Zaitsev 2001). The defect emitting at 596/597 nm is unassigned, but is thought to differ from that associated with the 596 nm absorption peak in brown CVD diamonds (Martineau et al. 2004).

HPHT annealing destroys the defects responsible for the 389, 468, 533, and 596/597 nm features, while also reducing the intensity of NV centers (Charles et al. 2004; Martineau et al. 2004; Wang et al. 2012; Zaitsev et al. 2021). Yet these conditions result in the formation of more complex nitrogen-related defects such as N3 (N_3V^0, 415 nm), H3 (N_2V^0, 503.2 nm), and its negatively charged counterpart, H2 (986 nm). Additionally, the treatment introduces unidentified peaks at 850 and 875.5 nm, and a series of lines in the 451–459 and 520–580 nm regions.

The PL spectra for CVD diamonds that have been treated pink by irradiation and annealing for nitrogen-vacancy formation are unsurprisingly dominated by emission from both NV^0 and NV^- centers, but also include peaks at 389, 495.9 (H4, N_4V^0), 503.5 (3H, interstitial-related), 796.9, 806.4, and 949.0 nm (Wang et al. 2010; Eaton-Magaña and Shigley 2016; Song et al. 2021). Strong absorption from the "595 nm" (594.3 nm) and GR1 (V^0, 741 nm) centers, which overlap with the vibronic bands associated with NV^0 and NV^- luminescence, are detected as negative peaks. Further peaks will be present as outlined above, depending on whether the material was as-grown or underwent HPHT treatment prior to irradiation and annealing.

CONCLUDING REMARKS

The development and global expansion of diamond synthesis using HPHT and CVD technologies has led to rapid improvements in material quality and sizes. These dynamic and competitive fields continue to be actively researched by academic and industrial scientists alike, who characterize diamond and its crystal defects to exploit many of its unrivalled properties and find new avenues of use. The nascent laboratory-grown gem diamond sector is showing signs of maturity, benefiting from decades of synthesis research for industrial and technological applications. Despite the similarities between natural and laboratory-grown diamonds, the fundamental differences in their formation provide evidence of their growth origin, enabling their conclusive identification.

ACKNOWLEDGEMENTS

UFSDJ would like to thank the diamond research and gemology team members at GIA, whose comprehensive data collection and examination of both natural and laboratory-grown diamonds are the basis of the identification section. Also, she would like to acknowledge the work by Alex Balter (GIA) who conducted a lot of the referenced statistical analysis of diamonds submitted to our laboratories. JEB thanks the CVD diamond research community for many years of open, supportive, and collaborative discussions which rapidly advanced our understanding prior to the current commercialization efforts. ANK is deeply grateful to all the specialists who contributed to the fascinating research process of growing new and ultra large diamond crystals. Special recognition go to Mr. Roman Isakov, the Chief Technology Officer of New Diamond Technology Ltd. (NDT), for his exceptional engineering talent in the diamond production field, and to Dr. Alexander Koliadin, the former CTO of NDT, whose innovative ideas made it possible to start the growth project. Thank you also to all the teams at NDT and Alkor-D Ltd. who daily provide the technological support necessary to create world record-breaking laboratory-grown diamonds. The authors are also thankful to Dr. Sally Eaton-Magaña and Dr. Christopher M. Breeding for providing helpful comments on an early draft of the manuscript. Dr. Evan M. Smith is thanked for help with Figure 1. We are also grateful for reviews by Prof. Michael Ashfold, Dr. Boris N. Feigelson, and Dr. Daniel J. Twitchen.

REFERENCES

Achard J, Silva F, Brinza O, Tallaire A, Gicquel A (2007) Coupled effect of nitrogen addition and surface temperature on the morphology and the kinetics of thick CVD diamond single crystals. Diamond Relat Mater 16:685–689

Achard J, Issaoui R, Tallaire A, Silva F, Barjon J, Jomard F, Gicquel A (2012) Freestanding CVD boron doped diamond single crystals: A substrate for vertical power electronic devices? Phys Stat Sol (a) 209:1651–1658

Achard J, Jacques V, Tallaire A (2020) CVD diamond single crystals with NV centres: A review of material synthesis and technology for quantum sensing applications. J Phys D: Appl Phys, 53:313001

Angus JC (1994) Development of CVD diamond growth in the United States. *In*: Synthetic Diamond: Emerging CVD Science and Technology, The Electrochemical Society Series. Spear KE, Dismukes JP (eds) John Wiley, Interscience, New York, p. 21–39

Angus JC (2014) Diamond synthesis by chemical vapor deposition: The early years. Diamond Relat Mater 49:77–86

Angus JC, Sunkara M, Sahaida SR, Glass JT (1992) Twinning and faceting in early stages of diamond growth by chemical vapor deposition. J Mater Res 7:3001–3009

Ardon T, Eaton-Magaña S (2018) Lab Notes: 15 carat HPHT synthetic diamond. Gems Gemol 54:217–218

Ardon T, McElhenny G (2019) Lab Notes: CVD layer grown on natural diamond. Gems Gemol 55:97–99

Ardon T, Wang W (2014) Lab Notes: Heavily irradiated CVD synthetic diamond. Gems Gemol 50:240–241

Ashfold MNR, Goss JP, Green BL, May PW, Newton ME, Peaker CV (2020) Nitrogen in diamond. Chem Rev 120:5745–5794

Asmussen J, Grotjohn TA, Schuelke T, Becker MF, Yaran MK, King DJ, Wicklein S, Reinhard DK (2008) Multiple substrate microwave plasma-assisted chemical vapor deposition single crystal diamond synthesis. Appl Phys Lett 93:130–132

Auciello O, Sumant AV (2010) Status review of the science and technology of ultrananocrystalline diamond (UNCD ™) films and application to multifunctional devices. Diamond Relat Mater 19:699–718
Awschalom DD, Hanson R, Wrachtrup J, Zhou BB (2018) Quantum technologies with optically interfaced solid-state spins. Nat Photonics 12:516–527
Babich YV, Feigelson BN, Fisher D, Yelisseyev AP, Nadolinny VA, Baker JM (2000) The growth rate effect on the nitrogen aggregation in HPHT grown synthetic diamonds. Diamond Relat Mater 9:893–896
Babich YV, Feigelson BN, Yelisseyev AP (2004) Nitrogen aggregation and linear growth rate in HPHT synthetic diamonds. Diamond Relat Mater 13:1802–1806
Balmer RS, Brandon JR, Clewes SL, Dhillon HK, Dodson JM, Friel I, Inglis PN, Madgwick, Markham ML, Mollart TP, Perkins N, Scarsbrook GA, Twitchen DJ, Whitehead AJ, Wilman JJ, Woollard SM. (2009) Chemical vapour deposition synthetic diamond: Materials, technology and applications. J Phys: Condens Matter 21:364221
Barjon J, Rzepka E, Jomard F, Laroche, JM, Ballutaud D, Kociniewski T, Chevallier J (2005) Silicon incorporation in CVD diamond layers. Phys Stat Sol (a) 202:2177–2181
Barnes R, Bangert U, Martineau P (2006) HR-TEM imaging and image simulation of vacancy clusters in brown diamond. Phys Stat Sol (a) 203:3081–3087
Bovenkerk HP, Bundy FP, Hall HT, Strong HM, Wentorf RH (1959) Preparation of diamond. Nature 194:1094–1098
Boyd SR, Kiflawi I, Woods GS (1994) The relationship between infrared absorption and the A defect concentration in diamond. Philos Mag B 69:1149–1153
Boyd SR, Kiflawi I, Woods GS (1995) Infrared absorption by the B nitrogen aggregate in diamond. Philos Mag B 72:351–361
Branstrator B (2022) Measuring the lab-grown diamond market: Size, growth, and future opportunities. National Jeweler, *https://www.nationaljeweler.com/articles/10624-measuring-the-lab-grown-diamond-market-size-growth-and-future-opportunities*
Breeding CM, Shigley JE (2009) The "Type" classification system of diamonds and its importance in gemology. Gems Gemol 45:96–111
Breeding CM, Wang W (2008) Occurrence of the Si-V defect center in natural colorless gem diamonds. Diamond Relat Mater 17:1335–1344
Breeding CM, Eaton-Magaña S, Shigley JE (2018) Natural-color green diamonds: A beautiful conundrum. Gems Gemol 54:2–27
Breeze BG, Meara CJ, Wu XX, Michaels CP, Gupta R, Diggle PL, Dale MW, Cann BL, Ardon T, D'Haenens-Johansson UFS, Friel I, Rayson MJ, Briddon PR, Goss JP, Newton ME, Green BL (2020) Doubly charged silicon vacancy center, Si–N complexes, and photochromism in N and Si codoped diamond. Phys Rev B 101:184115
Brinza O, Achard J, Silva F, Bonnin X, Barroy P, De Corte K, Gicquel A (2008) Dependence of CVD diamond growth rate on substrate orientation as a function of process parameters in the high microwave power density regime. Phys Stat Sol (a) 205:2114–2120
Brozel MR, Evans T, Stephenson RF (1978) Partial dissociation of nitrogen aggregates in diamond by high temperature-high pressure treatments. Proc R Soc A 361:109–127
Buijnsters JG, Shankar P, van Enckevort WJP, Schermer JJ, ter Meulen JJ (2005) Adhesion analysis of polycrystalline diamond films on molybdenum by means of scratch, indentation and sand abrasion testing. Thin Solid Films 474:186–196
Bundy FP (1962) Direct conversion of graphite to diamond in static pressure apparatus. Science 137:1057–1058
Bundy FP (1963) Direct conversion of graphite to diamond in static pressure apparatus. J Chem Phys 38:631–643
Bundy FP (1980) The P, T phase and reaction diagram for elemental carbon, 1979. J Geophys Res 85:6930–6936
Bundy FP (1988) Ultra-high pressure apparatus. Phys Rep 167:133–176
Bundy FP, Hall HT, Strong HM, Wentorf RH (1955) Man-made diamonds. Nature 176:51–55
Bundy FP, Bassett WA, Wathers MS, Hemley RJ, Mao HK, Goncharov AF (1996) The pressure-temperature phase and transformation diagram for carbon; updated through 1994. Carbon 34:141–153
Burns RC, Cvetkovic V, Dodge CN, Evans DJF, Rooney MLT, Spear PM, Welbourn CM (1990) Growth-sector dependence of optical features in large synthetic diamonds. J Cryst Growth 104:257–279
Burns RC, Hansen JO, Spits RA, Sibanda M, Welbourn CM, Welch DL (1999) Growth of high purity large synthetic diamond crystals. Diamond Relat Mater 8:1433–1437
Burns RC, Chumakov AI, Connell SH, Dube D, Godfried HP, Hansen JO, Härtwig J, Hoszowska J, Masiello F, Mkhonza L, Rebak M, Rommevaux A, Setshedi R, Van Vaerenbergh P (2009) HPHT growth and x-ray characterization of high-quality Type IIa diamond. J Phys: Condens Matter 21:364224
Burton NC, Steeds JW, Meaden GM, Shreter YG, Butler JE (1995) Strain and microstructure variation in grains of CVD diamond film. Diamond Relat Mater 4:1222–1234
Butler JE, Oleynik I (2008) A mechanism for crystal twinning in the growth of diamond by chemical vapour deposition. Philos Trans R Soc, A 366:295–310
Butler JE, Sumant AV (2008) The CVD of nanodiamond materials. Chem Vap Deposition 14:145–160
Butler JE, Windischmann H (1998) Developments in CVD-diamond synthesis during the past decade. MRS Bull 23:22–27
Butler JE, Woodin RL (1993) Thin-film diamond growth mechanisms. Philos Trans R Soc, A 342:209–224

Butler JE, Celii FG, Oakes DB, Hanssen LM, Carrington WA, Snail KA (1989) Studies of diamond chemical vapor-deposition. High Temp Sci 27:183–197
Butler JE, Cheesman A, Ashfold MNR (2009a) Recent progress in the understanding of CVD growth of diamond. *In*: CVD Diamond for Electronic Devices and Sensors. Sussmann RS (ed) John Wiley & Sons, Chichester, p 103–124
Butler JE, Mankelevich YA, Cheesman A, Ma J, Ashfold MNR (2009b) Understanding the chemical vapor deposition of diamond: Recent progress. J Phys: Condens Matter 21:364201
Byrne KS, Anstie JD, Chapman JG, Luiten AN (2012) Optically reversible photochromism in natural pink diamond. Diamond Relat Mater 30:31–36
Byrne KS, Chapman JG, Luiten AN (2014a) Photochromic charge transfer processes in natural pink and brown diamonds. J Phys: Condens Matter 26:035501
Byrne KS, Chapman JG, Luiten AN (2014b) Corrigendum: Photochromic charge transfer processes in natural pink and brown diamonds (2014 J. Phys.: Condens. Matter 26 035501). J Phys: Condens Matter 26:239502
Calvert JG, Pitts JN (1966) Photochemistry. John Wiley & Sons, New York
Celii FG, Butler JE (1989) Hydrogen atom detection in the filament-assisted diamond deposition environment. Appl Phys Lett 54:1031–1033
Celii FG, Butler JE (1991) Diamond chemical vapor deposition. Annu Rev Phys Chem 42:643–684
Celii FG, Pehrsson PE, Wang HT, Butler JE (1988) Infrared detection of gaseous species during the filament-assisted growth of diamond. Appl Phys Lett 52:2043–2045
Celii FG, Thorsheim HR, Butler JE (1990a) In-situ THG detection of gas phase atomic hydrogen in diamond CVD processes. Carbon 28:808
Celii FG, Thorsheim HR, Butler JE, Plano LS, Pinneo JM (1990b) Detection of ground-state atomic-hydrogen in a dc plasma using third-harmonic generation. J Appl Phys 68:3814–3817
Chalain J-P (2003) Gem News International: A natural yellow diamond with nickel-related optical centers. Gems Gemol 39:325–326
Charles SJ, Butler JE, Feygelson BN, Newton ME, Carroll DL, Steeds JW, Darwish H, Yan CS, Mao HK, Hemley RJ (2004) Characterization of nitrogen doped chemical vapor deposited single crystal diamond before and after high pressure, high temperature annealing. Phys Stat Sol (a) 201:2473–2485
Chayahara A, Mokuno Y, Horino Y, Takasu Y, Kato H, Yoshikawa H, Fujimori N (2004) The effect of nitrogen addition during high-rate homoepitaxial growth of diamond by microwave plasma CVD. Diamond Relat Mater 13:1954–1958
Chen N, Ma H, Yan B, Chen L, Chen L, Guo L (2018) Characterization of various centers in synthetic Type Ib diamond under HPHT annealing. Cryst Growth Des 18:3870–3876
Chrenko RM, Strong HM, Tuft RE (1971) Dispersed paramagnetic nitrogen content of large laboratory diamonds. Philos Mag 23:313–318
Chrenko RM, Tuft RE, Strong HM (1977) Transformation of the state of nitrogen in diamond. Nature 270:141–144
Chu HN, Denhartog EA, Lefkow AR, Jacobs J, Anderson LW, Lagally MG, Lawler JE (1991) Measurements of the gas kinetic temperature in a CH_4-H_2 discharge during the growth of diamond. Phys Rev A 44:3796–3803
Clark CD (1959) The absorption edge spectrum of diamond. J Phys Chem Solids 8:481–484
Clark CD, Dickerson CB (1991) The 1.681 eV centre in polycrystalline diamond. Surf Coat Tech 47:336–343
Clark CD, Walker J (1973) The neutral vacancy in diamond. Proc R Soc Lond A 334:241–257
Clark CD, Ditchburn RW, Dyer HB (1956) The absorption spectra of irradiated diamonds after heat treatment. Proc R Soc Lond A 237:75–89
Clark CD, Kanda H, Kiflawi I, Sittas G (1995) Silicon defects in diamond. Phys Rev B 51:16681–16688
Clausing RE, Heatherly L, More KL, Begun GM (1989) Electron-microscopy of the growth features and crystal-structures of filament assisted CVD diamond films. Surf Coat Technol 39:199–210
Cobb SJ, Ayres ZJ, Macpherson JV (2018) Boron doped diamond: A designer electrode material for the twenty-first century. Ann Rev Anal Chem 11:463–484
Collins AT (1978) Investigating artificially coloured diamonds. Nature 273:654–655
Collins AT (1980) Vacancy enhanced aggregation of nitrogen in diamond. J Phys C: Solid State Phys 13:2641–2650
Collins AT (1982) Colour centres in diamond. J Gemmol 18:37–75
Collins AT (1989) The polarised absorption and cathodoluminescence associated with the 1.40 eV centre in synthetic diamond. J Phys: Condens Matter 1:439–450
Collins AT (1992) The characterisation of point defects in diamond by luminescence spectroscopy. Diamond Relat Mater 1:457–469
Collins AT (1993a) Intrinsic and extrinsic absorption and luminescence in diamond. Phys B 185:284–296
Collins AT (1993b) The optical and electronic properties of semiconducting diamond. Phil Trans R Soc Lond A 342:233–244
Collins AT (2000) Spectroscopy of defects and transition metals in diamond. Diamond Relat Mater 9:417–423
Collins AT (2001) The colour of diamond and how it may be changed. J Gemmol 27:341–359
Collins AT, Lawson SC (1989) Cathodoluminescence studies of isotope shifts associated with localised vibrational modes in synthetic diamond. J Phys: Condens Matter 39:6929–6937
Collins AT, Spear PM (1982) Optically active nickel in synthetic diamond. J Phys D: Appl Phys 15:83–87
Collins AT, Spear PM (1983) The 1.40 eV and 2.56 eV centres in synthetic diamond. J Phys C: Solid State Phys 16:963–973

Collins AT, Williams AWS (1971) The nature of the acceptor centre in semiconducting diamond. J Phys C: Solid State Phys 4:1789–1800
Collins AT, Woods GS (1982) An anomaly in the infrared absorption spectrum of synthetic diamond. Philos Mag B 46:77–83
Collins AT, Woods GS (1987) Isotope shifts of nitrogen-related localised mode vibrations in diamond. J Phys C: Solid State Phys 20:L797–L801
Collins AT, Davies G, Kanda H, Woods GS (1988) Spectroscopic studies of carbon-13 synthetic diamond. J Phys C: Solid State Phys 21:1363–1376
Collins AT, Kanda H, Burns RC (1990) The segregation of nickel-related optical centres in the octahedral growth sectors of synthetic diamond. Philos Mag B 61:797–810
Coulson CA, Larkins FP (1971) Isolated single vacancy in diamonds - I. Electronic structure. J Phys Chem Solids 32:2245–2257
Crisci A, Baillet F, Mermoux M, Bogdan G, Nesládek M, Haenen K (2011) Residual strain around grown-in defects in CVD diamond single crystals: A 2D and 3D Raman imaging study. Phys Stat Sol (a) 208:2038–2044
Crowningshield R (1971) General Electric's cuttable synthetic diamonds. Gems Gemol 2:302–314
Cruddace RC (2007) Magnetic Resonance and Optical Studies of Point Defects in Single Crystal CVD Diamond. PhD Dissertation, University of Warwick, Coventry, United Kingdom
Davies G (1976) The A nitrogen aggregate in diamond—its symmetry and possible structure. J Phys C: Solid State Phys 9: L537–L542
Davies G (1977) Charge state of the vacancy in diamond. Nature 269:498–500
Davies G (1981) Decomposing the IR absorption spectra of diamonds. Nature 290:40–41
Davies G, Hamer MF (1976) Optical studies of the 1.945 eV vibronic band in diamond. Proc R Soc Lond A 348:285–298
Davies G, Nazaré MH (1980) Uniaxial stress splitting of E to E transitions at trigonal centres in cubic crystals: The 594 nm band in diamond. J Phys C: Solid State Phys 13:4127–4136
Davies G, Nazaré MH, Hamer MF (1976) H3 (2.463 eV) vibronic band in diamond: Uniaxial stress effects and the breakdown of mirror symmetry. Proc R Soc Lond A 351:245–265
Davies G, Welbourn CM, Loubser JHN (1978) Optical and electron paramagnetic effects in yellow Type Ia diamonds. Diamond Res 23–30
Davies G, Neves AJ, Nazaré MH (1989) Nickel isotope effects in the 1.4 eV centre in synthetic diamond. Europhys Lett 9:47–52
Davies G, Lawson SC, Collins AT, Mainwood A, Sharp SJ (1992) Vacancy-related centers in diamond. Phys Rev B 46:13157–13170
Dean PJ (1965) Bound exciton and donor-acceptor pairs in natural and synthetic diamond. Phys Rev 139:A588-A602
Deljanin B, Alessandri M, Peretti A, Åström (2015) NDT breaking the 10 carat barrier: World record faceted and gem-quality synthetic diamonds investigated. Contrib Gemol 15:1–7, *http://gemresearch.ch/ndt-breaking-the-10-carat-barrier-world-record-faceted-and-synthetic-diamonds-investigated/*
de Sa ES, Davies G (1977) Uniaxial stress studies of the 2.498 eV (H4), 2.417 eV and 2.536 eV vibronic bands in diamond. Proc R Soc Lond A 357:231–251
de Theije FK, Schermer JJ, van Enckevort WJP (2000) Effects of nitrogen impurities on the CVD growth of diamond: Step bunching in theory and experiment. Diamond Relat Mater 9:1439–1449
D'Haenens-Johansson UFS, Edmonds AM, Newton ME, Goss JP, Briddon PR, Baker JM, Martineau PM, Khan RUA, Twitchen DJ, Williams SD (2010) EPR of a defect in CVD diamond involving both silicon and hydrogen that shows preferential alignment. Phys Rev B 82:155205
D'Haenens-Johansson UFS, Edmonds AM, Green BL, Newton ME, Davies G, Martineau PM, Khan RUA, Twitchen DJ (2011) Optical properties of the neutral silicon split-vacancy center in diamond. Phys Rev B 84:245208
D'Haenens-Johansson UFS, Moe KS, Johnson P, Wong SY, Lu R, Wang W (2014) Near-colorless HPHT synthetic diamonds from AOTC Group. Gems Gemol 50:30–45
D'Haenens-Johansson UFS, Katrusha AN, Moe KS, Johnson P, Wang W (2015a) Large colorless HPHT-grown synthetic gem diamonds from New Diamond Technology, Russia. Gems Gemol 51:260–279
D'Haenens-Johansson U.F.S., Ardon T., Wang W. (2015b) CVD synthetic gem diamonds with high silicon-vacancy concentrations. Conference on New Diamond and Nano Carbons, Shizuoka, Japan, May 2015
Dieck C, Loudin L, D'Haenens-Johansson UFS (2015) Lab Notes: Two large CVD-grown synthetic diamonds tested by GIA. Gems Gemol 51:437–439
Doherty MW, Manson NB, Delaney P, Jelezko F, Wrachtrup J, Hollenberg LCL (2013) The nitrogen-vacancy colour centre in diamond. Phys Rep 528:1–45
Donato N, Rouger N, Pernot J, Longobardi G, Udrea F (2019) Diamond power devices: State of the art, modelling, figures of merit and future perspective. J Phys D: Appl Phys 53:093001
Dyer HB, Du Preez L (1965) Irradiation damage in Type I diamond. J Chem Phys 42:1898–1906
Dyer HB, Raal FA, Du Preez L, Loubser JHN (1965) Optical absorption features associated with paramagnetic nitrogen in diamond. Philos Mag 11:763–774
Eaton-Magaña S (2018) Lab Notes: Three irradiated CVD synthetic diamonds. Gems Gemol 54:215–216
Eaton-Magaña S (2019) Lab Notes: Faint green HPHT synthetic diamonds. Gems Gemol 55:99–101

Eaton-Magaña S, Breeding CM (2016) An introduction to photoluminescence spectroscopy for diamond and its application in gemology. Gems Gemol 52:2–17
Eaton-Magaña S, Lu R (2011) Phosphorescence in Type IIb diamonds. Diamond Relat Mater 20:983–989
Eaton-Magaña S, Shigley JE (2016) Observations on CVD-grown synthetic diamonds: A review. Gems Gemol 52:222–245
Eaton-Magaña S, Post JE, Heaney PJ, Freitas J, Klein P, Walters R, Butler JE (2008) Using phosphorescence as a fingerprint for the Hope and other blue diamonds. Geology 36:83–86
Eaton-Magaña S, Shigley JE, Breeding CM (2017) Observations on HPHT-grown synthetic diamonds: a review. Gems Gemol 53:262–284
Eaton-Magaña S, Ardon T, Smit KV, Breeding CM, Shigley JE (2018a) Natural-color pink, purple, red, and brown diamonds: Band of many colors. Gems Gemol 54:352–377
Eaton-Magaña S, Breeding CM, Shigley JE (2018b) Natural-color blue, gray, and violet diamonds: Allure of the deep. Gems Gemol 54:112–131
Eaton-Magaña S, McElhenny G, Breeding CM, Ardon T (2020) Comparison of gemological and spectroscopic features in Type IIa and Ia natural pink diamonds. Diamond Relat Mater 105:107784
Eaton-Magaña S, Ardon T, Breeding CM (2021) Laboratory-grown diamond: A gemological laboratory perspective. J Gems Gemmol 23:25–39
Edmonds AM, D'Haenens-Johansson UFS, Cruddace RJ, Newton ME, Fu K-MC, Santori C, Beausoleil RG, Twitchen DJ, Markham ML (2012) Production of oriented nitrogen-vacancy color centers in synthetic diamond. Phys Rev B 86:035201
Evans T (1979) Changes produced by high temperature treatment of diamond. *In*: The Properties of Diamond. Field JE, (ed) Academic Press, London, p 403–424
Evans T, Qi Z (1982) The kinetics of the aggregation of nitrogen atoms in diamond. Proc R Soc Lond A 381:159–178
Evans T, Qi Z, Maguire J (1981) The stages of nitrogen aggregation in diamond. J Phys C 14:379–384
Eversole WG (1962) Synthesis of diamond, US3030187 and US3003188
Fedoseev DV (1994) Summary of research on diamond growth from the gas phase in Russia. *In*: Synthetic Diamond: Emerging CVD Science and Technology, The Electrochemical Society Series. Spear KE, Dismukes JP (eds) John Wiley, Interscience, New York, p 41–56
Feigelson BN (1983) Some questions of pressure generation in the multianvil apparatus. *In:* Silicate Systems at High Pressures, Proceedings of the Institute of Geology and Geophysics. Siberian Branch of the Academy of Sciences of the USSR, Novosibirsk, p 62–76 (in Russian)
Field JE (2012) The mechanical and strength properties of diamond, Rep Prog Phys 72:126505
Fisher D, Sibley SJ, Kelly CJ (2009) Brown colour in natural diamond and interaction between the brown related and other colour-inducing defects. J Phys: Condens Matter 21:364213
Frank FC, Lang AR, Evans DJF, Rooney MLT, Spear PM, Welbourn CM (1990) Orientation-dependent nitrogen incorporation on vicinals on synthetic diamond cube growth surfaces. J Cryst Growth 100:354–376
Friel I, Clewes SL, Dhillon HK, Perkins N, Twitchen DJ, Scarsbrook GA (2009) Control of surface and bulk crystalline quality in single crystal diamond grown by chemical vapour deposition. Diamond Relat Mater 18:808–815
Fritsch E (1998) The nature of color in diamonds. *In*: The Nature of Diamonds. Harlow G (ed) Cambridge University Press, Cambridge, p 23–47
Fritsch E, Phelps AW (1993) Type IIb diamond thin films deposited onto near-colorless natural gem diamonds. Diamond Relat Mater 2:70–74
Fritsch E, Shigley J (1989) Contribution to the identification of treated colored diamonds: diamonds with peculiar color-zoned pavilions. Gems Gemol 25:95–101
Fritsch E, Shigley JE (1993) The separation of natural from synthetic gem-quality diamonds on the basis of crystal growth criteria. J Cryst Growth 128:425–428
Fuchs F, Wild C, Schwarz K, Koidl P (1995a) Hydrogen-related IR absorption in chemical vapour deposited diamond. Diamond Relat Mater 4:652–656
Fuchs F, Wild C, Schwarz K, Müller-Sebert W, Koidl P (1995b) Hydrogen induced vibrational and electronic transitions in chemical vapor deposited diamond, identified by isotopic substitution. Appl Phys Lett 66:177–179
Fujita N, Blumenau AT, Jones R, Öberg S, Briddon PR (2006) Theoretical studies on ⟨100⟩ dislocations in single crystal CVD diamond. Phys Stat Sol (a) 203:3070–3075
Gaillou E, Post JE, Bassim ND, Zaitsev AM, Rose T, Fries MD, Stroud RM, Steele A, Butler JE (2010) Spectroscopic and microscopic characterizations of color lamellae in natural pink diamonds. Diamond Relat Mater 19:1207–1220
Gallheber BC, Fischer M, Mayr M, Straub J, Schreck M (2018) Growth, stress, and defects of heteroepitaxial diamond on Ir/YSZ/Si(111). J Appl Phys 123:225302
Gaukroger MP, Martineau PM, Crowder MJ, Friel I, Williams SD, Twitchen DJ (2008) X-ray topography studies of dislocations in single crystal CVD diamond. Diamond Relat Mater 17:262–269
Glover C (2003) A Study of Defects in Single Crystal CVD Diamond. PhD Dissertation, University of Warwick, Coventry, United Kingdom
Goodwin DG, Butler JE (1997) Theory of diamond chemical vapor deposition. *In*: Handbook of Industrial Diamonds. Prelas MA, Popovici G, Bigelow LK (eds) Marcel Dekker, New York, p 527–581

Goss JP, Jones R, Breuer SJ, Briddon PR, Öberg S (1996) The twelve-line 1.682 eV luminescence center in diamond and the vacancy-silicon complex. Phys Rev Lett 77:3041–3044
Goss JP, Briddon PR, Jones R, Öberg S (2004) The lattice location of Ni in diamond: A theoretical study. J Phys C: Condens Matter 16:4567–4578
Goss JP, Briddon PR, Hill V, Jones R, Rayson MJ (2014) Identification of the structure of the 3107 cm^{-1} H-related defect in diamond. J Phys: Condens Matter 14:145801
Green BL, Mottishaw S, Breeze BG, Edmonds AM, D'Haenens-Johansson UFS, Doherty MW, Williams SD, Twitchen DJ, Newton ME (2017) Neutral silicon-vacancy center in diamond: Spin polarization and lifetimes. Phys Rev Lett 119:096402
Green BL, Doherty MW, Nako E, Manson NB, D'Haenens-Johansson UFS, Williams SD, Twitchen DJ, Newton ME (2019) Electronic structure of the neutral silicon-vacancy center in diamond. Phys Rev B 99:161112(R)
Green BL, Collins AL, Breeding CM (2022) Diamond spectroscopy, defect centers, diamond color and treatments. Rev Mineral Geochem XX:xxx-xxx
Hainschwang T, Katrusha A (2003) Gem News International: A bicolored synthetic diamond. Gems Gemol 39:163–164
Hall HT (1960a) High temperature high pressure apparatus, US2941248
Hall HT (1960b) Ultra-high-pressure, high-temperature apparatus: The "belt." Rev Sci Instrum 31:125–131
Hamza AV, Kubiak GD, Stulen RH (1990) Hydrogen chemisorption and the structure of the diamond C(100)-(2×1) surface. Surf Sci 237:35–52
Hanssen LM, Carrington WA, Butler JE, Snail KA (1988) Diamond synthesis using an oxygen-acetylene torch. Mater Lett 7:289–292
Harris JW, Smit KV, Fedortchouck Y, Moore M (2022) Morphology of monocrystalline diamond and its inclusions. Rev Mineral Geochem XX:xxx-xxx
Harris SJ, Weiner AM (1990) Methyl radical and H-atom concentrations during diamond growth. J Appl Phys 67:6520–6526
Harris SJ, Weiner AM, Perry TA (1988) Measurement of stable species present during filament-assisted diamond growth. Appl Phys Lett 53:1605–1607
Hepp C, Müller T, Waselowski V, Becker JN, Pingault B, Sternschulte H, Steinmüller-Nethl D, Gali A, Maze JR, Atatüre M, Becher C (2014) Electronic structure of the silicon vacancy color center in diamond. Phys Rev Lett 112:036405
Hofer S (1985) Pink diamonds from Australia. Gems Gemol 21:147–155
Howell D (2012) Strain-induced birefringence in natural diamond: A review. Eur J Mineral 24:575–585
Howell D, Fisher D, Piazolo S, Griffin WL, Sibley SJ (2015) Pink color in Type I diamonds: Is deformation twinning the cause? Am Mineral 100:1518–1527
Howell D, Collins AT, Loudin LC, Diggle PL, D'Haenens-Johansson UFS, Smit KV, Katrusha AN, Butler JE, Nestola F (2019) Automated FTIR mapping of boron distribution in diamond. Diamond Relat Mater 96:207–215
Hsu WL (1991) Mole fractions of H, CH_3, and other species during filament-assisted diamond growth. Appl Phys Lett 59:1427–1429
Hsu WL, McMaster MC, Coltrin ME, Dandy DS (1994) Molecular-beam mass-spectrometry studies of chemical-vapor-deposition of diamond. Jpn J Appl Phys 33:2231–2239
Iakoubovskii K, Adriaenssens GJ (2000a) Luminescence excitation spectra in diamond. Phys Rev B 61:174–182
Iakoubovskii K, Adriaenssens GJ (2000b) Optical study of some interstitial-related centres in CVD diamond. Phys Stat Sol (a) 181:59–64
Iakoubovskii K, Adriaenssens GJ (2002) Evidence for a Fe-related defect centre in diamond. J Phys C: Condens Matter 14:L95–L98
Iakoubovskii K, Stesmans A (2002) Chemical vapour deposition diamond studied by optical and electron spin resonance techniques. J Phys: Condens Matter 14:R467–R499
Iakoubovskii K, Adriaenssens GJ, Vohra YK (2000) Nitrogen incorporation in diamond films homoepitaxially grown by chemical vapour deposition. J Phys C: Condens Matter 12:L519–L524
Iakoubovskii K, Adriaenssens GJ, Dogadkin NN, Shiryaev AA (2001) Optical characterization of some irradiation-induced centers in diamond. Diamond Relat Mater 10:18–26
Iakoubovskii K, Kiflawi I, Johnston K, Collins A, Davies G, Stesmans A (2003) Annealing of vacancies and interstitials in diamond. Phys B 340–342:67–75
IGI (2022) IGI analyzes record 150 carat rough lab grown diamond. IGI Press Room, *https://www.igi.org/press/igi-analyzes-record-150-carat-rough-lab-grown-diamond*
Inspektor A, Liou Y, McKenna T, Messier R (1989) Plasma CVD diamond deposition in C–H–O systems. Surf Coat Technol 39:211–221
Irifune T, Kurio A, Sakamoto S, Inoue T, Sumiya H (2003) Ultrahard polycrystalline diamond from graphite. Nature 421:599–560
Irifune T, Kurio A, Sakamoto S, Inoue T, Sumiya H, Funakoshi K-I (2004) Formation of pure polycrystalline diamond by direct conversion of graphite at high pressure and high temperature. Phys Earth Planet Inter 143:593–600
Irifune T, Isobe F, Shinmei T (2014) A novel large-volume Kawai-type apparatus and its application to the synthesis of sintered bodies of nano-polycrystalline diamond. Phys Earth Planet Inter 228:255–261

Isberg J, Hammersberg J, Johansson E, Wikström T, Twitchen DJ, Whitehead AJ, Coe SE, Scarsbrook GA (2002) High carrier mobility in single-crystal plasma-deposited diamond. Science 297:1670–1672

Isoya J, Kanda H, Uchida Y (1990) EPR studies of interstitial Ni centers in synthetic diamond crystals. Phys Rev B 42:9843–9852

Jacob DE, Kronz A, Viljoen KS (2004) Cohenite, native iron and troilite inclusions in garnets from polycrystalline diamond ag- gregates. Contrib Mineral Petrol 146:566–576

Janssen G, van Enckevort WJ, Vollenberg W, Giling LJ (1992) Characterization of single-crystal diamond grown by chemical vapour deposition processes. Diamond Relat Mater 1:789–800

Johnson CE, Weimer WA, Hasting MAS (1990) Mass-spectroscopy of deposition exhaust-gases and oxidation of diamond films. Carbon 28:791–791

Johnson P, Myagkaya E (2017) Lab Notes: HPHT synthetic diamond with intense green color. Gems Gemol 53:96–98

Jones R (2009) Dislocations, vacancies and the brown colour of CVD and natural diamond. Diamond Relat Mater 18:820–826

Jones R, Briddon PR, Öberg S (1992) First-principles theory of nitrogen aggregates in diamond. Philos Mag Lett 66:67–74

Jones R, Torres VJB, Briddon PR, Öberg S (1994) Theory of nitrogen aggregates in diamond: The H3 and H4 defects. Mater Sci Forum 143–147:45–50

Jones R, Hounsome LS, Fujita N, Öberg S, Briddon PR (2007) Electrical and optical properties of multivacancy centres in diamond. Phys Stat Sol (a) 204:3059–3064

Kaminsky FV, Wirth R (2011) Iron carbide inclusions in lower- mantle diamond from Juina, Brazil. Can Mineral 49:555–572

Kammerling RC, Reinitz I, Fritsch E (1995) Lab Notes: Synthetic diamond suite. Gems Gemol 31:122–123

Kanda H (2000) Large diamonds grown at high pressure conditions. Braz J Phys 30:482–489

Kanda H (2005) Crystal growth of diamond. *In:* Bulk Crystal Growth of Electronic, Optical and Optoelectronic Materials. Capper P (ed) John Wiley & Sons, Ltd., Chichester, p 407–432

Kanda H, Lawson SC (1995) Growth temperature effects of impurities in HP/HT diamonds. Industrial Diamond Rev. 55:56–61

Kanda H, Watanabe K (1999) Distribution of nickel related luminescence centers in HPHT diamond. Diamond Relat Mater 8:1463–1469

Kanda H, Yamaoka S (1993) Inhomogeneous distribution of nitrogen impurities in {111} growth sectors of high pressure synthetic diamond. Diamond Relat Mater 2:1420–1423

Kanda H, Akaishi M, Setaka N, Yamaoka S, Fukunaga O (1980) Surface structures of synthetic diamonds. J Mater Sci 15:2743–2748

Kanda H, Ohsawa T, Fukunaga O, Sunagawa I (1989) Effect of solvent metals upon the morphology of synthetic diamonds. J Cryst Growth 94:115–124

Kanda H, Ohsawa T, Yamaoka S (1990) Formation of nitrogen pairs in synthetic diamond during growth. *In*: Science and Technology of New Diamond. Saito S, Fukunaga O, Yoshikawa M (eds) KTK Scientific Publishers/Terra Scientific Publishing Co., Tokyo, p 1420–1423

Kane RE (1980) The elusive nature of graining in gem quality diamonds. Gems Gemol 16:294–314

Kazuchits NM, Rusetsky MS, Kazuchits, VN, Zaitsev AM (2016) Aggregation of nitrogen in synthetic diamonds annealed at high temperature without stabilizing pressure. Diamond Relat Mater 64:202–207

Kennedy L, Johnson P (2016) Lab Notes: Yellow synthetic diamond with nickel-related green fluorescence. Gems Gemol 52:196–197

Khan RUA, Martineau PM, Cann BL, Newton ME, Twitchen DJ (2009) Charge transfer effects, thermo and photochromism in single crystal CVD synthetic diamond. J Phys: Condens Matter 21:364214

Khan RUA, Martineau PM, Cann BL, Newton ME, Dhillon HK, Twitchen DJ (2010) Color alterations in CVD synthetic diamond with heat and UV exposure: Implications for color grading and identification. Gems Gemol 46:18–26

Khan RUA, Cann BL, Martineau PM, Samartseva J, Freeth JJP, Sibley SJ, Hartland CB, Newton ME, Dhillon HK, Twitchen DJ (2013) Colour-causing defects and their related optoelectronic transitions in single crystal CVD diamond. J Phys: Condens Matter 25:275801

Khvostantsev LG, Slesarev VN, Brazhkin VV (2004) Toroid type high-pressure device: History and prospects. High Pressure Res 24:317–383

Kiflawi I, Mayer AE, Spear PM, Van Wyk JA, Woods GS (1994) Infrared absorption by the single nitrogen and A defect centres in diamond. Philos Mag B 69:1141–1147

Kiflawi I, Fisher D, Kanda H, Sittas G (1996) The creation of the 3107 cm^{-1} hydrogen absorption peak in synthetic diamond single crystals. Diamond Relat Mater 5:1516–1518

Kiflawi I, Kanda H, Mainwood A (1998) The effect of nickel and the kinetics of the aggregation of nitrogen in diamond. Diamond Relat Mater 7:327–332

Kim JR, Kim D-K, Zhu H, Abbaschian R (2011) High pressure and high temperature annealing on nitrogen aggregation in lab-grown diamonds. J Matter Sci 46:6264–6272

King JM, Moses TM, Shigley JE, Liu Y (1994) Color grading of colored diamonds in the GIA Gem Trade Laboratory. Gems Gemol 30:220–242
King JM, Moses TM, Shigley JE, Welbourn CM, Lawson SC, Cooper M (1998) Characterizing natural-color Type IIb blue diamonds. Gems Gemol 34:246–268
King JM, Shigley JE, Guhin SS, Gelb TH, Hall M (2002) Characterization and grading of natural-color pink diamonds. Gems Gemol 38:128–147
King JM, Shigley JE, Gelb TH, Guhin SS, Hall M, Wang W (2005) Characterization and grading of natural-color yellow diamonds. Gems Gemol 41:88–115
King JM, Geurts RH, Gilbertson AM, Shigley JE (2008) Color grading "D-to-Z" diamonds at the GIA Laboratory. Gems Gemol 44:296–321
Kocherzhinski YA, Kulik OG (1996) Equilibrium phase diagrams and manufacture of synthetic diamonds. Powder Metall Met Ceram 35:470–483
Kohn JA (1958) Twinning in diamond-type structures: a proposed boundary-structure model. Am Mineral 43:263–284
Koivula JI, Fryer CW (1984) Identifying gem-quality synthetic diamonds: An update. Gems Gemol 20:146–158
Koizumi S, Kamo M, Sato Y, Mita S, Sawabe A, Reznik A, Uzan-Saguy C, Kalish R (1998) Growth and characterization of phosphorus doped n-type diamond thin films. Diamond Relat Mater 7:540–544
Koizumi S, Umezawa H, Pernot J, Suzuki M (eds) (2018) Power Electronics Device Applications of Diamond Semiconductors. Woodhead Publishing, Duxford
Kolchin AV, Veprintsev VI, Klyachko LI, Novgorodov AS, Zubkov VM, Vereschagin LF, Khvostantsev LG, Novikov AP, Yanshin SI, Yanshina KM, Yanshina ES, Yanshin IS, Yanshina ZP (1981) Device for building-up high pressure. UA4290741
Koleske DD, Gates SM, Thoms BD, Russell JN, Butler JE (1994) Isothermal desorption of hydrogen from polycrystalline diamond films. Surf Sci 320:L105–L111
Koleske DD, Gates SM, Thoms BD, Russell JN, Butler JE (1995) Hydrogen on polycrystalline diamond films: Studies of isothermal desorption and atomic deuterium abstraction. J Chem Phys 102:992–1002
Kupriyanov IN, Khokhryakov AF, Borzdov YM, Palyanov YN (2016) HPHT growth and characterization of diamond from a copper-carbon system. Diamond Relat Mater 69:198–206
Lai MY, Breeding CM, Stachel T, Stern RA (2020) Spectroscopic features of natural and HPHT-treated yellow diamonds. Diamond Relat Mater 101:107642
Lang AR (1967) Causes of birefringence in diamond. Nature 213:248–251
Lang A (1979) Internal structure. *In*: The Properties of Diamond. Field JE, (ed) Academic Press, London, p 425–469
Lang AR, Moore M, Makepeace APW, Wierzchowski W, Welbourn CM (1991) On the dilatation of synthetic Type Ib diamond by substitutional nitrogen impurity. Phil Trans R Soc Lond A 337:497–520
Lang AR, Vincent R, Burton NC, Makepeace APW (1995) Studies of small inclusions in synthetic diamonds by optical microscopy, microradiography and transmission electron microscopy. J Appl Cryst 28:690–699
Lang AR, Yelisseyev AP, Pokhilenko NP, Steeds JW, Wotherspoon A (2004) Is dispersed nickel in natural diamonds associated with cuboid growth sectors in diamonds that exhibit a history of mixed-habit growth? J Cryst Growth 263:575–589
Law PL, Wang W (2016) Lab Notes: CVD synthetic diamond over 5 carats identified. Gems Gemol 52:414–416
Lawson SC, Kanda H (1993a) An annealing study of nickel point defects in high-pressure synthetic diamond. J Appl Phys 73:3967–3973
Lawson SC, Kanda H (1993b) Nickel in diamond: an annealing study. Diamond Relat Mater 2:130–135
Lawson SC, Davies G, Collins AT, Mainwood A (1992) The 'H2' optical transition in diamond: The effects of uniaxial stress perturbations, temperature and isotopic substitution. J phys: Condens Matter 4:3439–3452
Lawson SC, Kanda H, Watanabe K, Kiflawi I, Sato Y, Collins AT (1996) Spectroscopic study of cobalt-related optical centers in synthetic diamond. J Appl Phys 79:4348–4357
Lawson SC, Fisher D, Hunt DC, Newton ME (1998) On the existence of positively charged single-substitutional nitrogen in diamond. J Phys: Condens Matter 10:6171–6180
Lee SS, Minsek DW, Vestyck DJ, Chen P (1994) Growth of diamond from diamond from atomic-hydrogen and a supersonic free jet of methyl radicals. Science 263:1596–1598
Li Z-C, Jia X-P, Huang G-F, Hu M-H, Li Y, Yan B-M, Ma H-A (2013) FEM simulations and experimental studies of the temperature field in a large diamond crystal growth cell. Chin Phys B 22:014701
Liander H, Lundblad E (1960) Some observations on the synthesis of diamonds. Ark Kemi 16:139–149
Liang Q, Yan C-S, Meng Y, Lai J, Krasnicki S, Mao H-K, Hemley RJ (2009) Recent advances in high-growth rate single-crystal CVD diamond. Diamond Relat Mater 18:698–703
Liggins S (2010) Identification of Point Defects in Treated Single Crystal Diamond. PhD Dissertation, University of Warwick, Coventry, United Kingdom
Liggins S, Newton ME, Goss JP, Briddon PR, Fisher D (2010) Identification of the dinitrogen ⟨001⟩ split interstitial H1a in diamond. Phys Rev B 81:085214
Lightowlers EC, Collins AT (1976) Determination of boron in natural semiconducting diamond by prompt particle nuclear microanalysis and Schottky barrier differential-capacitance measurements. J Phys D: Appl Phys 9:951–963

Linde O, Kravchenko S, Epstein A, Rentmeesters (2021) The Global Diamond Industry 2020–21, Bain & Company, *https://www.bain.com/insights/global-diamond-industry-2020-21/*
Liu H, Dandy DS (1995) Diamond Chemical Vapor Deposition—Nucleation and Early Growth Stages. Noyes Publications, Park Ridge
Loubser JHN, van Wyk JA (1977) A triplet state in irradiated and annealed Type Ib diamonds. Diamond Res 11:11–14
Lowther JE (1993) Excited states of the vacancy in diamond. Phys Rev B 48:11592–11601
Luo Y, Breeding CM (2013) Fluorescence produced by optical defects in diamond: Measurement, characterization, and challenges. Gems Gemol 40:82–97
Ma J, Cheesman A, Ashfold MNR, Hay KG, Wright S, Langford N, Duxbury G, Mankelevich YA (2009) Quantum cascade laser investigations of CH_4 and C_2H_2 interconversion in hydrocarbon/H_2 gas mixtures during microwave plasma enhanced chemical vapor deposition of diamond. J Appl Phys 106:033305
Mäki JM, Tuomisto F, Kelly C, Fisher D, Martineau P (2007) Effects of thermal treatment on optically active vacancy defects in CVD diamonds. Phys B 401–402:613–616
Martineau PM, Lawson SC, Taylor AJ, Quinn SJ, Evans DJF, Crowder MJ (2004) Identification of synthetic diamond grow using Chemical Vapor Deposition (CVD). Gems Gemol 40:2–25
Martineau P, Gaukroger M, Khan R, Evans D (2009) Effect of steps on dislocations in CVD diamond grown on {001} substrates. Phys Status Solidi C 6:1953–1957
McGuinness CD, Wassell AM, Lanigan MP, Lynch SA (2020) Separation of natural from laboratory-grown diamond using time-gated luminescence imaging. Gems Gemol 56:220–229
Meng YF, Yan CS, Lai J, Krasnicki S, Shu H, Yu T, Liang Q, Mao HK, Hemley RJ (2008) Enhanced optical properties of chemical vapor deposited single crystal diamond by low-pressure/high-temperature annealing. PNAS 105:17620–17625
Mikhail S, Guillermier C, Franchi IA, Beard AD, Crispin K, Verchovsky AB, Jones AP, Milledge HJ (2014) Empirical evidence for the fractionation of carbon isotopes between diamond and iron carbide from the Earth's mantle. Geochem Geophys Geosyst 15:855–866
Mita, Y (1996) Change of absorption spectra in Type Ib diamond with heavy neutron irradiation. Phys Rev B 53:11360–11364
Mita Y, Nisida Y, Suito K, Onodera A, Yazu S (1990) Photochromism of H2 and H3 centres in synthetic Type Ib diamonds. J Phys: Condens Matter 2:8567–8574
Moe KS, D'Haenens-Johansson U, Wang W (2015) Lab Notes: Irradiated green-blue CVD synthetic diamonds. Gems Gemol 51:320–321
Moe KS, Johnson P, D'Haenens-Johansson U, Wang W (2017) Lab Notes: A synthetic diamond overgrowth on a natural diamond. Gems Gemol 53:237–239
Mokuno Y, Chayahara A,Soda Y, Horino Y, Fujimori N (2005) Synthesizing single-crystal diamond by repetition of high rate homoepitaxial growth by microwave plasma CVD. Diamond Relat Mater 14:1743–1746
Moses TM, Reinitz I, Fritsch E, Shigley JE (1993) Two treated-color synthetic red diamonds seen in the trade. Gems Gemol 29:182–190
Moses TM, Reinitz IM, Johnson ML, King JM, Shigley JE (1997) A contribution to understanding the effect of blue fluorescence on the appearance of diamonds. Gems Gemol 22:244–259
Muranaka Y, Yamashita H, Miyadera H (1991) Synthesis and purification of diamond films using the microwave plasma of a CO-H_2 system. J Mater Sci 26:3235–3243
Nad S, Gu Y, Asmussen J (2015) Growth strategies for large and high quality single crystal diamond substrates. Diamond Relat Mater 60:26–34
Nad S, Charris A, Asmussen, J (2016) MPACVD growth of single crystalline diamond substrates with PCD rimless and expanding surfaces. Appl Phys Lett 109:162103
Nadolinny VA, Yelisseyev AP (1993) New paramagnetic centres containing nickel ions in diamond. Diamond Relat Mater 3:17–21
Nadolinny VA, Yelisseyev AP, Yuryeva OP, Feygelson BN (1997) EPR study of the transformations in nickel containing centres at heated synthetic diamonds. Appl Magn Resol 12:543–554
Nadolinny V, Yelisseyev, A, Yurjeva, O, Hofstaetter A, Meyer B, Feigelson B (1998) Relationship between electronic states of nickel-containing centres and donor nitrogen in synthetic and natural diamonds. Diamond Relat Mater 7:1558–1561
Nadolinny VA, Yelisseyev AP, Baker JM, Newton ME, Twitchen DJ, Lawson SC, Yuryeva OP, Feigelson BN (1999) A study of ^{13}C hyperfine structure in the EPR of nickel-nitrogen-containing centres in diamond and correlation with their optical properties. J Phys: Condens Matter 11:7357–7376
Nazaré MH, Rino LM (1993) Synthetic diamond: the optical band at 1.883 eV. J Mater Sci Eng B 21:329–332
Nazaré MH, Neves AJ, Davies G (1991) Optical studies of the 1.40-eV Ni center in diamond. Phys Rev B 43:14196
Nazaré MH, Mason PW, Watkins GD, Kanda H (1995) Optical detection of magnetic resonance of nitrogen and nickel in high-pressure synthetic diamond. Phys Rev B 51:16741–16745
Nazaré MH, Rino LM, Kanda H (1996) High pressure synthetic diamond: optical studies of nickel related defects. Mater Sci Eng A 290:302–305
Nazaré MH, Lopes JC, Neves AJ (2001) Nickel related defects in diamond: The 2.51eV band. Phys B 308–310:616–620

Nemanich RJ, Carlisle JA, Hirata A, Haenen K (2014) CVD diamond—Research, applications, and challenges. MRS Bull 39:490–498
Noble CJ, Pawlik Th, Spaeth J-M (1998) Electron paramagnetic resonance investigations of nickel defects in natural diamonds. J Phys: Condens Matter 50:11781–11793
Palyanov YN, Borzdov YM, Khokhryakov AF, Kupriyanov IN, Sokol AG (2010) Effect of nitrogen impurity on diamond crystal growth processes. Cryst Growth Des 10:3169–3175
Palyanov YN, Kupriyanov IN, Khokhryakov AF, Ralchenko VG (2015a) Crystal growth of diamond. *In:* Handbook of Crystal Growth. Rudolph P (ed) Elsevier, Boston, p 671–713
Palyanov YN, Kupriyanov IN, Borzdov YM, Surovtsev NV (2015b) Germanium: A new catalyst for diamond synthesis and a new optically active impurity in diamond. Sci Rep 5:1–8. doi: 10.1038/srep14789
Palyanov YN, Kupriyanov IN, Khokhryakov AF, Borzdov YM (2017) High-pressure crystallization and properties of diamond from magnesium-based catalysts. CrystEngComm 19:4459–4475
Pate BB (1986) The diamond surface: Atomic and electronic structure. Surf Sci 165:83–142
Pehrsson PE, Celii FG, Butler JE (1993) Chemical Mechanisms of Diamond CVD. *In*: Diamond Films and Coatings. Davis R, (ed) Noyes Publications, Park Ridge, p 68–146
Pereira E, Santos L, Pereira L, Hofmann DM, Christmann P, Stadler W, Meyer BK (1994) Slow emission of the 2.56 eV centre in synthetic diamond. Diamond Relat Mater 4:53–58
Pereira E, Pereira L, Hofmann DM, Stadler W, Meyer BK (1995) Excited levels of the 2.56 eV emission in synthetic diamond. Radiat Eff Defects Solids 135:1–4
Peretti A, Herzog F, Bieri W, Alessandri M, Günther D, Frick DA, Cleveland E, Zaitsev AM, Deljanin B (2014) New generation of synthetic diamonds reches the market. Part A: Identification of CVD-grown blue diamonds. Contrib Gemol 14:3–20
Persaud S, Wang W, Johnson P, Balov IP (2018) Lab Notes: One natural melee diamond found in large batch of HPHT synthetic melee. Gems Gemol 54:208–209
Philip J, Hess P, Feygelson T, Butler JE, Chattopadhyay S, Chen KH, Chen LC (2003) Elastic, mechanical, and thermal properties of nanocrystalline diamond films. J Appl Phys 93:2164–2171
Pinto H, Jones R (2009) Theory of the birefringence due to dislocations in single crystal CVD diamond. J Phys Condens Matter 21:364220
Ponahlo J (1992) Cathodoluminescence (CL) and CL spectra of De Beers' experimental synthetic diamonds. J Gemmol 23:3–17
Poon TPY, Wang W (2016) Lab Notes: Blue HPHT synthetic diamond over 10 carats. Gems Gemol 52:416
Prelas MA, Popovici G, Biglow LK (eds) (1997) Handbook of Industrial Diamonds and Diamond Films. Marcel Dekker, Inc., New York
Renfro N (2015) Digital photomicrography for gemologists. Gems Gemol 51:144–159
Robertson R, Fox, JJ, Martin AE (1934) Two types of diamond. Philos Trans R Soc, A 232:463–535
Robins LH, Cook LP, Farabaugh EN, Feldman A (1989) Cathodoluminescence of defects in diamond films and particles grown by hot-filament chemical-vapor deposition. Phys Rev B 39:13367–13377
Robinson A (2018) Irradiated HPHT-grown diamonds might escape detection as synthetics, says lab. IDEX Online, *http://www.idexonline.com/FullArticle?Id=43871*
Rogers LJ, Jahnke KD, Doherty MW, Dietrich A, McGuinness LP, Müller C, Teraji T, Sumiya H, Isoya J, Manson NB, Jelezko F (2014) Electronic structure of the negatively charged silicon-vacancy center in diamond. Phys Rev B 89:235101
Rooney MLT (1992) {115} Growth in boron-doped synthetic diamonds. J Cryst Growth 116:15–21
Rooney MLT, Welbourn CM, Shigley JE, Fritsch E, Reinitz I (1993) De Beers near colorless-to-blue experimental gem-quality synthetic diamonds. Gems Gemol 29:38–45
Rose BC, Huang D, Zhang ZH, Stevenson P, Tyryshkin AM, Sangtawesin S, Srinivasan S, Loudin L, Markham ML, Edmonds AM, Twitchen DJ, Lyon SA, De Leon NP (2018) Observation of an environmentally insensitive solid-state spin defect in diamond. Science 361:60–63
Rossman G, Kirschvink J (1984) Magnetic properties of gem-quality synthetic diamonds. Gems Gemol 20:163–166
Ruan J, Choyke WJ, Partlow WD (1991) Cathodoluminescence and annealing study of plasma-deposited polycrystalline diamond films. J Appl Phys 69:6632–6636
Ruan J, Kobashi K, Choyke WJ (1992) On the "band-A" emission and boron related luminescence in diamond. Appl Phys Lett 60:3138–3140
Rzepka E, Silva F, Lusson A, Rivière A, Gicquel A (2001) Luminescence study of polycrystalline CVD diamond films containing a small amount of nitrogen. Diamond Relat Mater 10:542–545
Satoh S, Sumiya H, Tsuji K, Yazu S (1990) Differences in nitrogen concentration and aggregation among (111) and (100) growth sectors of large synthetic diamonds. *In*: Science and Technology of New Diamond. Saito S, Fukunaga O, Yoshikawa M (eds) KTK Scientific Publishers/Terra Scientific Publishing Co., Tokyo, p 351–355
Setaka N (1994) History of diamond synthesis in Japan. *In*: Synthetic Diamond: Emerging CVD Science and Technology, The Electrochemical Society Series. Spear KE, Dismukes JP (eds) John Wiley, Interscience, New York, p 57–90

Sharp WE (1966) Phyrrhotite: A common inclusion in South African diamonds. Nature 211:402–403
Shigley JE, Fritsch E (1990) Optical properties of some greenish blue-to-green diamonds. SPIE Proc 1325:315–324
Shigley JE, Fritsch E, Stockton CM, Koivula JI, Fryer CW, Kane RE (1986) The gemological properties of the Sumitomo gem-quality synthetic yellow diamonds. Gems Gemol 22:192–208
Shigley JE, Fritsch E, Stockton CM, Koivula JI, Fryer CW, Kane RE, Hargett DR, Welch CW (1987) The gemological properties of the De Beers gem-quality synthetic diamonds. Gems Gemol 23:187–206
Shigley JE, Fritsch E, Reinitz I, Moon M (1992) An update on Sumitomo gem-quality synthetic diamonds. Gems Gemol 28:116–122
Shigley JE, Fritsch E, Koivula JI, Sobolev NV, Malinovsky IY, Pal'yanov YN (1993a) The gemological properties of Russian gem-quality synthetic yellow diamonds. Gems Gemol 29:228–248
Shigley JE, Fritsch E, Reinitz I (1993b) Two near-colorless General Electric Type-IIa synthetic diamond crystals. Gems Gemol 29:191–197
Shigley JE, Moses TM, Reinitz I, Elen S, McClure SF, Fritsch E (1997) Gemological properties of near-colorless synthetic diamonds. Gems Gemol 33:42–53
Shigley JE, Abbaschian R, Clarke C (2002) Gemesis laboratory-created diamonds. Gems Gemol 38:301–309
Shigley JE, McClure SF, Breeding CM, Shen AHT, Muhlmeister SM (2004a) Lab-grown colored diamonds from Chatham created gems. Gems Gemol 40:128–145
Shigley JE, Breeding CM, Shen AHT (2004b) An updated chart on the characteristics of HPHT-grown synthetic diamonds. Gems Gemol 40:303–313
Shvyd'ko Y, Blank V, Terentyev S (2017) Diamond x-ray optics: Transparent, resilient, high-resolution, and wavefront preserving. MRS Bull 42:437–444
Silva F, Achard J, Bonnin X, Michau A, Tallaire A, Brinza O, Gicquel A (2006) 3D crystal growth model for understanding the role of plasma pre-treatment on CVD diamond crystal shape. Phys Stat Sol (a) 203:3049–3055
Silva F, Bonnin X, Achard J, Brinza O, Michau A, Gicquel A (2008) Geometric modeling of homoepitaxial CVD diamond growth: I. The {100}{111}{113} system. J Cryst Growth 310:187–203
Silva F, Achard J, Brinza O, Bonnin X, Hassouni K, Anthonis A, De Corte K, Barjon J (2009) High quality, large surface area, homoepitaxial MPACVD diamond growth. Diamond Relat Mater 18:683–697
Sittas G, Kanda H, Kiflawi I, Spear PM (1996) Growth and characterization of Si-doped diamond single crystals grown by the HPHT method. Diamond Relat Mater 5:866–869
Smith EM, Shirey SB, Nestola F, Bullock ES, Wang J, Richardson SH, Wang W (2016) Large gem diamonds from metallic liquid in Earth's deep mantle. Science 354:1403–1405
Smith EM, Shirey SB, Richardson SH, Nestola F, Bullock ES, Wang J, Wang W (2018a) Blue boron-bearing diamonds from Earth's lower mantle. Nature 560:84–87
Smith EM, Shirey SB, Wang W (2018b) The very deep origin of the world's biggest diamonds. Gems Gemol 53:388–403
Song Z, Lu T, Liu H, Dai H, Ke J, Zhu W, Zhang J (2020) Identification of Type IIa blue CVD synthetic diamonds from Huzhou SinoC Semiconductor Co. in China. J Gemmol 37:306–313
Song Z, Dai H, Gao B, Zhu W (2021) Identification of pink-coloured CVD synthetic diamonds from Huzhou Sino-C Semiconductor Co. in China. Crystals 11:872
Stalder KR, Sharpless RL (1990) Plasma properties of a hydrocarbon arcjet used in th eplasma deposition of diamond thin-films. J Appl Phys 68:6187–6190
Stachel T, Harris JW (2008) The origin of cratonic diamonds—Constraints from mineral inclusions. Ore Geol Rev 34:5–32
Steeds JW, Charles S, Davis TJ, Gilmore A, Hayes J, Pickard D, Butler JE (1999a) Creation and mobility of self-interstitials in diamond by use of a transmission electron microscope and their subsequent study by photoluminescence microscopy. Diamond Relat Mater 8:94–100
Steeds JW, Davis TJ, Charles SJ, Hayes JM, Butler JE (1999b) 3H luminescence in electron-irradiated diamond samples and its relationship to self-interstitials. Diamond Relat Mater 8:1847–1852
Stoupin S, Antipov S, Butler JE, Kolyadin AV, Katrusha A (2016) Large-surface-area diamond (111) crystal plates for applications in high-heat-load wavefront-preserving X-ray crystal optics. J Synchrotron Radiat 23:1118–1123
Strong HM (1977) Novel diamond products and the manufacture thereof. US4042673
Strong HM (1989) Early diamond making at General Electric. Am J Phys 57:794–801
Strong HM, Chrenko RM (1971) Further studies on diamond growth rates and physical properties of laboratory-made diamond. J Phys Chem 75:1838–1843
Sugano T, Ohashi N, Tsurumi T, Fukunaga O (1996) Pressure and temperature region of diamond formation in systems graphite and Fe containing alloy. Diamond Relat Mater 5:29–33
Sumida N, Lang AR (1981) Cathodoluminescence evidence of dislocation interactions in diamond. Philos Mag A 43:1277–1287
Sumiya H (2014) HPHT synthesis of large, high-quality, single crystal diamonds. *In*: Comprehensive Hard Materials. Sarin V (ed) Elsevier, Oxford, p 195–215
Sumiya H, Satoh S (1996) High-pressure synthesis of high-purity diamond crystal. Diamond Relat Mater 5:1359–1365
Sumiya H, Tamasaku K (2012) Large defect-free synthetic Type IIa diamond crystals synthesized via high pressure and high temperature. Jpn J Appl Phys 51:090102

Sumiya, H, Toda N, Nishibayashi Y, Satoh S (1997) Crystalline perfection of high purity synthetic diamond crystal. J Cryst Growth 178:485–494
Sumiya H, Toda N, Satoh S (2002) Growth rate of high-quality large diamond crystals. J Cryst Growth 237–239:1281–1285
Sumiya H, Harano K, Tamasaku K (2015) HPHT synthesis and crystalline quality of large high-quality (001) and (111) diamond crystals. Diamond Relat Mater 58:221–225
Sunagawa I (1984) Morphology of natural and synthetic diamond crystals. *In*: Materials Science of the Earth's Interior. Sunagawa I (ed) Terra Scientific Publishing Co., Tokyo, p 303–330
Sunagawa I (1995) The distinction of natural from synthetic diamond. J Gemmol 24:485–499
Takeuchi D, Watanabe H, Yamanaka S, Okushi H, Kajimura K. (2000) Homoepitaxial diamond films grown by step-flow mode in various misorientation angles of diamond substrates. Diamond Relat Mater 9:231–235
Takeuchi D, Watanabe H, Yamanaka S, Okushi H, Sawada H, Ichinose H, Sekiguchi T, Kajimura K (2001) Origin of band-A emission in diamond thin films. Phys Rev B 63:245328
Tallaire A, Collins AT, Charles D, Achard J, Sussmann R, Gicquel A, Newton ME, Edmonds AM, Cruddace RJ (2006) Characterisation of high-quality thick single-crystal diamond grown by CVD with a low nitrogen addition. Diamond Relat Mater 15:1700–1707
Tallaire A, Achard J, Silva F, Brinza O, Gicquel A (2013) Growth of large size diamond single crystals by plasma assisted chemical vapour deposition: Recent achievements and remaining challenges. C R Phys 14:169–184
Tallaire A, Mille V, Brinza O, Thi TNT, Brom JM, Loguinov Y, Katrusha A, Koliadin A, Achard J (2017a) Thick CVD diamond films grown on high-quality Type IIa HPHT diamond substrates from New Diamond Technology. Diamond Relat Mater 77:146–152
Tallaire A, Brinza O, Mille V, William L, Achard J (2017b) Reduction of dislocations in single crystal diamond by lateral growth over a macroscopic hole. Adv Mater 29:1604823
Tennant S (1797) On the nature of the diamond. Phil Trans R Soc Lond 87:123–127
Thomas RE, Rudder RA, Markunas RJ (1992) Thermal desorption from hydrogenated and oxygenated diamond (100) surfaces. J Vac Sci Technol A 10:2451–2457
Tolansky S (1966) Birefringence of diamond. Nature 211:158–160
Tolansky S, Sunagawa I (1959) Spiral and other growth forms of synthetic diamonds: A distinction between natural and synthetic diamond. Nature 184:1523–1527
Tran Thi TN, Morse J, Caliste D, Fernandez B, Eon D, Hartwig J, Barbay C, Mer-Calfati C, Tranchant N, Arnault JC, Lafford TA, Baruchel J (2017) Synchrotron Bragg diffraction imaging characterization of synthetic diamond crystals for optical and electronic power device applications. J Appl Cryst 50:561–569
Twitchen DJ, Hunt DC, Smart V, Newton ME, Baker JM (1999) Correlation between ND1 optical absorption and the concentration of negative vacancies determined by electron paramagnetic resonance (EPR). Diamond Relat Mater 8:1572–1575
van Wyk JA, Woods GS (1995) Electron spin resonance of excited states of the H3 and H4 centres in irradiated Type Ia diamonds. J Phys: Condens Matter 7:5901–5911
Varma CKR (1970) Evidence of deformation twinning in natural diamond crystals. J Phys Chem Solids 31:890
Vasil'ev EA, Ivanov-Omskii VI, Pomazanskii BS, Bogush IN (2004) The N3 center luminescence quenched by nitrogen impurity in natural diamond. Tech Phys Lett 30:802–803
Vins VG, Feigelson BN, Eliseev AP, Patrin NS, Patrenin YV, Nehaev PY (1991) Optically active defects in diamonds grown at 1350–1750 °C. Sverkhtverd. Mater. 3:21–26 (in Russian)
Wakatsuki M (1966) New catalysts for synthesis of diamond. Jap J Appl Phys 5:337
Wakatsuki M, Ohnishi A, Jia X, Kurosawa M, Sueno S, Hayakawa S, Gohshi Y (1999) Growth of diamond with Zr-containing molten metal solvents and metal elements as incorporated impurities. Diamond Relat Mater 8:1438–1440
Walker J (1977) An optical study of the TR12 and 3H defects in irradiated diamond. J Phys C: Solid State Phys 10:3031–3037
Walmsley JC, Lang AR (1983) Transmission electron-microscopic observations of deformation and microtwinning in a synthetic diamond compact. J Mater Sci Lett 2:785–788
Wang W, Moses T (2007) Lab Notes: Type IIa diamond with intense green color introduced by Ni-related defects. Gems Gemol 43:156–158
Wang W, Moses TM, Linares RC, Shigley JE, Hall MS, Butler JE (2003) Gem-quality synthetic diamonds grown by a chemical vapor deposition (CVD) method. Gems Gemol 39:268–283
Wang W, Smith CP, Hall MS, Breeding CM, Moses TM (2005a) Treated-color pink-to-red diamonds from Lucent Diamonds Inc. Gems Gemol 41:6–19
Wang W, Tallaire A, Hall MS, Moses TM, Achard J, Sussmann RS, Gicquel A (2005b) Experimental CVD synthetic diamonds from LIMHP-CNRS, France. Gems Gemol 41:234–244
Wang W, Hall M, Breeding CM (2007a) Natural Type Ia diamond with green-yellow color due to Ni-related defects. Gems Gemol 43:240–243
Wang W, Hall MS, Moe KS, Tower J, Moses TM (2007b) Latest-generation CVD-grown synthetic diamonds from Apollo Diamond Inc. Gems Gemol 43:294–312
Wang W, Doering P, Tower J, Lu R, Eaton-Magaña S, Johnson P, Emerson E, Moses TM (2010) Strongly colored pink CVD lab-grown diamonds. Gems Gemol 46:4–17

Wang W, D'Haenens-Johansson UFS, Johnson P, Moe KS, Emerson E, Newton ME, Moses TM (2012) CVD synthetic diamond from Gemesis Corp. Gems Gemol 48:80–97
Wang W, Persaud S, Myagkaya E (2022) New record size for CVD laboratory-grown diamond. GIA Research News, *https://www.gia.edu/gia-news-research/january-2022-largest-cvd*
Wassell AM, McGuiness CD, Hodges C, Lanigan PMP, Fisher D, Martineau PM, Newton ME, Lynch SA (2018) Anomalous green luminescent properties in CVD synthetic diamonds. Phys Stat Sol (a) 215:1800292
Watanabe K, Lawson SC, Isoya J, Kanda H, Sato Y (1997) Phosphorescence in high-pressure synthetic diamond. Diamond Relat Mater 6:99–106
Welbourn CM, Cooper M, Spear PM (1996) De Beers natural versus synthetic diamond verification instruments. Gems Gemol 32:156–169
Wentorf RH (1971) Some studies of diamond growth rates. J Phys Chem 75:1833–1837
Woods GS (1984) Infrared absorption studies of the annealing of irradiated diamonds. Philos Mag B 50:673–688
Woods GS, Collins AT (1982) The 1450 cm^{-1} infrared absorption in annealed, electron-irradiated Type I diamonds. J Phys C: Solid State Phys 15:L949–L952
Woods GS, Collins AT (1983) Infrared absorption spectra of hydrogen complexes in type I diamonds. J Phys Chem Solids 44:471–475
Woods G, Lang A (1975) Cathodoluminescence, optical absorption and x-ray topographic studies of synthetic diamonds. J Cryst Growth 28:215–226
Wort CJH, Balmer RS (2008) Diamond as an electronic material. Mater Today 11:22–28
Yamada H, Chayahara A, Mokuno Y, Umezawa H, Shikata SI, Fujimori N (2011) Fabrication of 1 inch mosaic crystal diamond wafers. Appl Phys Express 3:051301
Yamada H, Chayahara A, Mokuna Y, Tsubouchi N, Shikata SI (2013) Uniform growth and repeatable fabrication of inch-sized wafers of a single-crystal diamond. Diamond Relat Mater 33:27–31
Yamada H, Chayahara A, Mokuno Y, Kato Y, Shikata S (2014) A 2-in. mosaic wafer made of a single-crystal diamond. Appl Phys Lett 104:102110
Yamada H, Chayahara A, Mokuno Y (2016) Effects of intentionally introduced nitrogen and substrate temperature on growth of diamond bulk single crystals. Jpn J Appl Phys 55:01AC07
Yang NJ, Yu SY, Macpherson JV, Einaga Y, Zhao HY, Zhao GH, Swain GM, Jiang X (2019) Conductive diamond: synthesis, properties, and electrochemical applications. Chem Soc Rev 48:157–204
Yelisseyev A, Kanda H (2007) Optical centers related to 3d transition metals in diamond. New Diamond Front Carbon Technol 17:127–178
Yelisseyev AP, Nadolinny VA (1995) Photoinduced absorption lines related to nickel impurity in annealed synthetic diamonds. Diamond Relat Mater 4:177–185
Yelisseyev A, Nadolinny V, Feigelson B, Terentyev S, Nosukhin S (1996) Spatial distribution of impurity defects in synthetic diamonds obtained by the BARS technology. Diamond Relat Mater 5:1113–1117
Yelisseyev A, Babich Yu, Nadolinny V, Fisher D, Feigelson B (2002) Spectrospic study of HPHT synthetic diamonds, as grown at 1500 °C. Diamond Relat Mater 11:22–37
Yelisseyev A, Lawson S, Sildos I, Osvet A, Nadolinny V, Feigelson B, Baker JM, Newton M, Yuryeva O (2003) Effect of HPHT annealing on the photoluminescence of synthetic diamonds grown in the Fe–Ni–C system. Diamond Relat Mater 12:2147–2168
Yelisseyev AP, Steeds JW, Babich YV, Feigelson BN (2006) A new approach to investigation of nickel defect transformation in the HPHT synthetic diamonds using local optical spectroscopy. Diamond Relat Mater 15:1886–1890
Zaitsev AM (2000) Vibronic spectra of impurity-related optical centers in diamond. Phys Rev B 61:909–922
Zaitsev AM (2001) Optical Properties of Diamond: A Data Handbook. Springer, Berlin
Zaitsev AM, Moe KS, Wang W (2018) Defect transformations in nitrogen-doped CVD diamond during irradiation and annealing. Diamond Relat Mater 88:237–255
Zaitsev AM, Kazuchits NM, Kazuchits VN, Moe KS, Rusetsky MS, Korolik OV, Kitajima K, Butler JE, Wang W (2020) Nitrogen-doped CVD diamond: Nitrogen concentration, color and internal stress. Diamond Relat Mater 105:107794
Zaitsev AM, Kazuchits NM, Moe KS, Butler JE, Korolik OV, Rusetsky MS, Kazuchits VN (2021) Luminescence of brown CVD diamond: 468 nm luminescence center. Diamond Relat Mater 113:108255
Zeitlin A, Herman H, Brayman J (1961) Super-high pressure apparatus. US 2968837
Zhang Z-H, Stevenson P, Thiering G, Rose BC, Huang D, Edmonds AM, Markham ML, Lyon SA, Gali A, De Leon NP (2020) Optically detected magnetic resonance in neutral silicon vacancy centers in diamond via bound exciton states. Phys Rev Lett 125:237402
Zhu H, Pearson K, Sunset Peak International Limited (2019) Multi-heater method for growing high quality diamond. US10166518 B2
Zimnisky P (2020) State of the Diamond Market—Independent Monthly Data Analysis, August 2020, Volume 3, Issue 12
Zimnisky P (2021) Lab-grown diamond jewelry market forecast to almost double in size by 2025. Paul Zimnisky Diamond Analytics, *https://www.paulzimnisky.com/Lab-Grown-Diamond-Jewelry-Market-Forecast-to-Almost-Double-in-Size-by-2025*